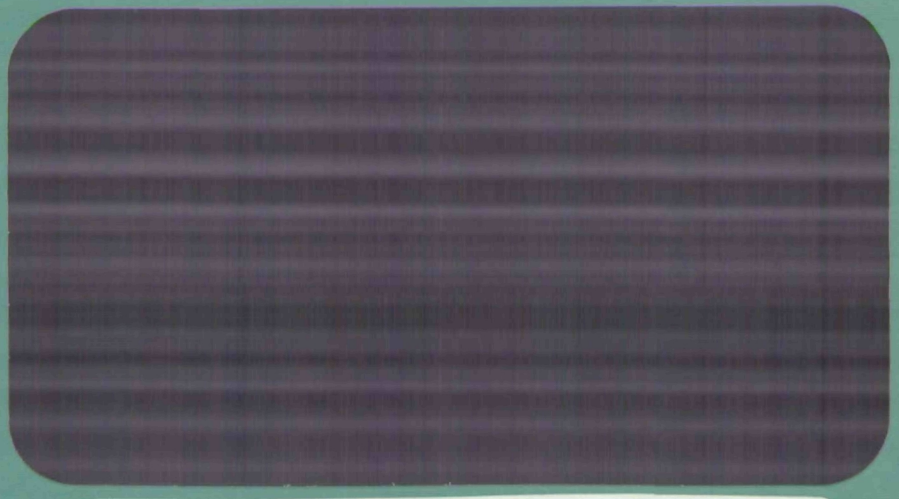

Z 65 16172

(ACCESSION NUMBER)

(THRU)

100

(PAGES)

(CODE)

03

(NASA CR OR TMX OR AD NUMBER)

(CATEGORY)

FACILITY FORM 602

AVAILABLE TO NASA HEADQUARTERS ONLY

NOV 1977

RECEIVED

NASA STI FACILITY

(NASA-CR-156962) LEM RADIATOR STUDY Final Report (Grumman Aircraft Engineering Corp.) 100 p

N78-76277

Unclas

00/18 33798

CONTRACT REQUIREMENTS	CONTRACT ITEM	MODEL	CONTRACT NO.
Exhibit E-Para.No.5.1	Line Item 13	LEM	NAS 9-1100

Type II Documentation

Primary Code 703

REPORT

NO. LED-510-11

DATE: 2 August 1965

FINAL REPORT
LEM RADIATOR STUDY

CODE 26512

PREPARED BY: A. Hoch A. Schmidt M. Tawil
A. Hoch A. Schmidt M. Tawil

CHECKED BY: M. Tawil R. H. Bullis
M. Tawil R. H. Bullis

DEPARTMENT: LEM Thermodynamics

SECTION:

TECHNICAL APPROVAL:

APPROVED BY: A. J. Katz

APPROVED BY: R. B. Whitaker

APPROVED BY:

REVISIONS

DATE	REV. BY	REVISIONS & ADDED PAGES	REMARKS

FORM G324 REV 1 8-64

AVAILABLE TO NASA HEADQUARTERS ONLY

This report is submitted in partial fulfillment of the requirements of Contract NAS 9-1100. Portions of the study discussed herein were conducted by Ling Temco Vought Astronautics Division under Grumman Purchase Order 2-24497-C.

TABLE OF CONTENTS

Page

Summary.....1

Introduction.....2

Design Constraints.....6

ECS Description.....8

Flat Radiators.....11

- Design.....11
- Startup Sequence.....12
- Thermal Performance.....13

Geometrically Selective Radiator.....34

- Principle of Operation.....34
- Design.....34
- Thermal Performance.....35
- LEM System Application.....37

Weight Savings.....61

Conclusions.....69

Recommendations.....70

Appendices.....

- A - GSR Construction Details.....71
- B - GSR Performance Analysis.....77
- C - GSR-ECS System Analysis Program.....86
- D - GSR Fin Effectiveness Program.....93

References.....95

LIST OF ILLUSTRATIONS & TABLES

Figure		Page
1a	EPS Two Phase Radiator System Schematic	4
1b	EPS Secondary Loop Radiator System Schematic	4
2	EPS-ECS Common Glycol Radiator Loop	5
3	Simplified ECS Heat Load Profile	7
4	ECS Loop Simplified with and without Space Radiators	9
5	ECS Final Schematic	10
6	Variation of Heat Rejection with Gimbal Angle	16
7	Radiator Locations on LEM	17
8	Side Radiator in Partially Unfolded Position	18
9	Aft Radiator in Unfolded Position	19
10	Aft Radiator Installation	20
11	Panel Assembly - Center Aft LEM Radiator	21
12	Radiator Main Swivel	22
13	Deployment Sequence - Rotate Radiators 180°	23
14	Deployment Sequence - Unfold with Lanyards	24
15	Deployment Sequence - Unfold without Lanyards	25
16	Deployment Sequence - Orient Aft Radiator to Horizontal Position	26
17	Radiator - Vehicle Radiant Interchange Modes	27
18	Six Panel Configuration used for Final Mission Analysis	28
19	ECS Radiator Heat Rejection for ECS Design Heat Load	29
20	Design Heat Load Performance of Final Radiator Configuration	30
21	Radiator Heat Rejection for Minimum ECS Load	31
22	Minimum Heat Load Performance of Final Radiator Configuration	32
23	Comparison of Radiator Heat Rejection with and without Shading	33
24	Principle of Operation	41
25	Energy Interchanges within the GSR	42
26	GSR Deployable Radiator	43
27	Heat Rejection of GSR as a Function of Solar and Azimuth Angles	44
28	Effects of Radiator Properties on GSR Performance	45
29	Effects of Reflector Properties on GSR Performance	46

LIST OF ILLUSTRATIONS & TABLES (Cont'd)

Figure		Page
30	Effects of Reflector Non-Specularity on GSR Performance	47
31	Effects of Radiator Temperature on GSR Performance	48
32	GSR Deployment - Stowed Radiator	49
33	GSR Deployment - Swinging Panel Out	50
34	GSR Deployment - Final Vertical Position	51
35	Water Boiler Estimated Performance	52
36	Water Consumption, GSR with Vehicle Input	56
37	Water Consumption, GSR without Vehicle Input	57
38	Water Consumption, GSR Carry Off Design	58
39	GSR Carry Off Design	60
40	Separation Weight Savings for Radiators with Radiant Interchange	63
41	Effect of Radiant Interchange and Shadowing on Weight Savings	64
42	Weight Savings at Separation-Boom Suspended GSR	65
43	Separation Weight Savings	67
44	Separation Weight Savings Oversized Panels	68
45	GSR Panel Design	76

Table		Page
I	GSR Design Parameters	36
II	LEM Vehicle Load on GSR	38
III	Cycle Calculation Results - with Vehicle Inputs, Deployable GSR	53
IV	Cycle Calculation Results - without Vehicle Inputs, Deployable GSR	54
V	Cycle Calculation Results - with Vehicle Inputs, Carry Off GSR	55
VI	GSR Water Savings	59
VII	GSR Weight Summary	66

SUMMARY

This report presents the results of a feasibility study of the use of space radiators for the LEM. The design as it finally evolved consists of two types of mechanically interchangeable radiators each suitable for its intended range of lunar landing locations. For all but the night-time landings, the radiators must be deployed to achieve an overall vehicle weight saving. As a general rule, the Geometrically Selective Radiator (GSR) is preferable for near subsolar missions and flat radiators for near terminator landings. The optimum size of the radiator is decreased as displacement from the subsolar point increases.

For a nominal 35-hour lunar stay, with the present ECS load profile, the inclusion of an ECS radiator would increase the separation weight by approximately 200 lbs. while the maximum water saving approaches 340 lbs. (separation weight). A significant increase in this weight saving would almost certainly be realized by any extension of the active radiator life and/or increase in the ECS heat load profile.

Information on the flat radiator panels is somewhat condensed since this phase of the study is well documented in the Ling Temco Vought report covering their efforts for the Grumman Aircraft Engineering Corporation (Reference 1). A large part of the flat panel discussion contained herein is taken from that document as are the illustrations. The GSR is covered in greater detail in this report.

INTRODUCTION

The subject of the study at its inception was the investigation of various applications of space radiators to assist in LEM heat rejection with the end goal of reducing LEM weight.

Without the inclusion of a radiator, the ECS system relies on a porous plate water boiler to remove waste heat. The fuel cells (now defunct) used excess hydrogen flow to cool the cells and purge waste water vapor; the wet hydrogen was vented to space. Maximum weight savings were to be obtained by using a radiator system to cool the vented hydrogen for recirculation and, at the same time, reclaim the associated water. In addition, part or all of the water boiler load would be carried by a radiator.

The study was divided into three main areas:

1. ECS radiator system
2. EPS radiator system
3. Combined radiator system

The ECS system involved the inclusion of a radiator to share the water boiler load. An EPS system would include either a single high temperature, two phase hydrogen radiator (Figure 1a) or a heat exchanger and a secondary heat transport loop for a low temperature radiator (Figure 1b). The combined system would use the ECS glycol loop as the heat transport media for the hydrogen loop (Figure 2) so that a low temperature radiator would handle both the ECS and EPS loads.

Approximately six weeks after the start of the study, Grumman was directed by NASA (CCA #103) to eliminate the fuel cells from the LEM design, and to stop all work connected with them. This made inapplicable a good deal of the weight saving potential associated with the conversion from open to closed or even semi-closed cycle operation and terminated efforts on items 2 and 3 above. A significant side effect was caused by the fuel cells having to operate from launch pad through the entire mission. Because of this, electronic equipment and the ECS loop were active throughout the mission. With the change to batteries, Grumman was directed to shut down the ECS loop during the translunar phase of the mission. This, coupled with provisions of the LEM Thermal Design Mission which specified arbitrary orientations for most of the remaining mission

time, limited operation of the ECS radiator to the lunar stay portion of the mission. An additional savings potential of about 200 pounds (separation weight) which could have been obtained through the use of a relatively unsophisticated radiator handling the translunar loads was therefore lost.

The major portion of this report is concerned with the application of radiators to the ECS waste heat rejection problem during lunar stay.

The main objective of this study was to devise a radiator system which would show the maximum amount of weight saved for the least additional compexity in the LEM design and operation.

The results of those portions of the study completed, prior to CCA #103, are presented in the appendices of Reference 1 and they include: EPS radiator analysis, characterization of the two phase flow for the high temperature EPS radiator, combined ECS-EPS radiator analysis and ECS translunar analysis. These preliminary results indicate that a total of approximately 300 pounds of separation weight could have been saved with the fuel cell configuration.

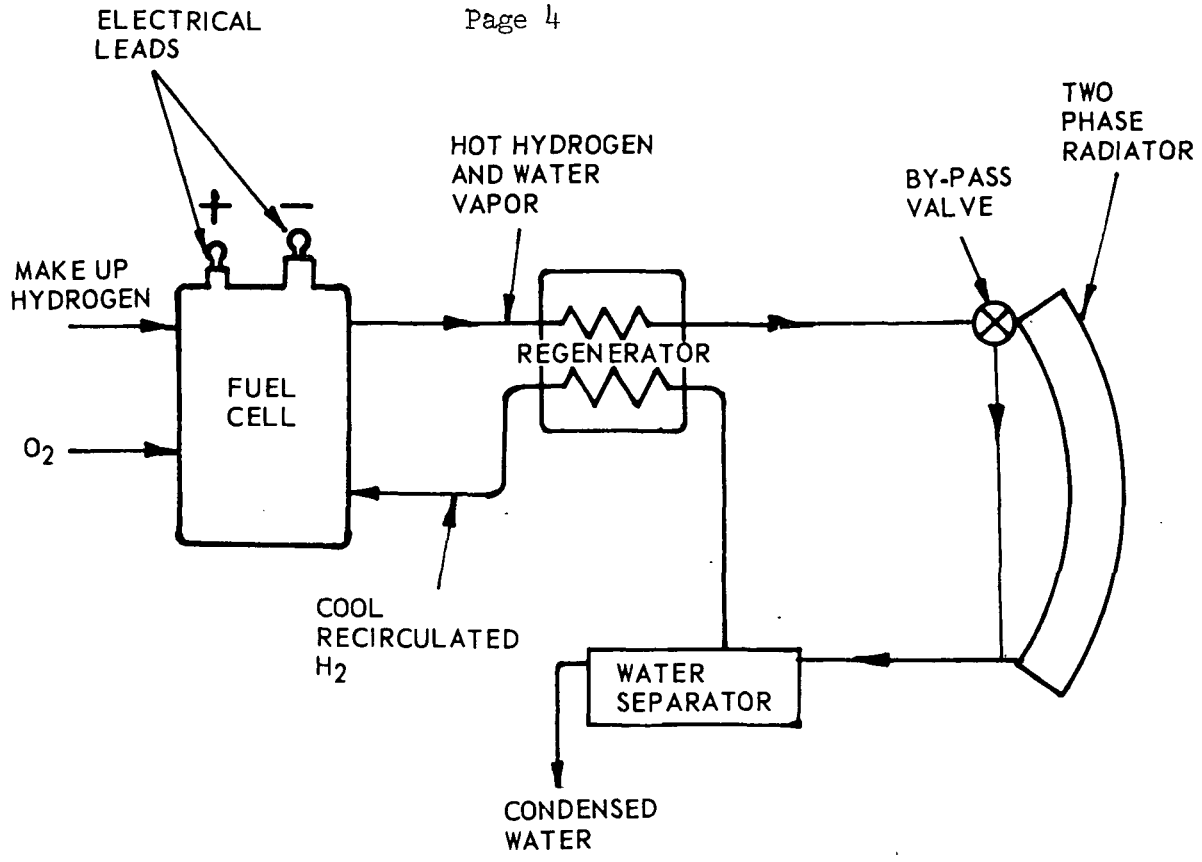

FIGURE 1a - EPS TWO PHASE RADIATOR SYSTEM SCHEMATIC

FIGURE 1b - EPS SECONDARY LOOP RADIATOR SYSTEM SCHEMATIC

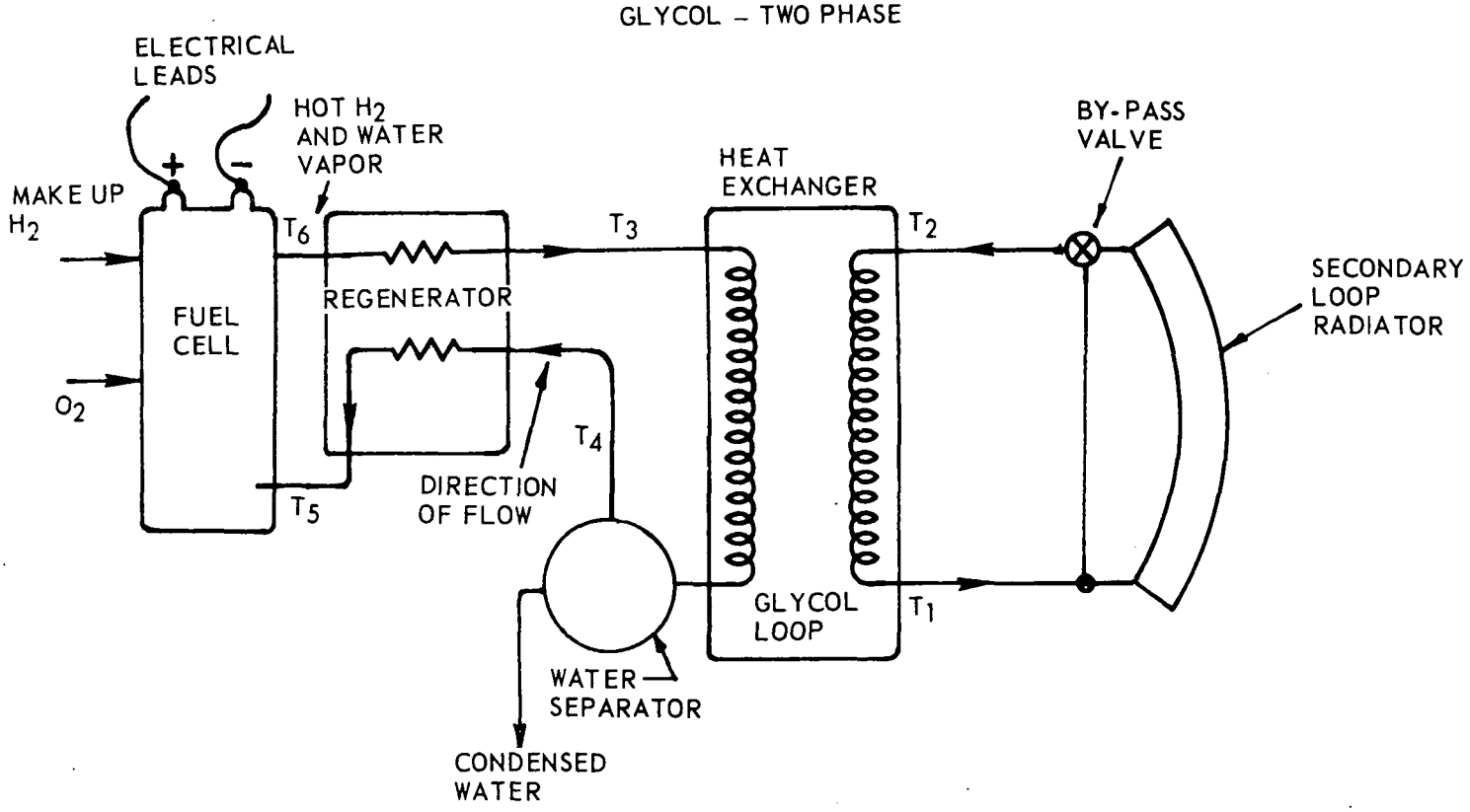

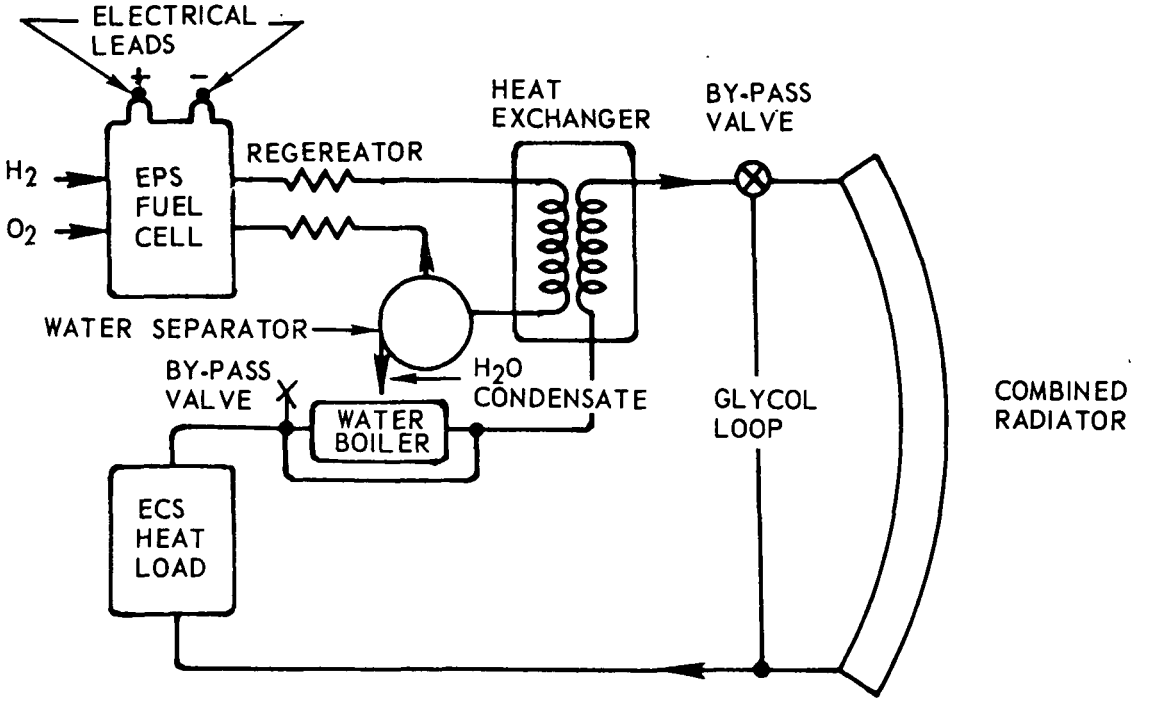

FIGURE 2- EPS-ECS COMMON GLYCOL RADIATOR LOOP

DESIGN CONSTRAINTS

The design constraints for this study are outlined below. In cases where they have been extracted from another document it is called out as a reference:

1. The ECS glycol loop will be inactive during the pre-separation phases. Hence, radiators can only be employed in the post separation phases.

2. The ECS heat load for the All Battery LEM (Figure 3) shall apply.

3. Total glycol flow rate is continuous at 222 lbs/hr.

4. The radiators shall be included in the system with a minimum of changes.

5. Micrometeroroid protection is not required for the radiators.

6. Prior knowledge of the landing site is assumed so that external changes (skins, radiator panels, etc) can be made on the vehicle before launch.

7. The entire thermal design mission from Reference 2 is applicable.

8. The vehicle orientation during lunar orbit is essentially arbitrary.

9. The lunar landing site shall be within ± 5° of selenographic latitude and ± 45° longitude.

10. The yaw orientation of the vehicle is arbitrary during the lunar stay; i.e. the sun position with respect to the vehicle shall not be constrained in any way other than that defined by the above latitude constraint.

11. The vehicle X-axis can be inclined to the local vertical within ± 30° during lunar stay.

FIGURE 3

SIMPLIFIED ECS HEAT LOAD PROFILE

ON LUNAR SURFACE
-WORST LEM ORIENTATION-

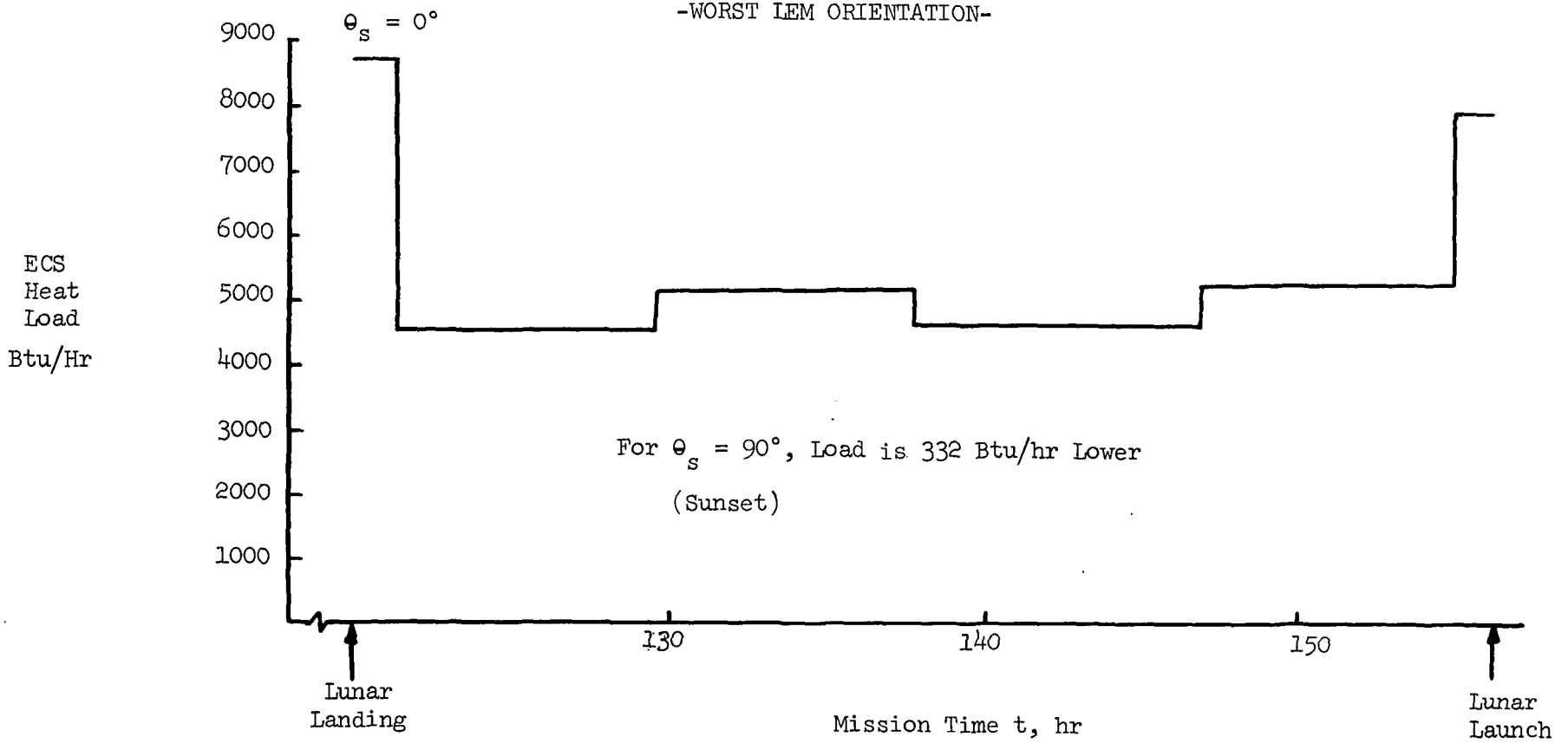

ECS DESCRIPTION

The ECS loop can be simplified to the point of consisting of a few major components (Figure 4):

1. The heat load made up of electronic equipment, metabolic and structural loads.

2. The water boiler where the load is rejected to space by subliming water.

3. The heat transfer fluid (water-glycol) which is pumped around the loop to carry the load from its source to the boiler.

Glycol temperature entering the water boiler does not exceed 90°F and its temperature leaving is not less than 32°F. In keeping with the desire for simplicity, the radiators are added to the loop without major modifications as shown in Figure 4.

In order to make the radiators work effectively, additions to the system are needed. Variations in the heat load could cause unacceptably low glycol return temperatures. For the load range used in this study, a control in the form of a proportioning radiator bypass valve is sufficient, however, two redundant valves are used to improve the reliability of the system. Since the radiators are not active prior to landing on the lunar surface, the panels need not contain glycol until that time. By leaving glycol out of the tubes, each panel can be designed to carry only its own weight from earth launch through lunar touchdown, resulting in considerable savings. However, the glycol must still be carried along to fill the tubing at the proper time. This is accomplished by storing the liquid in a precharged reservoir connected to the lines by a pair of redundant solenoid valves. Equipment carried on the ascent stage must pay an additional staging factor penalty. Therefore, wherever possible, equipment is located on the descent stage. This results in the addition of separation hardware on lines running down to the descent stage and increased complexity in the valving located in the ascent stage. That is, the valving now serves as a backup to the sealing of the interstage disconnects on separation. The final loop with all the added hardware in shown in Figure 5. It should be noted that the ascent stage accumulator must be made larger in order to handle the greater volume of fluid in the system. In addition, any resizing of the pump to handle the increased pressure drop must be charged to the radiators. For the flat radiator analysis, a water boiler bypass leg is used to limit the return temperature to 40°F. The GSR system does not use this feature.

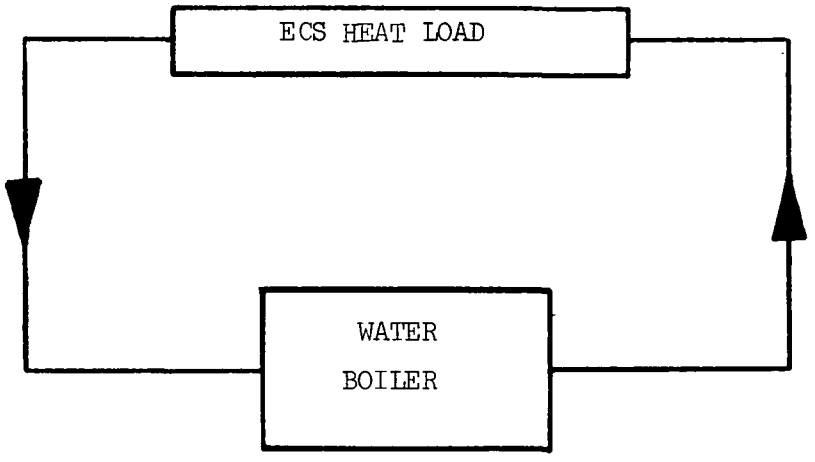

BASIC LOOP WITHOUT RADIATORS

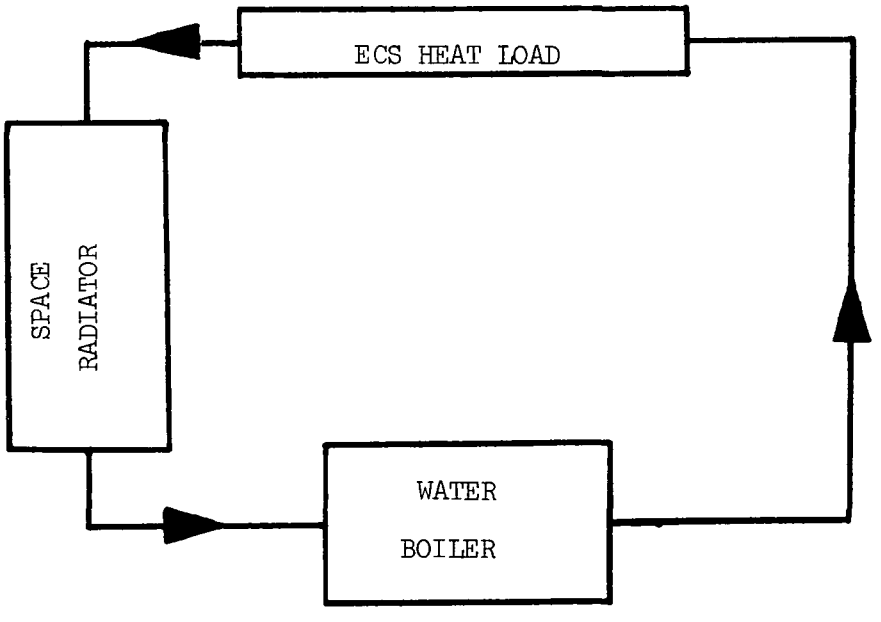

ECS LOOP-SIMPLIFIED, WITH & WITHOUT SPACE RADIATOR

FIGURE 4

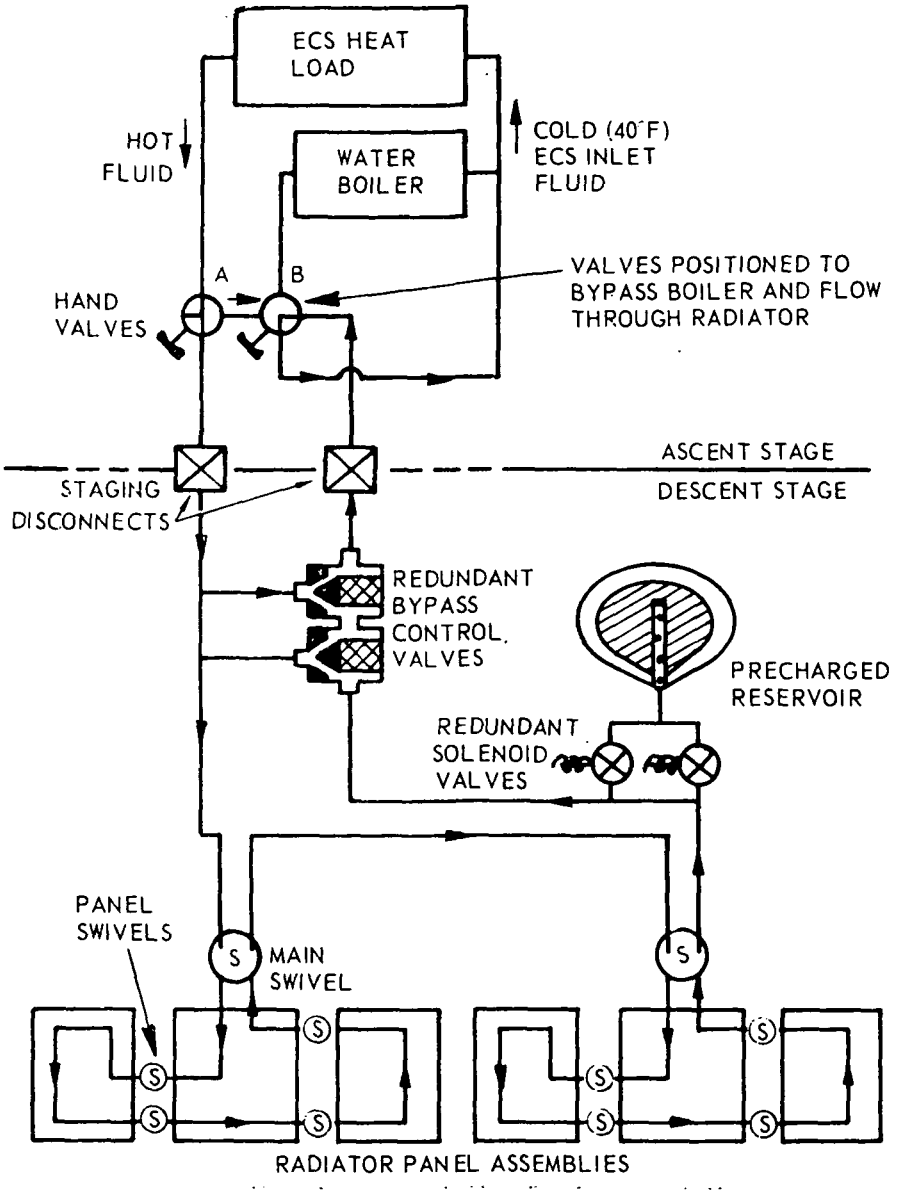

ECS FINAL SCHEMATIC

FIGURE 5

FLAT RADIATORS

Design

The initial emphasis was placed on the use of lightweight flat panels. The results of earlier Grumman studies indicated that vertical radiators would be of doubtful value on the lunar surface. This is due to the very large IR (infra-red) input from the hot lunar surface to a high emittance radiator. It was desirable to have a horizontal or near horizontal radiator so as to reject the largest possible amount of heat. It quickly became apparent that horizontal areas on the LEM available for mounting radiators were severely limited if fixed panels were to be kept within the confines of the spacecraft-LEM adapter (SLA). This led to the development of panels which could fit within the SLA and could be unfolded after landing on the lunar surface so as to provide the required surface area. Further investigation indicated that for any landing site, the heat rejection capability of the panel could be varied by changing its orientation with respect to the sun and moon. The results of this analysis are summarized in Figure 6. While the optimum gimbal (or orientation) angle varies with the landing site, it was felt that gimbaling to the horizontal was sufficient. This decision was made because the effects of vehicle radiation (discussed in the next section) would make the optimum orientation extremely difficult for the astronaut to determine. (The effects of vehicle orientation are not included in Figure 6)

The resulting design consists of two sets of folding radiator panel assemblies which are deployed by the astronaut after a lunar landing.

Throughout the study, the structural design and the thermal analyses were coordinated in order to achieve an optimum weight savings potential. Structural details such as tube wall thickness, tube spacing, and fin thickness resulted from an iteration process involving required thermal characteristics, structural soundness, and producibility. Many processes and materials were investigated during the course of the design development. Reference 1 contains detailed discussions of the aforementioned items.

The position of the radiator panel assemblies on the vehicle is shown in Figure 7. Figures 8 and 9 show the panels in the folded and partially deployed configuration. The three panels of each

assembly fold on top of each other and are stored over the descent stage landing gear outriggers during the earth launch, translunar and lunar descent mission phases. Each panel is supported by the descent stage structure and by the apex fitting of a landing gear support truss. Figures 10 and 11 show the structural details of the aft radiator and in particular its center panels. A complete set of design drawings is contained in Reference 1.

The radiator deployment requires a two way flow swivel sketched in Figure 12. The swivel is mounted to the LEM landing gear apex fitting and provides 180° rotation in the Y-Z plane, and ± 35° rotation in each of the two other mutually perpendicular planes. The frictional drag of the swivel holds the radiators in place after they have been oriented by the astronaut. The swivel torque will be adjusted before launch to a setting which will insure that the radiators maintain their orientation once they have been deployed.

Startup Sequence

The Radiator Startup Sequence is as follows:

(1) For all mission phases prior to lunar landing, hand valve A is positioned to bypass the radiator system and valve B is positioned to direct the flow from valve A through the water boiler (Figure 5). The radiator subsystem remains evacuated during all mission phases through lunar landing.

(2) After landing, the descent stage solenoid valves are energized to fill the radiator subsystem from the precharged reservoir, after filling they are de-energized (closed). A radiator subsystem pressure gage is monitored to insure that the subsystem pressure is stable before the radiators are coupled to the ECS.

(3) Approximately 1.5 hours after lunar touchdown, an astronaut emerges to rotate the panels away from the vehicle, unfold them, and orient them to a position to establish a favorable radiating environment. All astronaut tasks required for deployment and positioning are compatible with the present physical restrictions on the Apollo space suit. These deployment operations are accomplished with the aid of lanyards and a walking staff if the vehicle attitude is such that the astronaut cannot reach the panel for hand deployment (Figures 13 thru 16).

(4) When the radiator panels are fully deployed, the astronaut in the LEM positions three way valve A to direct flow through the radiator panels. Valve B is set to continue directing flow through the water boiler.

(5) When temperatures and pressures have stabilized, and if the return line temperature from the radiator subsystem is 40°F or below, the astronaut positions valve B to bypass the water boiler.

Thermal Performance

The radiating surfaces initially considered were subject to the same tipping condition (Design Constraint #11) experienced by the entire vehicle since they were considered to be rigidly attached to the LEM structure. The poor performance of these surfaces led to the consideration of gimballed radiators. The effect of re-orienting the radiators after the lunar landing is shown in Figure 6. The gimbal angle (ϕ) is defined as the angle between the local horizontal and the radiator surface. The +30° gimbal angle curves correspond to the 30° tilt away from the sun, and conversely for the -30° gimbal angle. The effect of gimbal angle on radiator performance is quite pronounced. For instance, at a landing site 60° from subsolar, the radiator performance can be increased by a factor of 2.85 if the radiator is rotated from ϕ = -30° (a possible landing configuration) to ϕ = +30°. The performance improvement available by gimballing the radiators was utilized for the final flat radiator configuration.

It was considered practical for the astronaut to orient the radiators to a horizontal position after the lunar landing. For the 60° landing site example above, gimballing the panel to a horizontal position could improve the performance to 62 percent of the maximum possible gain, assuming no shadowing or radiator vehicle thermal interchange. The actual radiant interchange couples are illustrated in Figure 17. Vehicle interchange encompasses direct IR radiation from the LEM and lunar IR, lunar albedo, and solar input reflected from the vehicle.

Thermal performance analyses were performed on six, five, four and three panel radiators at daytime landing sites from subsolar to 85° from subsolar.

The numbering scheme for the set of six radiator panels, the radiating areas, and the panel orientations, with respect to the vehicle, are shown in Figure 18.

A single panel radiating on both sides was considered for a night-time landing. No analyses were conducted to define performance at the terminator point (90° from subsolar) because of the discontinuity in heat load and thermal environment which existed at that point.

The panels are basically thin sheets with the fluid carrying tubing welded to them, the entire assembly stiffened with additional load carrying members. They are coated on the radiating side with a paint having an α_s/ϵ = .17/.92. The opposite side is shielded from lunar input with a superinsulation blanket.

The total system heat rejection for each of the above combinations of panels is compared with the design heat load in Figure 19. For landing sites, where the radiators cannot handle the entire design load, the difference is made up by the water boiler. The percent of flow through the radiator, the radiator subsystem pressure loss, and the radiator outlet temperature upstream of the bypass valve is shown in Figure 20 for the design heat load. The set of curves in Figure 20 shows the ability of combinations of panels to control the heat rejection over a range of landing sites. Flow is bypassed around the radiators when the landing sites are such that the radiator capacity exceeds the required heat rejection. Bypassing flow around the radiator reduces heat rejection by reducing the average radiating temperature and therefore reducing the radiator outlet temperature. For example, in Figure 20, when the outlet temperature of the six panel configuration drops to the 40°F control point, bypassing commences and outlet temperature continues to drop as solar angle and bypass flow increase. Bypassing also reduces radiator subsystem pressure drop until a point is reached where the high viscosity of the cold fluid more than offsets the decrease in pressure caused by a lower flow rate. Under these conditions, fewer panels are required.

For an actual mission, prior knowledge of the landing site allows for the mounting of the required number of panels. No change to the system occurs when one or more panels are left off the vehicle.

Performance analyses were conducted for minimum heat load performance of sets of six, five and three panels at various lunar sites. The LTV digital computer program used for the analyses accounts for all the inefficiencies inherent in the radiator as a heat rejection device, (e.g. fin efficiency, fluid flow model, incoming radiation, etc.). The radiator heat rejection is compared with minimum heat load in Figure 21. The percent of flow bypassed around the radiator is shown in Figure 22.

The radiator control description is completed with the curves of radiator outlet temperature and pressure drop in Figure 22. The data shows that a six panel configuration should not be used to satisfy the minimum heat load beyond 60° from subsolar. The radiator subsystem pressure loss becomes excessively high and the low fluid outlet temperature yields an extremely viscous glycol-water solution which may cease to flow. Combinations of five panels or less appear satisfactory for satisfying the minimum heat load requirement. Even a set of three panels will match the night-time minimum heat load.

A six panel radiator case was analyzed in order to establish the increase in radiator performance attainable by vehicle shadowing of the radiator and to define whether shadowing could upset the "full sun on" bypass control of heat rejection. Figure 23 shows the effect of partial shadowing caused by a solar input from the +Z direction. The heat rejection rate is increased because there is less direct solar flux on the radiator surfaces and no solar flux on many of the LEM surfaces which the radiator sees. The strong influence of vehicle shadowing shows that a method of controlling flat radiators must be devised which will allow their use in a shadowed condition for which they were not designed. One technique could simply require not unfolding the complete set of panels.

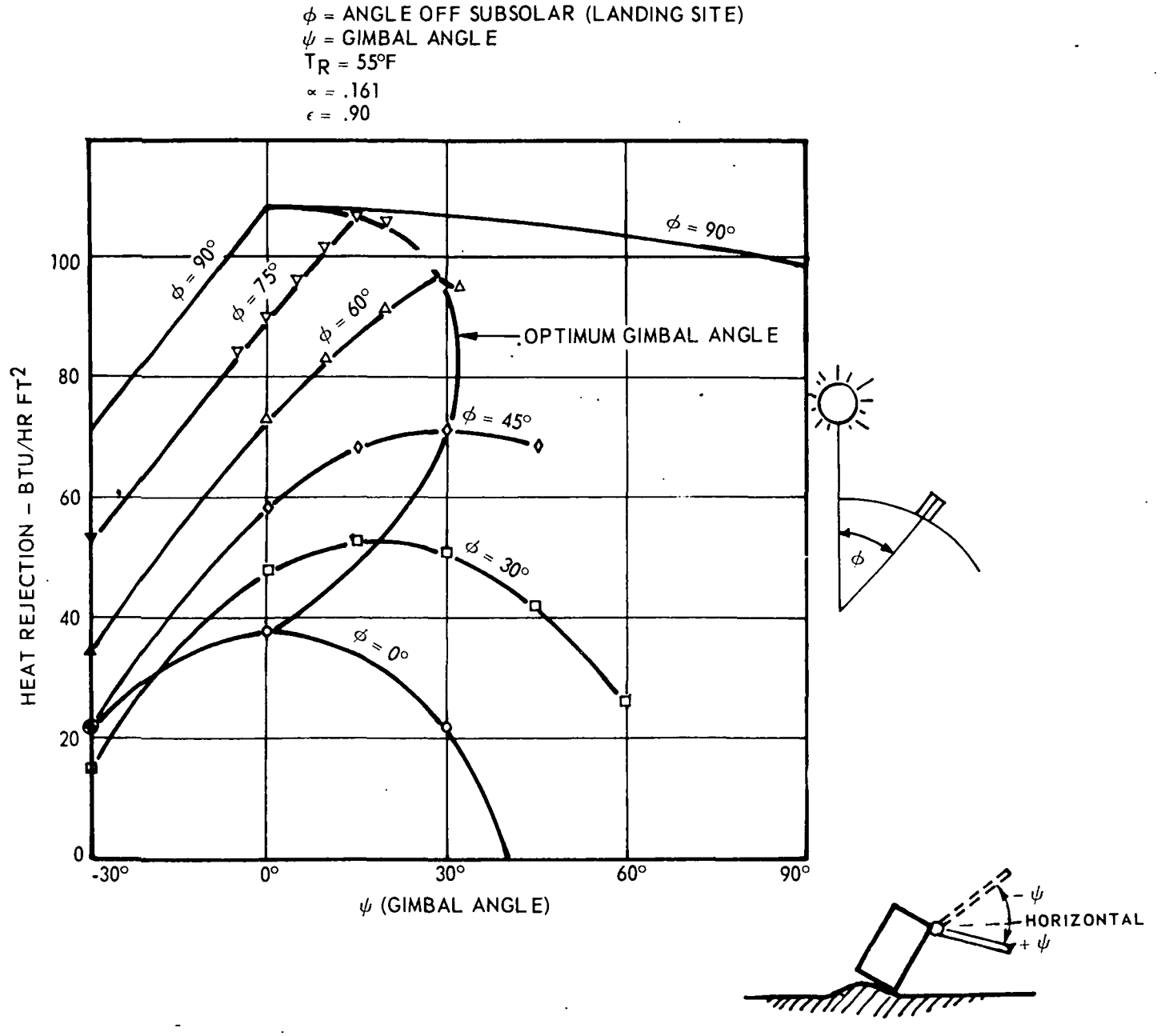

VARIATION OF HEAT REJECTION PER UNIT AREA WITH GIMBAL ANGLE

FIGURE 6

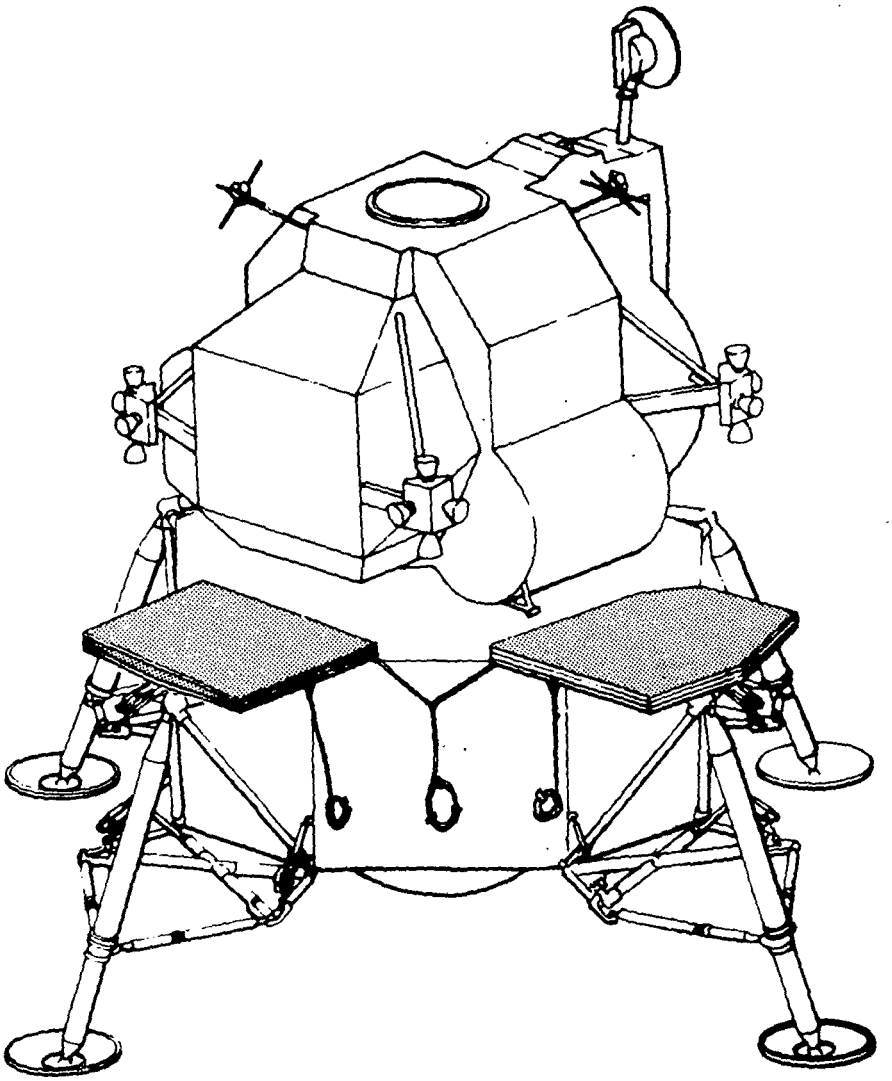

RADIATOR LOCATIONS ON LUNAR EXCURSION MODULE

FIGURE 7

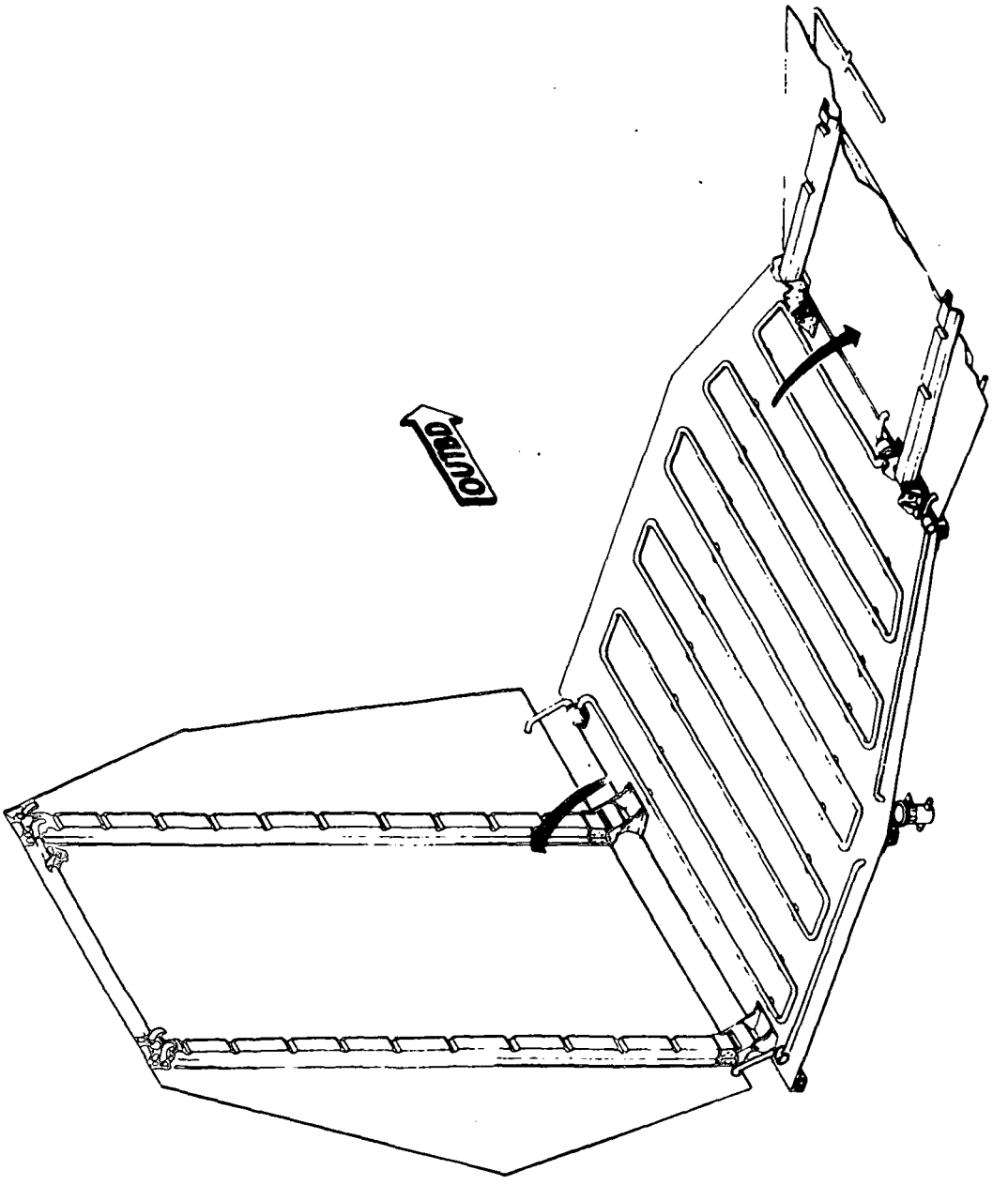

SIDE RADIATOR IN PARTIALLY UNFOLDED POSITION

FIGURE 8

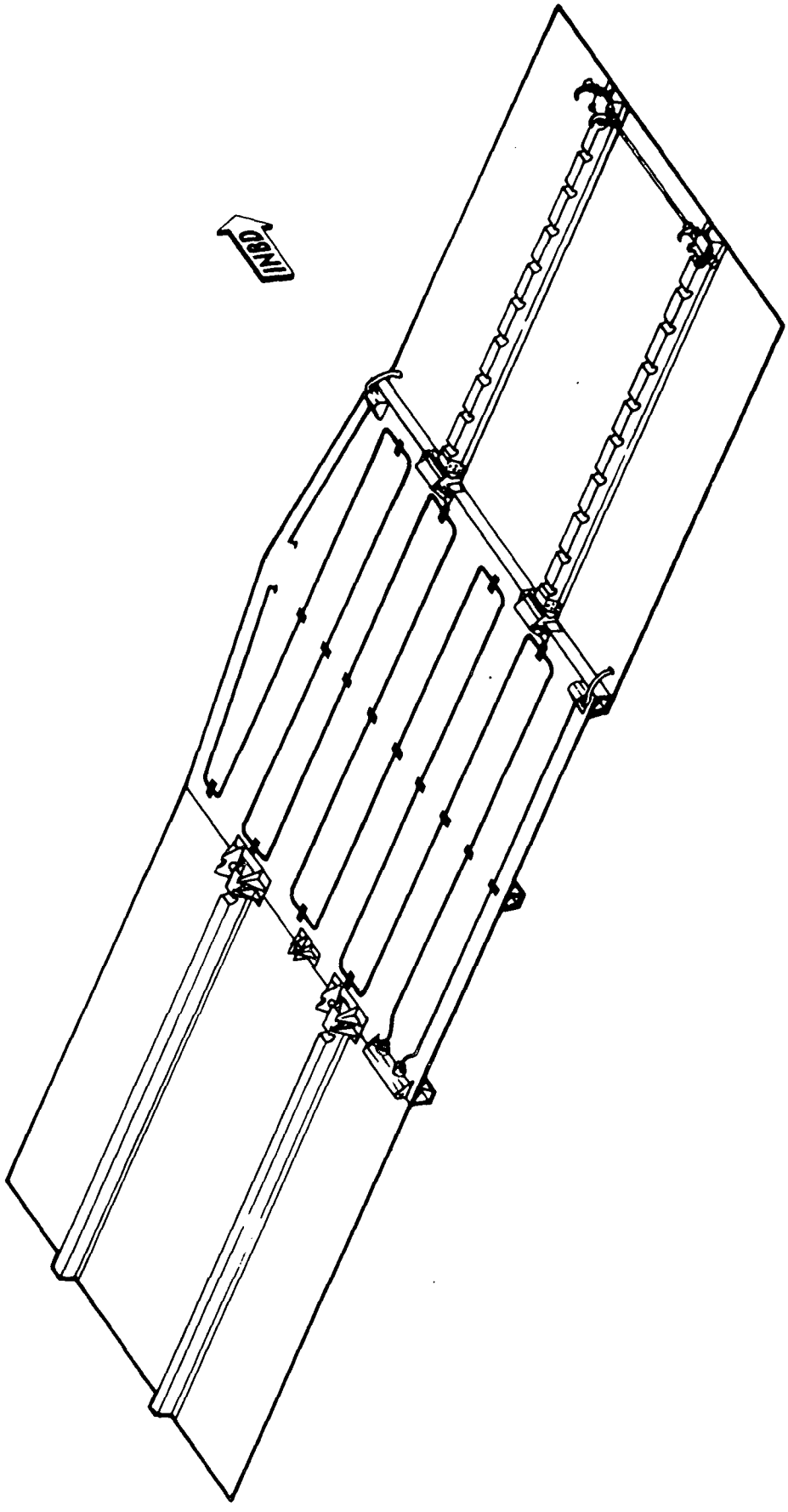

AFT RADIATOR IN UNFOLDED POSITION

FIGURE 9

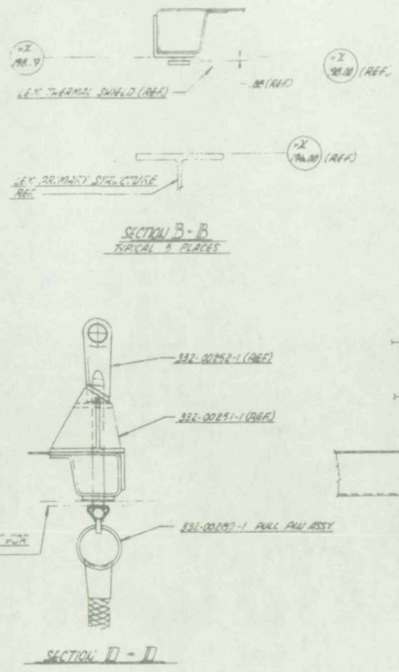

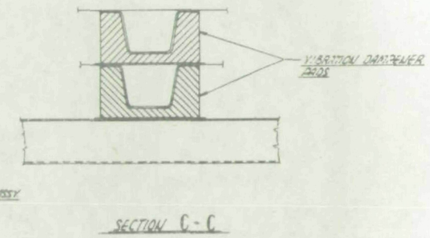

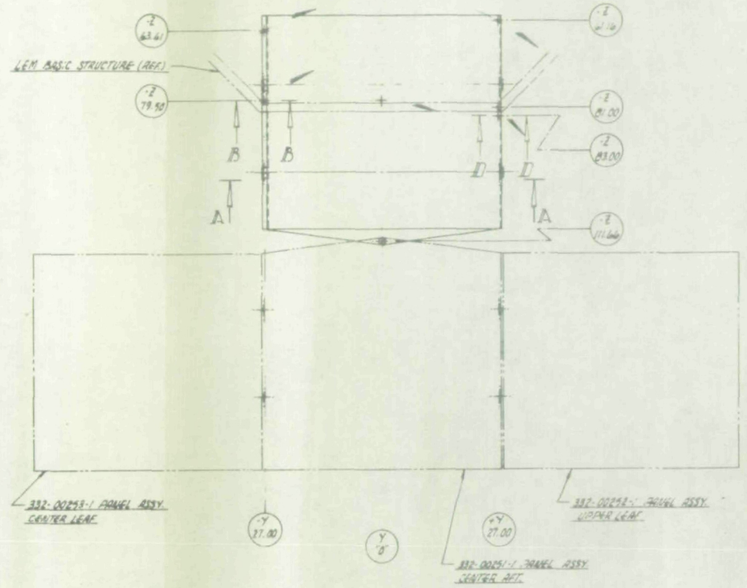

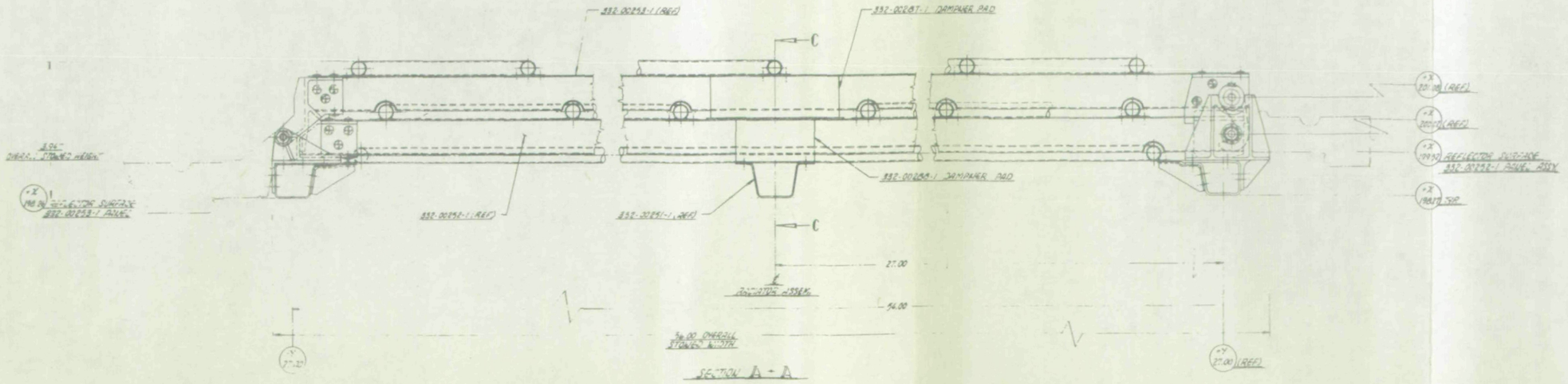

NOTES

1. 332-00251-1 & 332-00252-1 & 332-00258-1 LATCHING MECHANISMS TO BE ABLE TO FITTED AT ASSEMBLY TO ENSURE A NO TOLERANCE CONDITION IN METAL TO METAL CONTACT AT ALL PRESSURE SEALING UNDER STATIC CONDITIONS

FIGURE 10

1	332-00207-1	PULL PIN ASSY
1	332-00209-1	DAMPENER PADS
1	332-00207-1	DAMPENER PADS
1	332-00253-1	PANEL ASSY
1	332-00254-1	PANEL ASSY
1	332-00255-1	PANEL ASSY

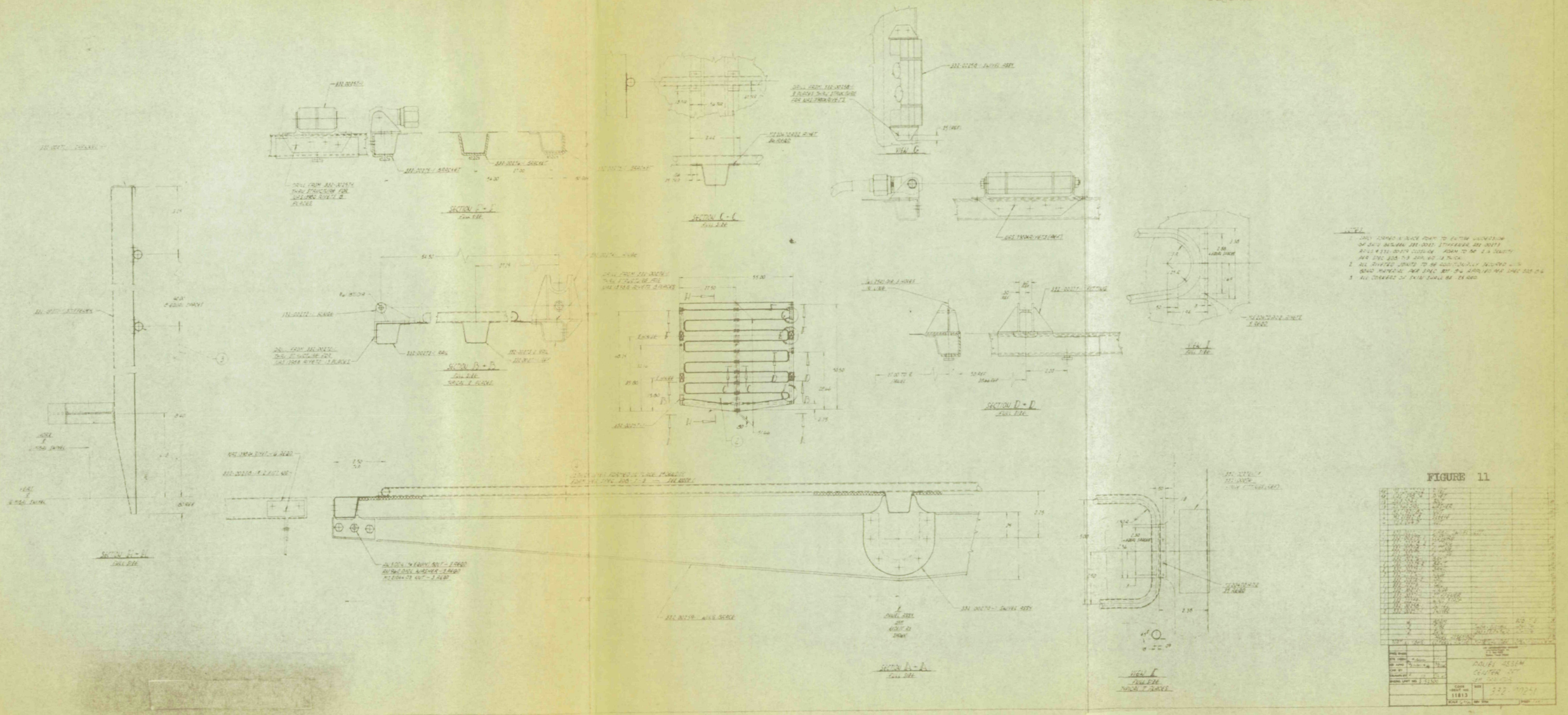

FIGURE 11

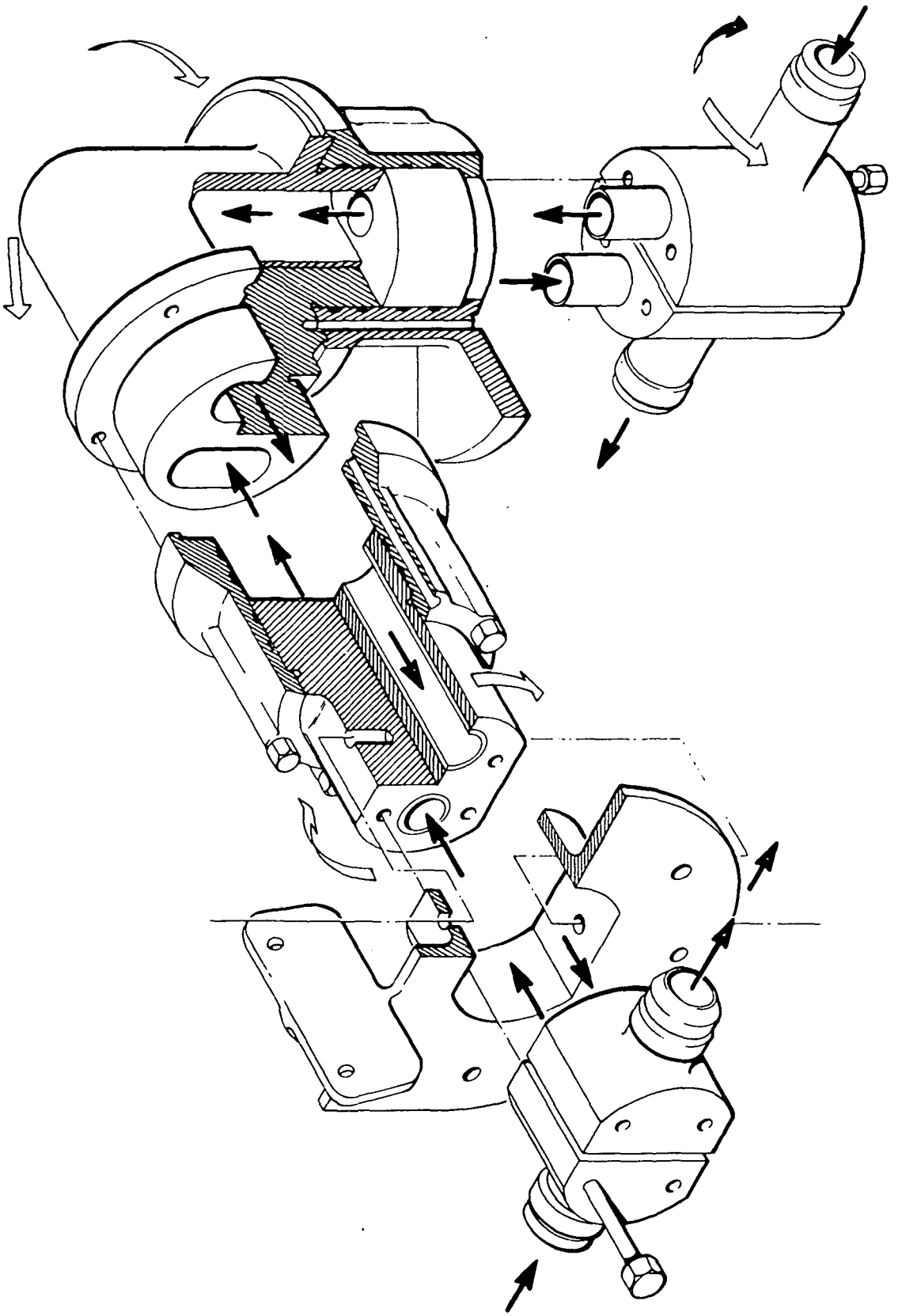

RADIATOR MAIN SWIVEL

FIGURE 12

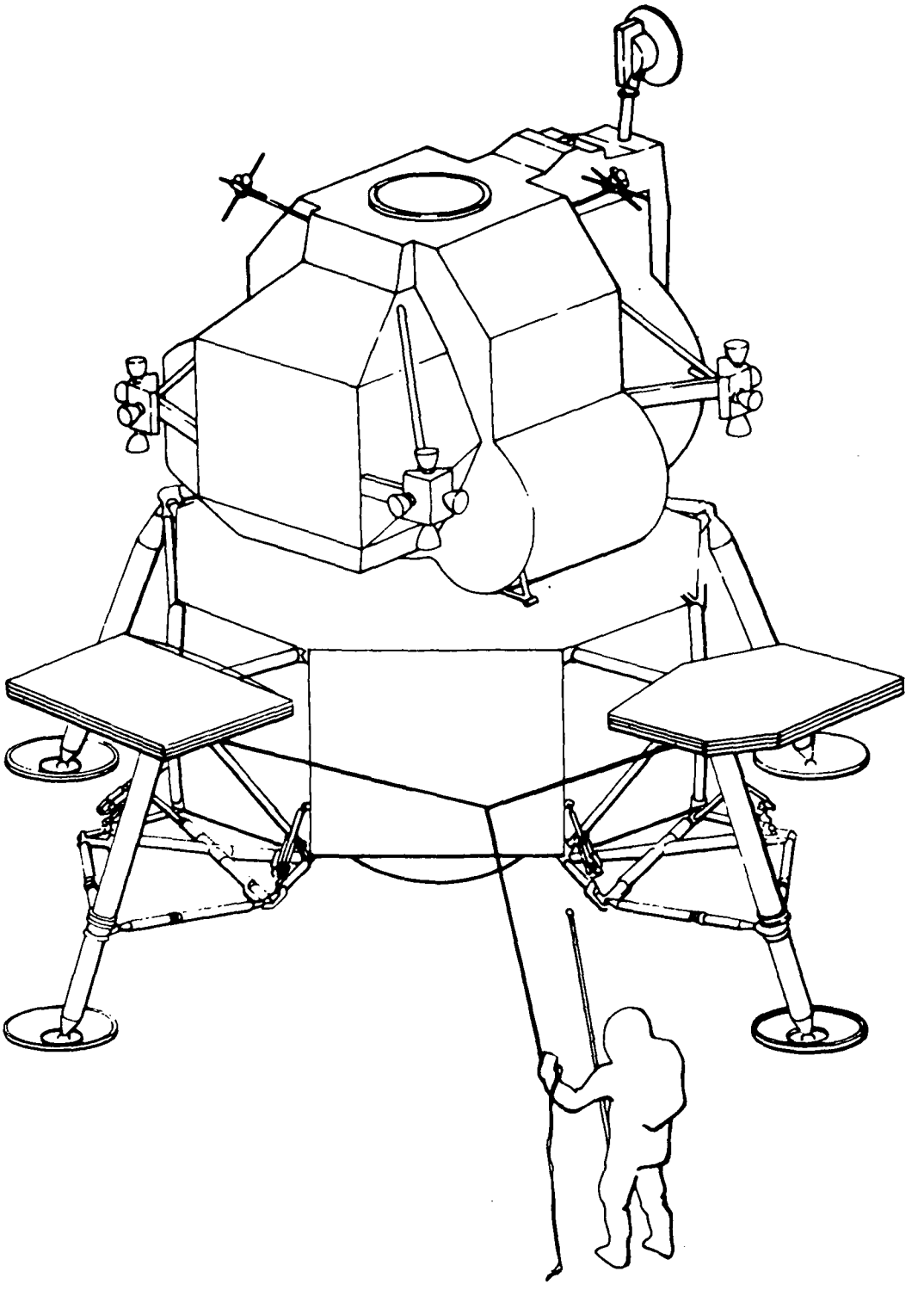

DEPLOYMENT SEQUENCE - ROTATE RADIATORS 180°

FIGURE 13

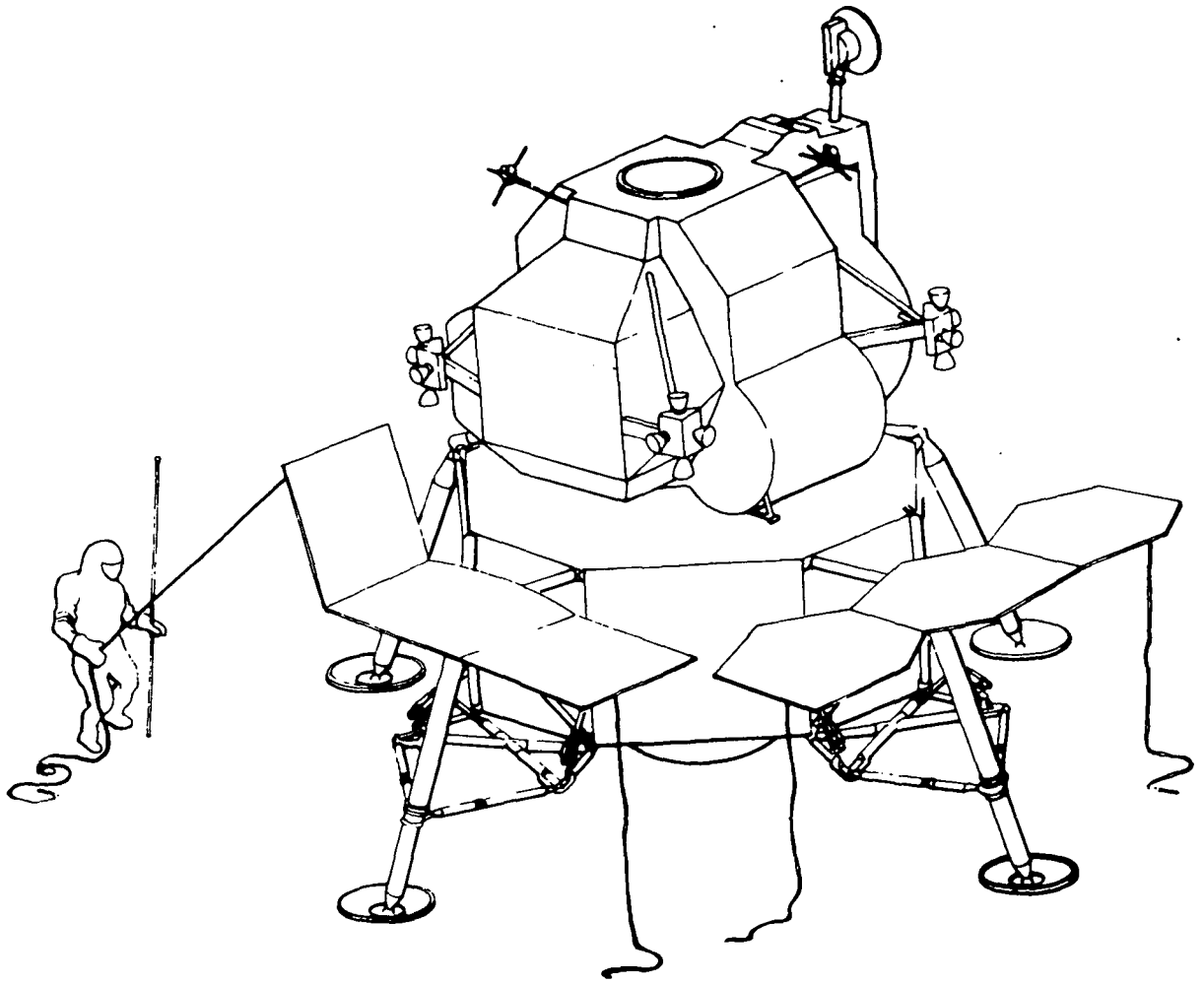

DEPLOYMENT SEQUENCE - UNFOLD WITH LANYARDS

FIGURE 14

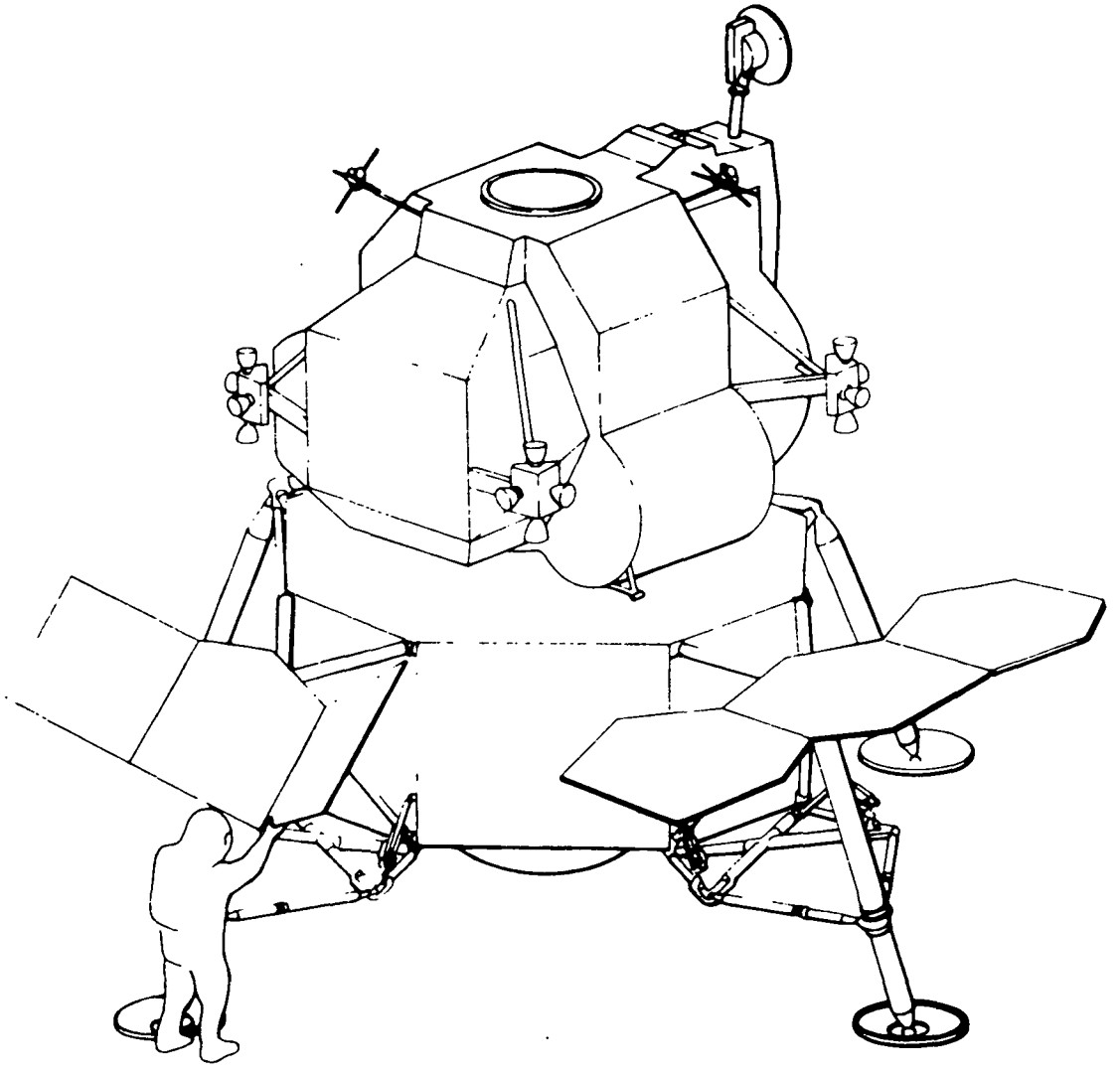

DEPLOYMENT SEQUENCE – UNFOLD WITHOUT LANYARDS

FIGURE 15

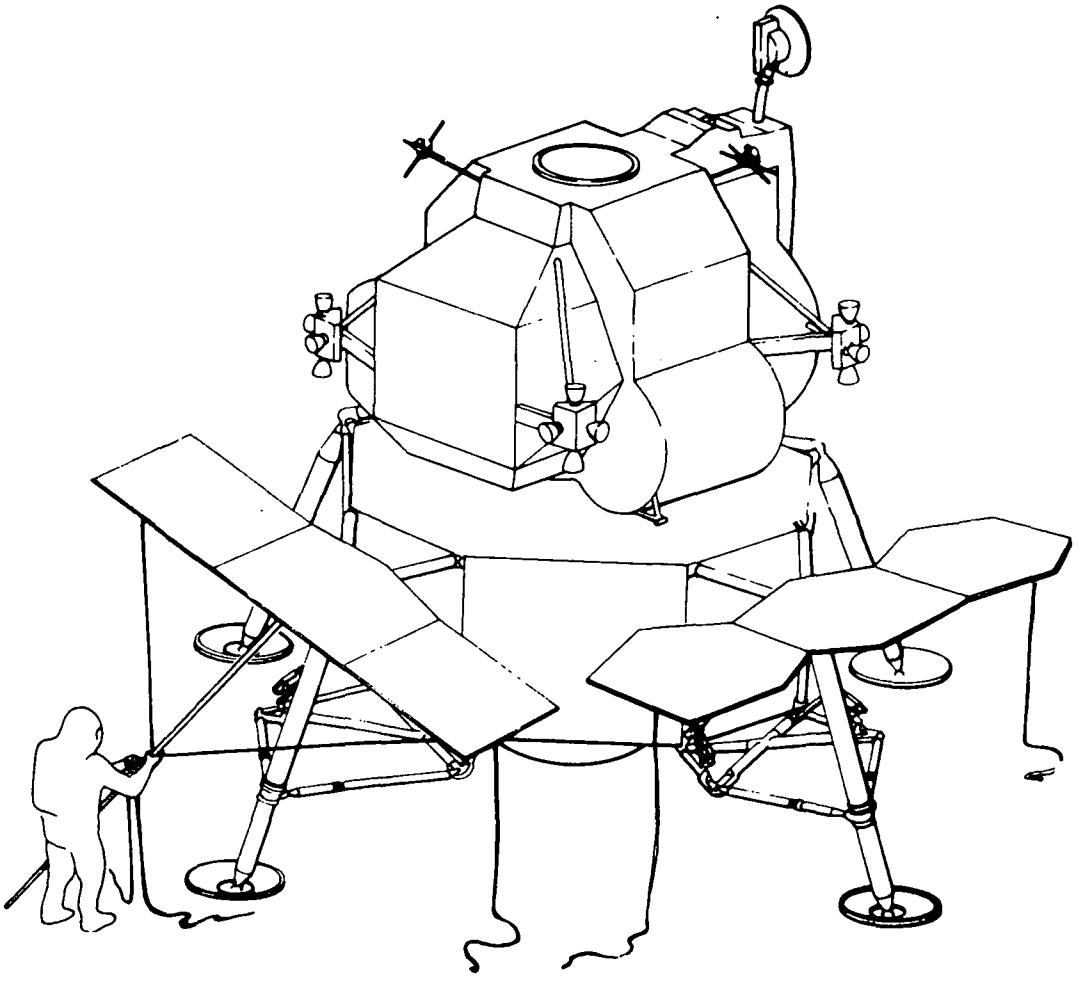

DEPLOYMENT SEQUENCE - ORIENT AFT RADIATOR TO HORIZONTAL POSITION

FIGURE 16

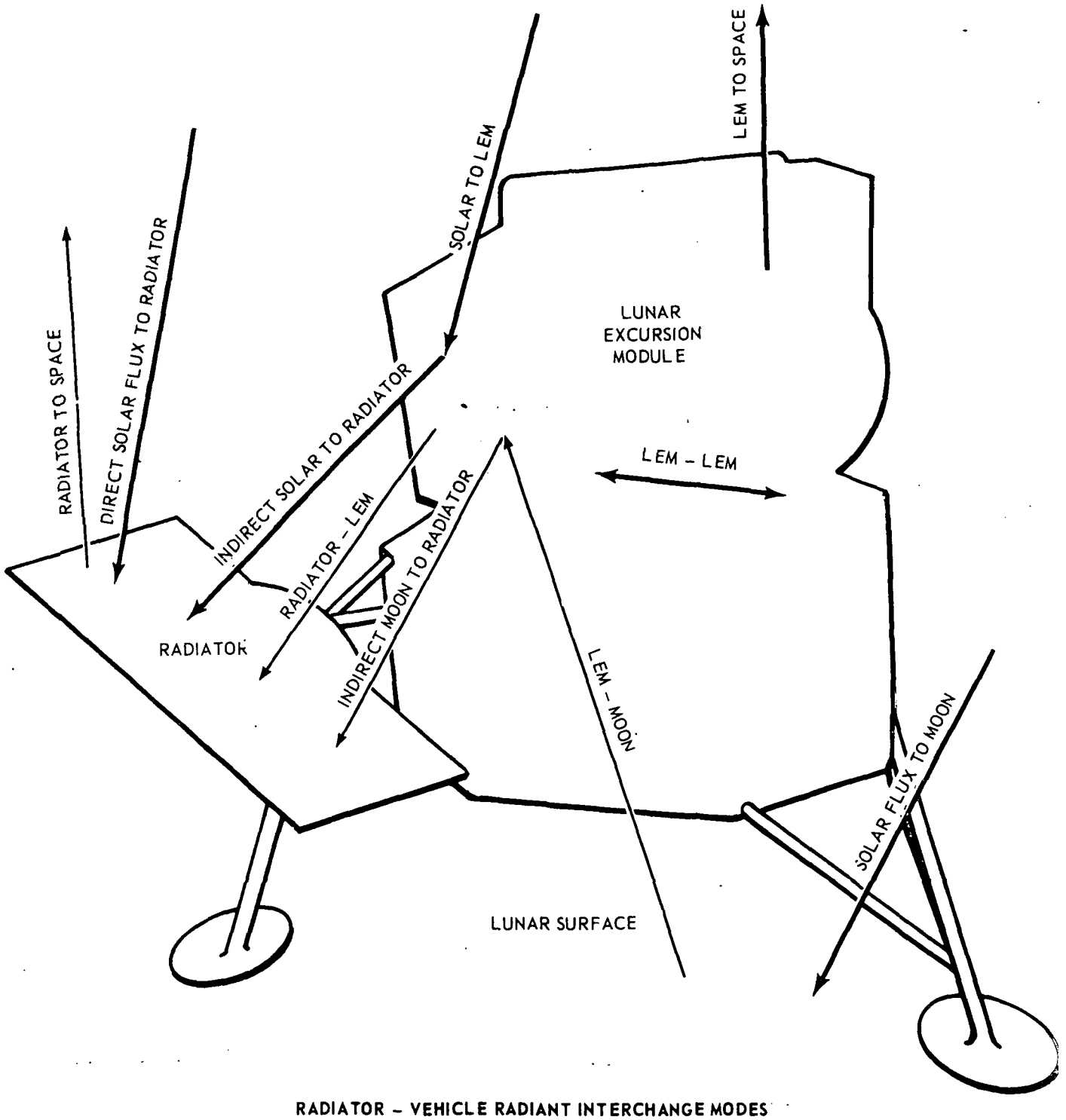

RADIATOR - VEHICLE RADIANT INTERCHANGE MODES

FIGURE 17

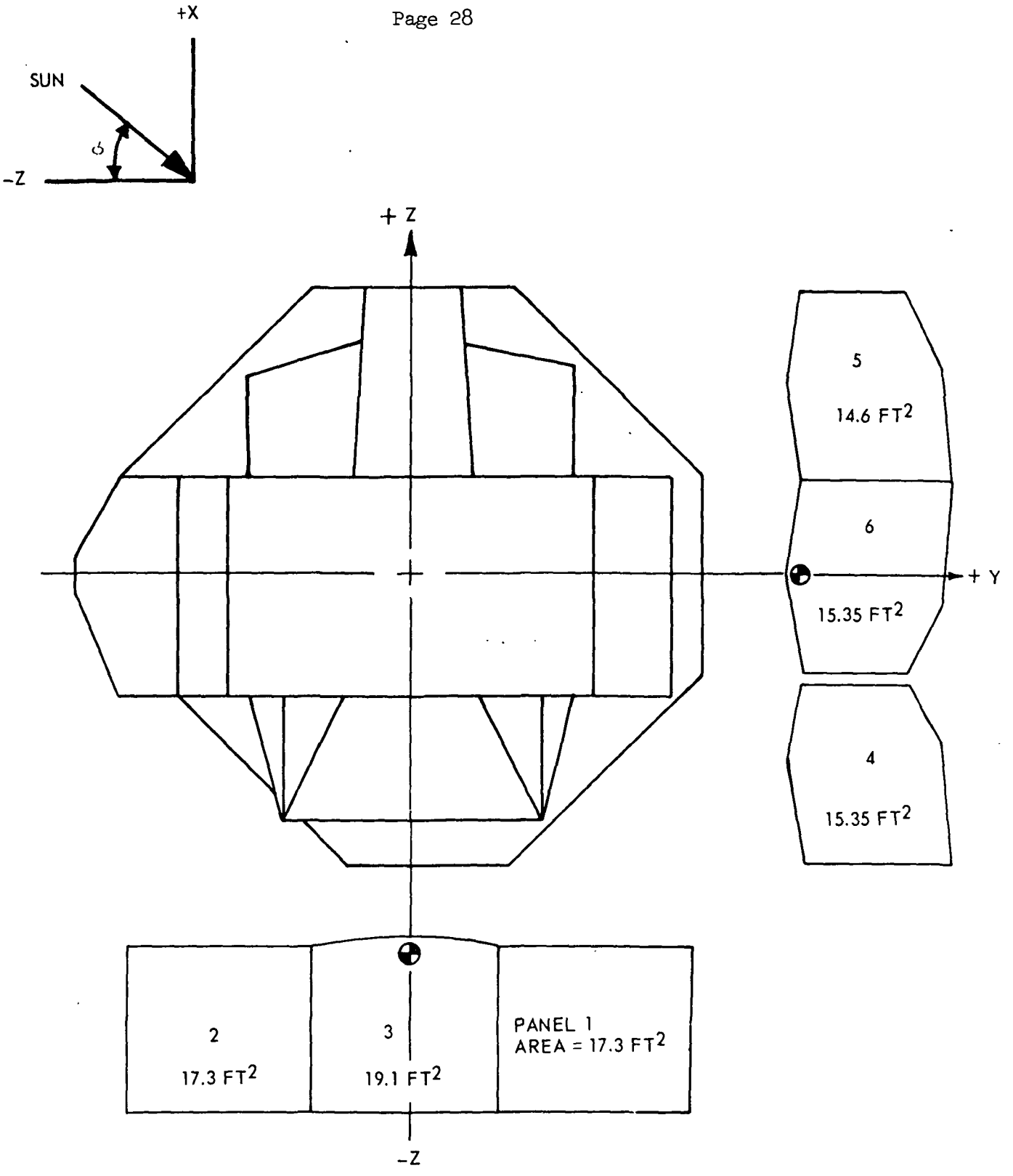

SIX PANEL CONFIGURATION USED FOR FINAL MISSION ANALYSIS

FIGURE 18

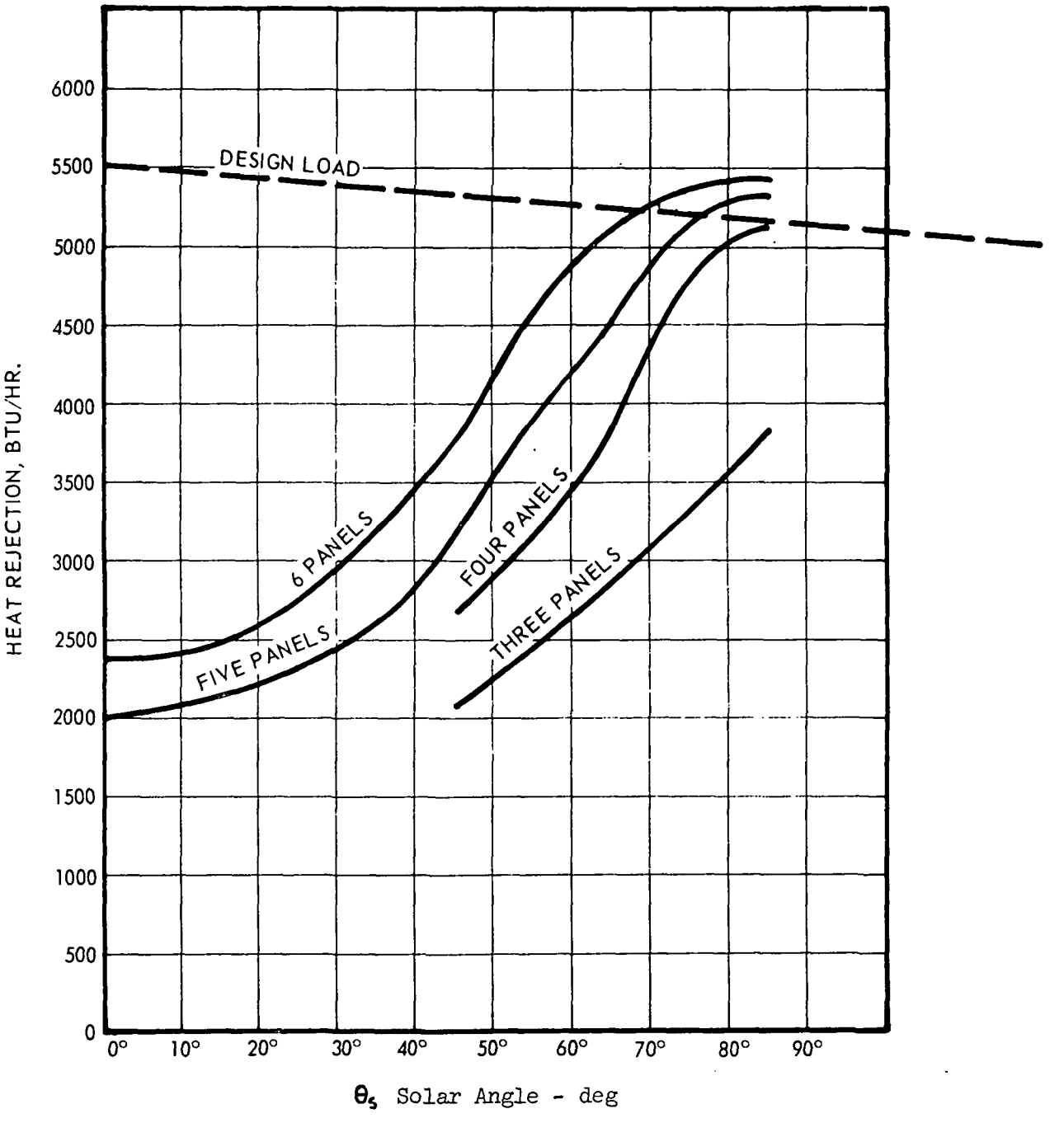

ECS RADIATOR HEAT REJECTION FOR ECS DESIGN HEAT LOAD

FIGURE 19

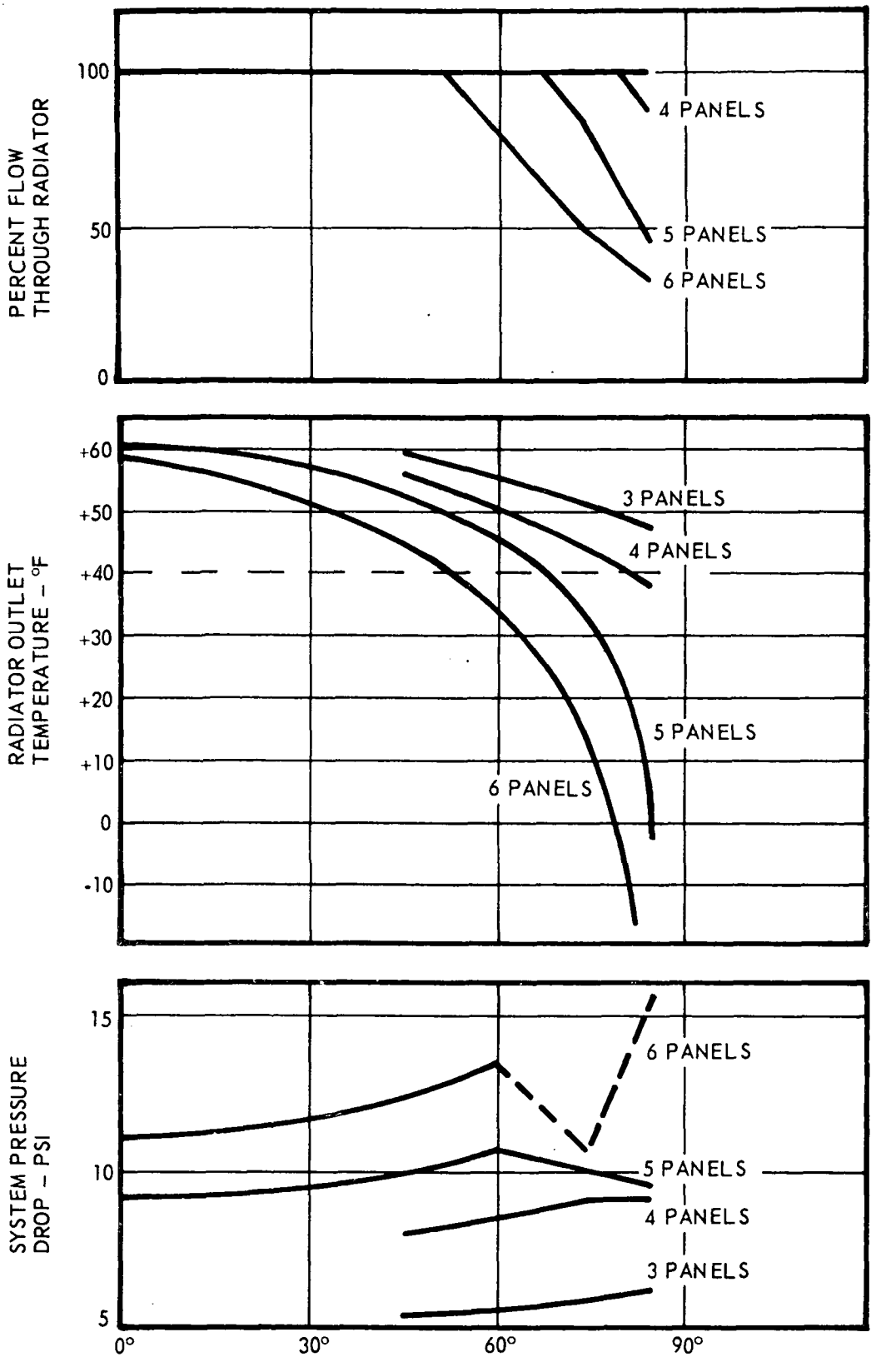

DESIGN HEAT LOAD PERFORMANCE OF FINAL RADIATOR CONFIGURATION

FIGURE 20

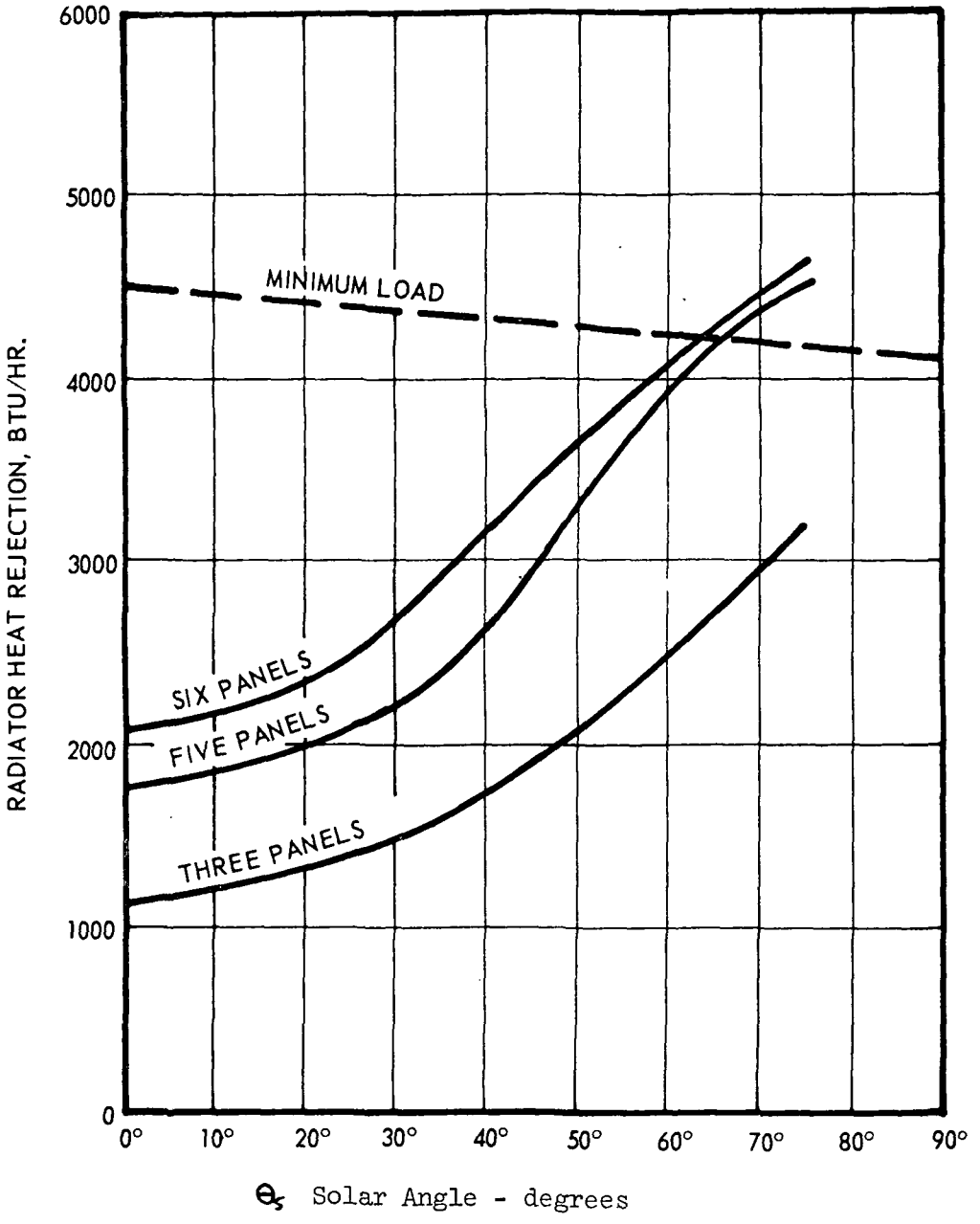

RADIATOR HEAT REJECTION FOR MINIMUM ECS HEAT LOAD

FIGURE 21

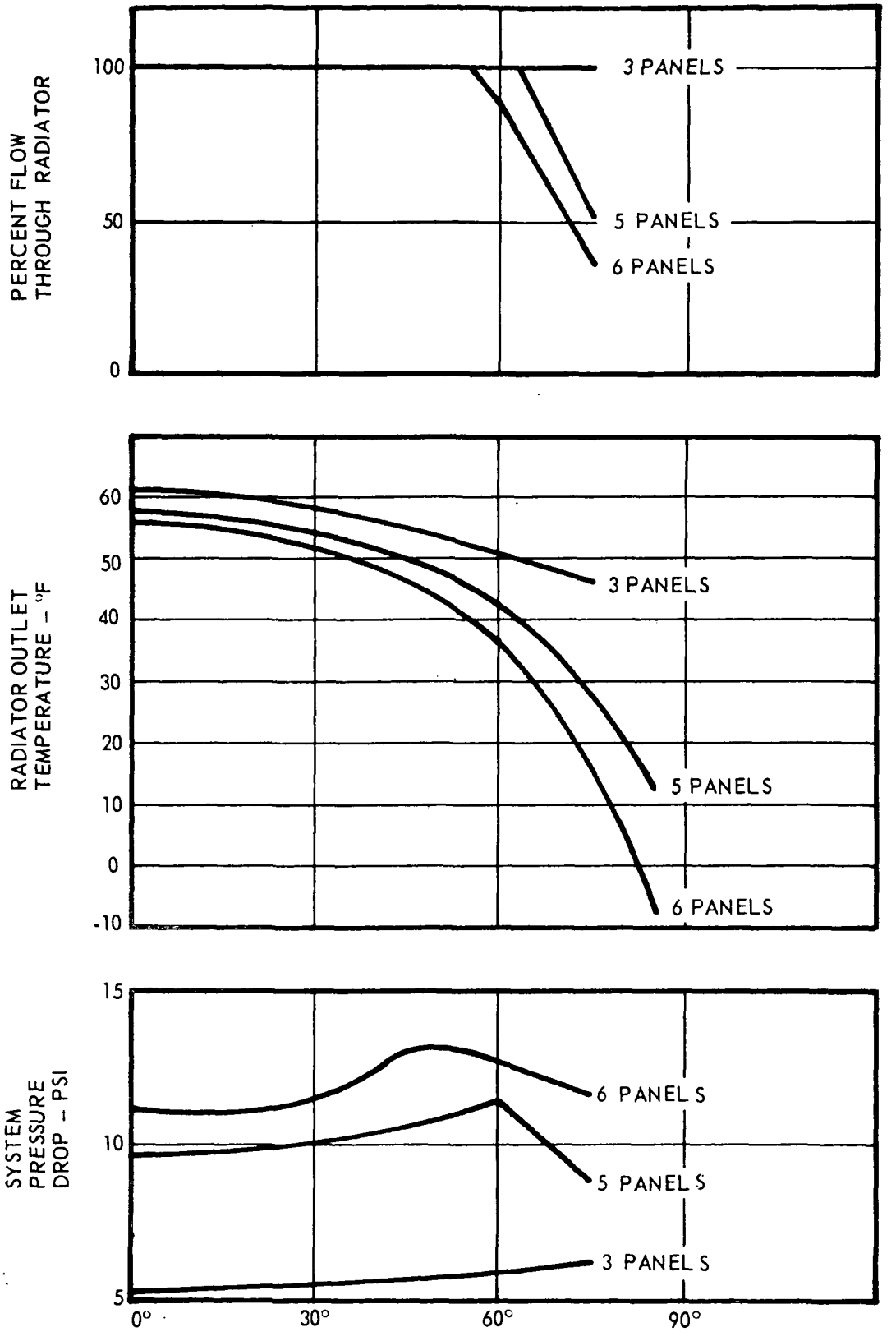

MINIMUM HEAT LOAD PERFORMANCE OF FINAL RADIATOR CONFIGURATION

FIGURE 22

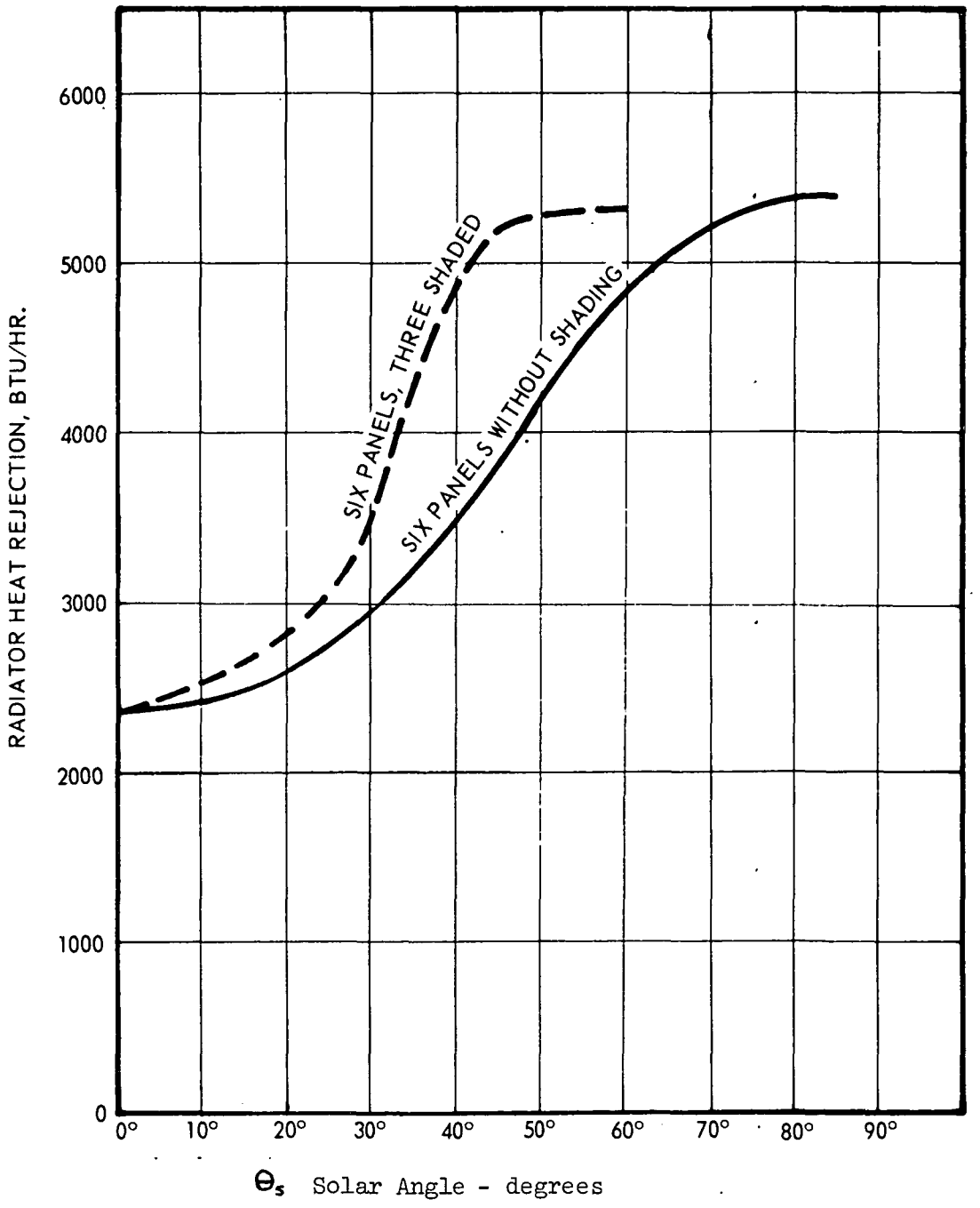

COMPARISON OF RADIATOR HEAT REJECTION WITH AND WITHOUT VEHICLE SHADING

FIGURE 23

GEOMETRICALLY SELECTIVE RADIATOR

At subsolar or near subsolar landing sites, the performance of flat radiators falls off sharply. An effective low temperature radiator operating at these landing locations would have to be capable of minimizing both solar and lunar surface thermal inputs. The following section of this report describes such a device. It is referred to as a Geometrically Selective Radiator (GSR). Figure 24 shows a cross section of a radiating element (the element extends into the plane of the paper). The two main components are the parabolic reflector, which has a perfectly specular coating on the concave surface, and the radiating element which lies on the axis of the parabola and extends from the parabola to the focus. The radiator surface has a diffuse coating with a high IR emittance on the side facing the reflector.

Principle of Operation

The performance of this device is based on the fact that radiation emanating from the focus and impinging on the parabola is reflected parallel to the axis, and that for a specular surface the angle of incidence equals the angle of reflection. Any rays entering between the parallel ray (1) and the normal to the parabola tangent (3) at the incident point must exit between the focus (2) and the normal (3). The converse is also true. Similarly, (for all but very small incident angles) rays coming from the radiator surface (6) are reflected out above the parallel ray (1). Thus, if the radiating surface is parallel to the lunar surface, all lunar radiation (which comes from below) is reflected to space without impinging on the radiating surface. Any solar input, coming from above, must hit the radiating surface. Figure 25 depicts the paths within the GSR traced by radiation from various external and internal sources. The interchanges shown in the figure are based on the assumption of the reflector being perfectly specular. The effect of the absorbed solar energy is minimized by using a low absorptance coating on the radiating surface and on the reflector.

Design

The actual radiator panel consists of pairs of these radiator and reflector elements joined back to back and stacked vertically as shown in Figure 26. The basic building module is triangular and consists of the radiating fin, heated by the glycol carrying tube, and two reflectors. The tubes of the panel are in series, with the connecting lines running up the sides of the panel and across the top to the mounting swivel. The fins are thermally isolated from

the reflectors by a superinsulation radiation barrier between the two. In addition, fiberglass stiffeners are used to join the reflectors to the fins in order to eliminate heat conduction. There is no mechanical connection between the radiation fin and its reflectors. This eliminates the conduction of heat into the fin in addition to saving some weight and simplifying the design. Fiberglass covers on the ends of the panel are used to join the modules together as well as to shield them from direct solar input (as discussed in Appendix A).

The double sided radiator panel has a number of advantages, for example:

a) Both sides of the radiator share a common fluid tube. The "wet" tubes comprise the single heaviest item in a radiator panel.

b) Structural rigidity is enhanced by adding to the width of the panel.

c) Superinsulation between the radiating surface and the reflecting surface (on the back side) is shared, minimized and protected from direct sunlight.

d) Twice the radiating surface area, for a given panel size, is available as compared to that of a single sided radiator.

The arrangement of the radiators in the glycol loop and the changes to the ECS will be similar to the arrangement and changes of the flat radiator approach. The schematic in Figure 5 is applicable to the GSR designs.

Thermal Performance

The parameters listed in Table I were used to calculate the operating characteristics of the GSR. The radiator thermal coatings are the same as those used for the flat panels.

TABLE I - GSR DESIGN PARAMETERS

Radiator Fin Area, sq. ft.	52.25
Fin Thickness, in.	0.01
Fin Width, in.	4.75

TABLE I - GSR DESIGN PARAMETERS (Cont'd)

Emittance - Radiator Fin	0.92
Absorptance - Radiator Fin	0.17
Emittance - Reflector	0.10
Absorptance - Reflector	0.30

The general performance curves (excluding vehicle interchange) are presented in Figure 27, as a function of the landing site (as measured by solar angle θ_S) and the azimuth angle γ. Appendix B presents the details of the performance analysis. With no insolation on the radiating surfaces i.e., sun on edge, the radiator performance is comparatively constant for varying lunar landing location. As the solar input increases, performance degrades so that the GSR absorbs rather than rejects heat for approximately half of the possible sunlight landing locations.

The system concept employed in this study is one where the radiator panel is always aligned with the sun vector ($\gamma = 90°$). With this constraint established, the absorptance (α_s) of the radiator surfaces has no effect on performance. However, the emittance (ϵ) and the degree of specularity of the coatings are important. These effects are shown in Figures 28, 29 and 30.

Figure 28 shows that if the radiator ϵ has a value as low as .8, net radiator heat rejection is decreased by about 13%. A realistic lower limit on ϵ is .86 and for such a coating, there is a decrease in Q_{net} of less than 7% from the ideal. Coatings having values of $\epsilon = 0.86$, and the other properties specified in Figure 28, are available. For the reflector, Figure 29 indicates that for ϵ varying from 0.03 to 0.1, performance is off a maximum of 7%. With regard to the reflector specularity, Figure 30 indicates that for 95% specularity the performance penalty is minimal. All of the values discussed are obtainable with standard vapor deposited aluminum coatings.

The aforementioned curves apply for a 65°F radiating temperature. The impact of other temperatures is depicted in Figure 31 and is mainly due to the fourth power variation characteristic of radiant heat transfer. Obviously, a temperature gradient from the fin root to fin tip exists. The radiator fin temperature described in the general performance curves is based on a constant temperature.

Incorporation of the classical definition of fin effectiveness,

$$\eta_{fin} = \frac{\text{Net Heat Rejected}}{\text{Net Heat Rejected if Radiator were at Fluid Temp.}}$$

allows conversion of constant temperature general performance data into specific radiator performance which is a function of materials, geometry and fluid flow characteristics.

Fin effectiveness analyses which were developed for flat radiators were applied to the GSR as an expedient. Derivation of an analytical technique, especially tailored to GSR designs, was begun but the analyses were not finished at the program's completion. However, sufficient results were obtained to substantiate that the flat radiator fin effectiveness technique is a good approximation, and that the performance results presented are accurate.

LEM System Application

The basic geometry of GSRs result in the ability to eliminate lunar thermal and solar albedo radiation as a direct heat input to a vertical radiator panel. A vertical panel can be oriented so that the sun vector is in the plane of the radiator while the radiation "shelves" are parallel to the lunar surface. This orientation eliminates the solar input to the radiator. The LEM thermal design mission dictates a landing within 5° of the lunar equator. Thus, once the panel is oriented parallel to the equatorial plane, the largest possible misalignment of azimuth angle as a result of sun translation is 5° for a full lunar cycle. For the period of design lunar stay, the maximum misalignment that can occur due to sun translation is approximately 1/2°. Figure 27 shows that a 5° misalignment has scant affect on heat rejection, therefore, a 1/2° effect is insignificant. This is particularly attractive for longer missions because once the radiator is aligned no further adjustment is required.

With this goal in mind, the deployment mechanism depicted in Figure 26 was evolved. The radiator panel is hung from the boom using a ball swivel located on the vertical axis passing through its center of gravity. After the astronaut exits from the LEM, he unlatches the panel from its stowed position on the side of the descent stage (Figure 32) and swings it away from the stage (Figure 33). When the boom is in its proper position, the panel is released so that it hangs vertically (Figure 34). The panel is then positioned so that the sun shines on its edge, completely or almost completely shadowing the radiator from insolation.

The deployment procedure is then repeated for the other radiator panel. Total deployment time is between 15 and 30 minutes.

For each landing orientation, there are a number of boom positions that could satisfy the sun on edge constraint. However, for any position of the boom and panel, there is some radiant interchange between the vehicle and the radiating fins. The numerical results for worst case vehicle heat inputs to the radiators are summarized in Table II.

TABLE II LEM HEAT INPUT TO GSR

Solar Angle Degrees	Heat Input Btu/hr-ft^2
0	35.6
45	30.6
75	20.2

Performance of the glycol loop with space radiators was obtained from a steady state cycle analysis of the simplified ECS (Figure 4). The heat load profile of Figure 3 provides the basic input to the porous plate water boiler whose performance is defined in Figure 35. Radiator performance is incorporated in the loop by using a digital computer routine specifically developed to represent GSR heat rejection. This program requires, as input data, the average radiator temperature. Since this temperature is unknown, an iterative procedure is employed in order to obtain the value. The fin effectiveness is used to relate fluid temperatures to average radiator temperature. Heat rejection is then obtained by known relationships involving fin geometry, materials, fluid flow rates and fin effectiveness. The specific analysis was developed for a flat radiator fin effectiveness technique. However, the results were verified for the GSR configuration. The performance analysis determines the total heat received and absorbed by the radiator from the reflector; to this is added the vehicle heat input. It also determines the total heat absorbed by the reflector and space from the radiator. The difference represents the net heat rejected by the GSR. This value is used in the cycle calculation of the heat balance to determine specific radiator performance.

The cycle calculation was performed for each phase of the active radiator life for solar angles of 0° (subsolar), 45° and 75°. Near terminator landing locations were not investigated because of the relative inefficiency of the GSR under those conditions. The results of the analyses are presented in three tables. Table III summarizes the cycle calculations for the boom mounted deployable radiator with vehicle heat inputs. Table IV deals with the same radiator except that vehicle inputs are assumed to be zero. Table V shows what could be accomplished by using a larger radiator panel without vehicle inputs, (in this case a 61.7 ft^2 radiator).

The amount of cooling water required by the water boiler was determined for each phase of radiator operation. Water requirements are reduced by an amount equivalent to the heat rejected by the space radiator. The water use rate without a radiator in the system is readily determined from the heat load. The difference in use rates, with appropriate consideration of phase times results in the water weight savings. Figures 36, 37 and 38 show water consumption rates as a function of mission time for the radiator active life. Also shown for comparison is the use rate for the system without radiators. Figure 36 shows that for the swing out boom design at a subsolar landing, approximately 93 pounds of water are saved. If the input due to vehicle radiant interchange could be eliminated, almost 137 pounds of water could be saved (Figure 37). This represents more than 90% of the total water boiler supply during the proposed active life of the radiator system. The elimination of vehicle input could be accomplished in a number of ways:

1. Mounting a single sided panel flush against the descent stage.

2. Deploying the radiator above the ascent stage.

3. Carrying the panels a sufficient distance (approximately 15 feet) away from the vehicle (Figure 39).

Figure 38 shows the water use rate for a 61.2 ft^2 carry off design which accommodates essentially all of the lunar stay heat load.

Table VI summarizes the GSR water weight savings for the radiators discussed both with and without vehicle input.

Because of the slight performance variation with landing location, the GSR bypass control does not divert any significant amount of fluid. Consequently, glycol temperatures through the radiator do not drop significantly below 30°F and no freezing or near freezing conditions exist. As a result, no reorientation of radiators is required to prevent flow stagnation.

PRINCIPLE OF OPERATION

Radiation Emanating From The Focus and Impinging On The Parabola Is Reflected Parallel To The Axis.

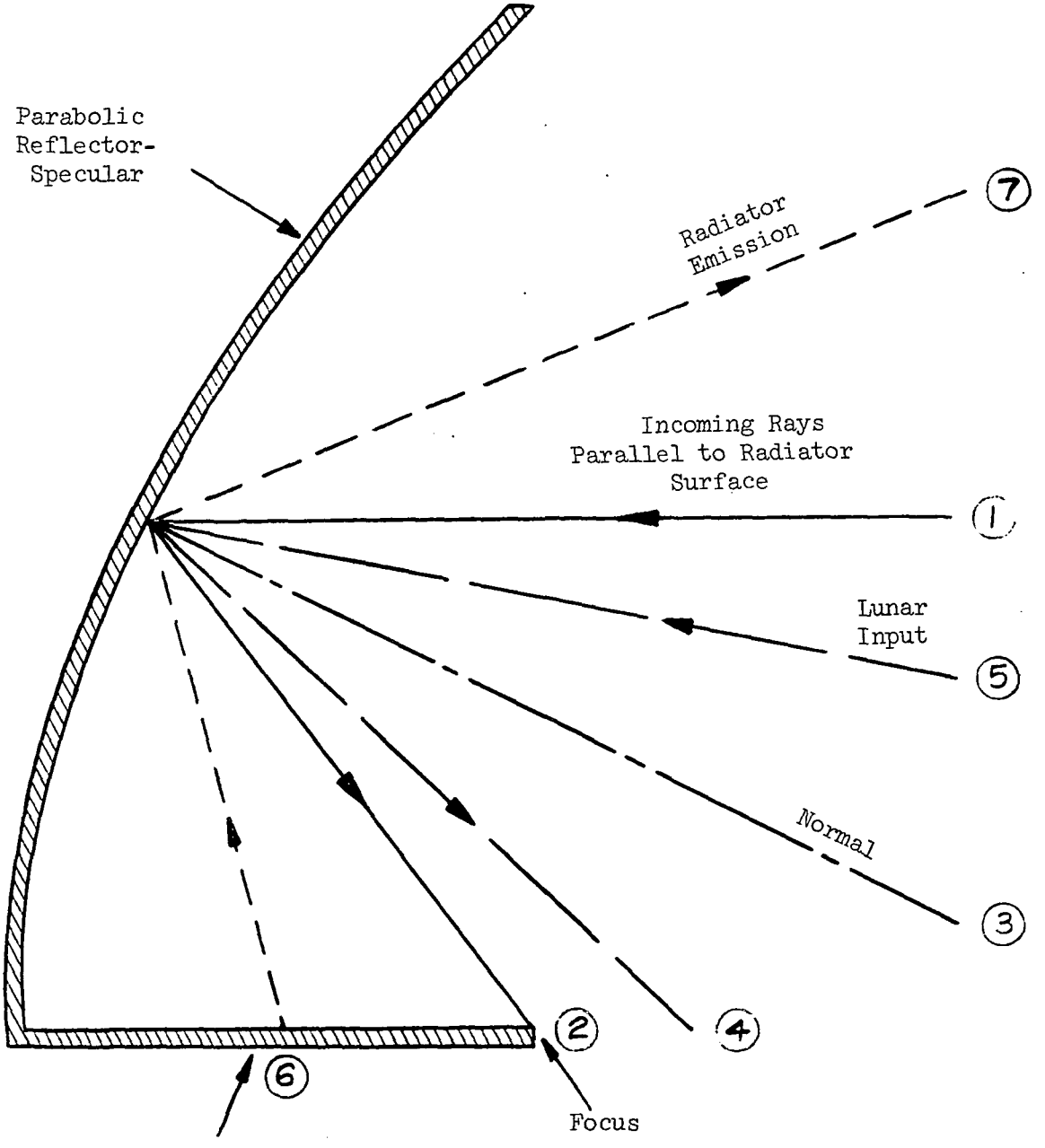

FIGURE 24

FIGURE 25

ENERGY INTERCHANGES WITHIN THE GSR

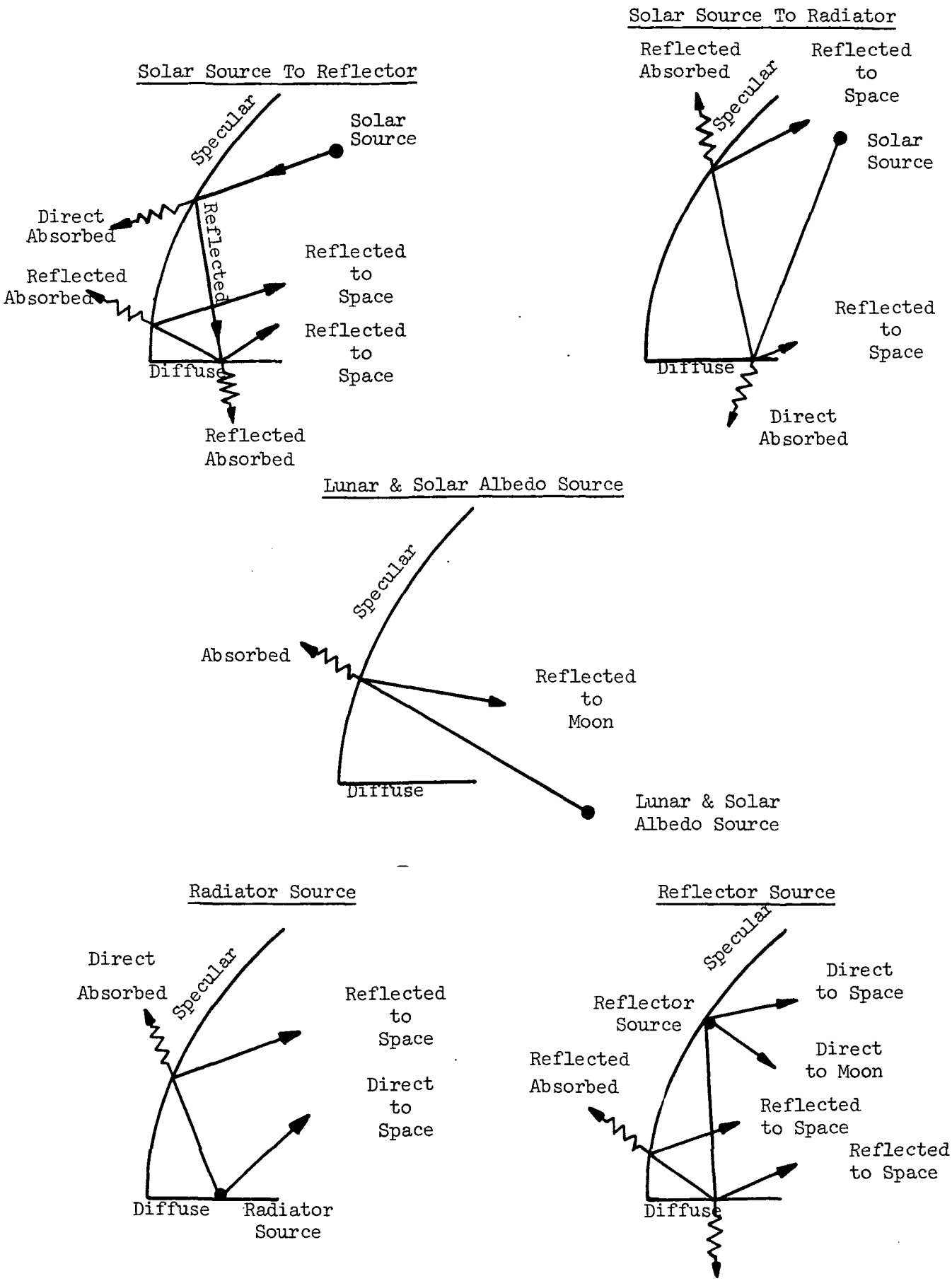

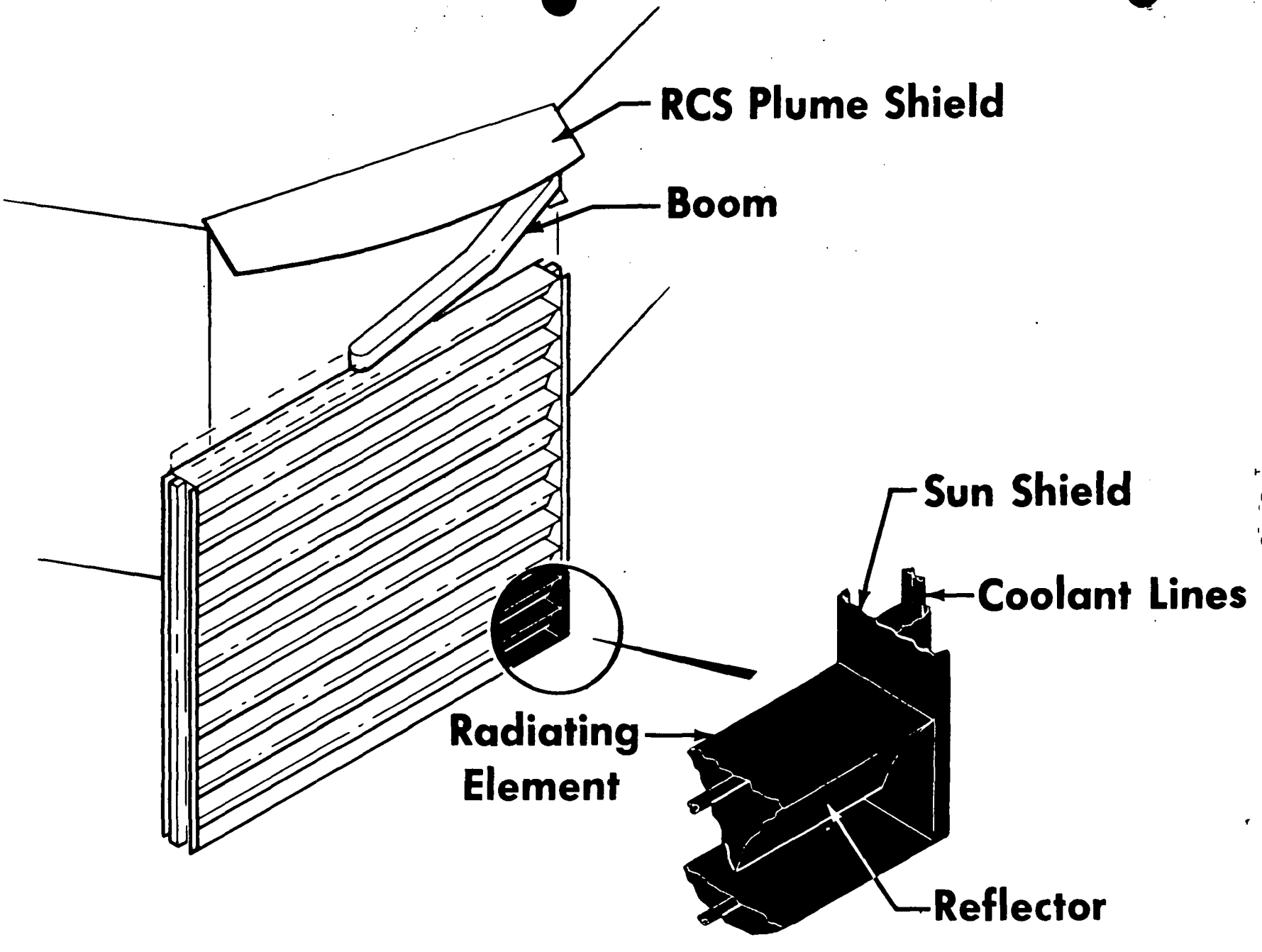

FIGURE 26 - GSR DEPLOYABLE RADIATOR

FIGURE 27

HEAT REJECTION OF GSR AS A FUNCTION OF SOLAR ANGLE AND AZIMUTH ANGLE

$\alpha_{s\,Ref.} = .3$
$\epsilon_{Ref.} = .1$
$\alpha_{s\,Rad.} = .17$
$\epsilon_{Rad.} = .92$
$T_{Rad.} = 65°F$

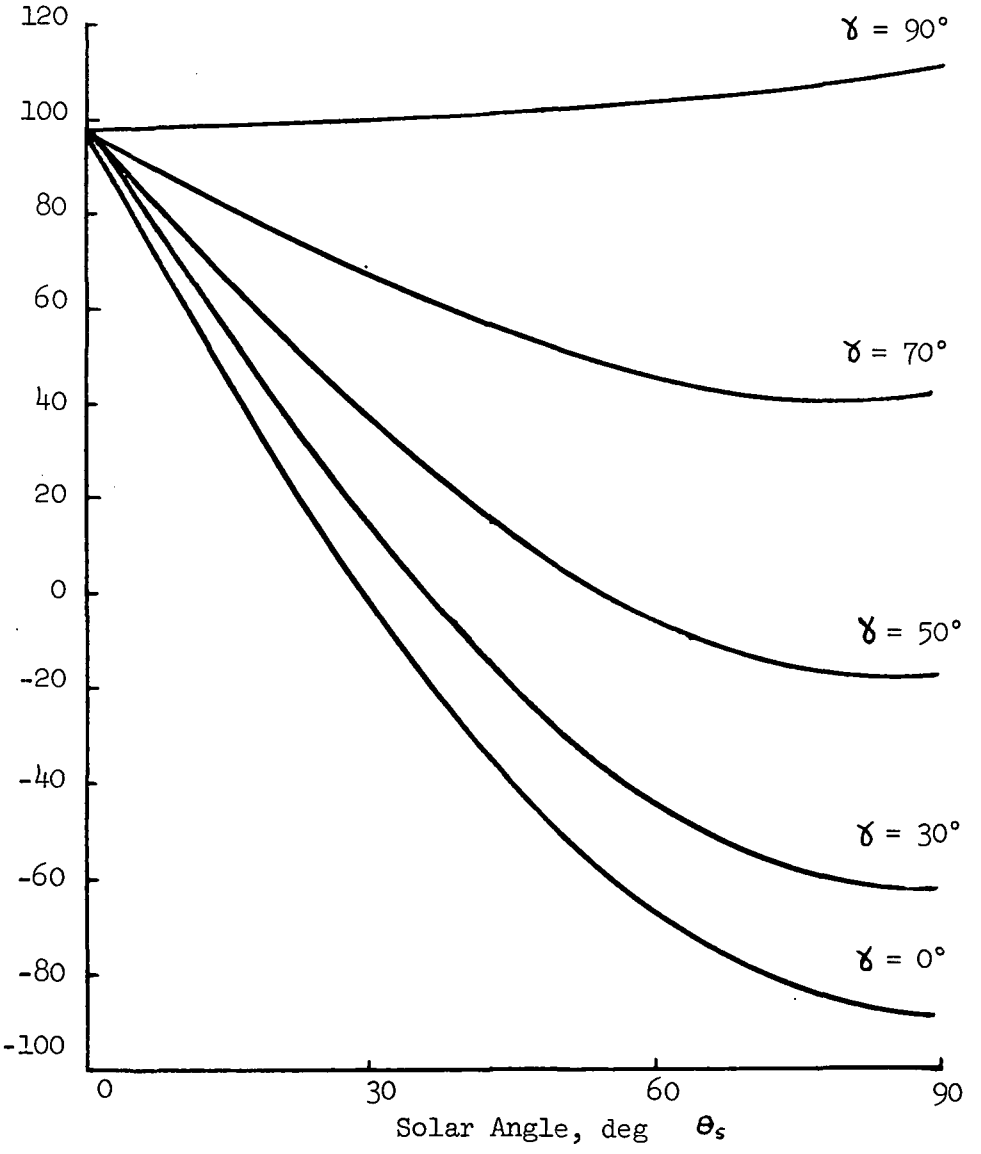

FIGURE 28

EFFECTS OF RADIATOR PROPERTIES

ON GSR PERFORMANCE

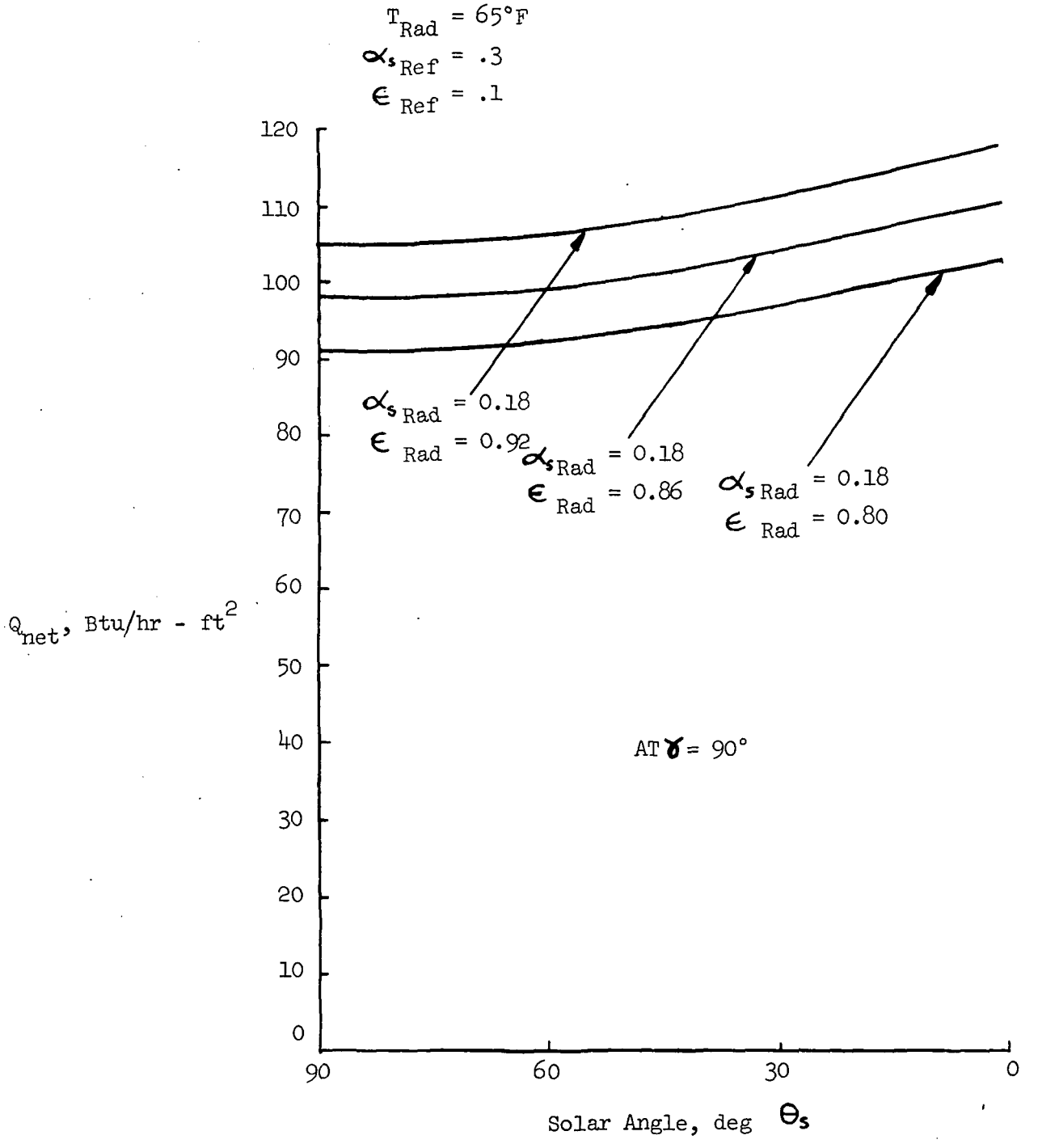

FIGURE 29

EFFECTS OF REFLECTOR PROPERTIES

ON GSR PERFORMANCE

$T_{Rad} = 65°F$

$\alpha_{Rad} = .17$

$\epsilon_{Rad} = .92$

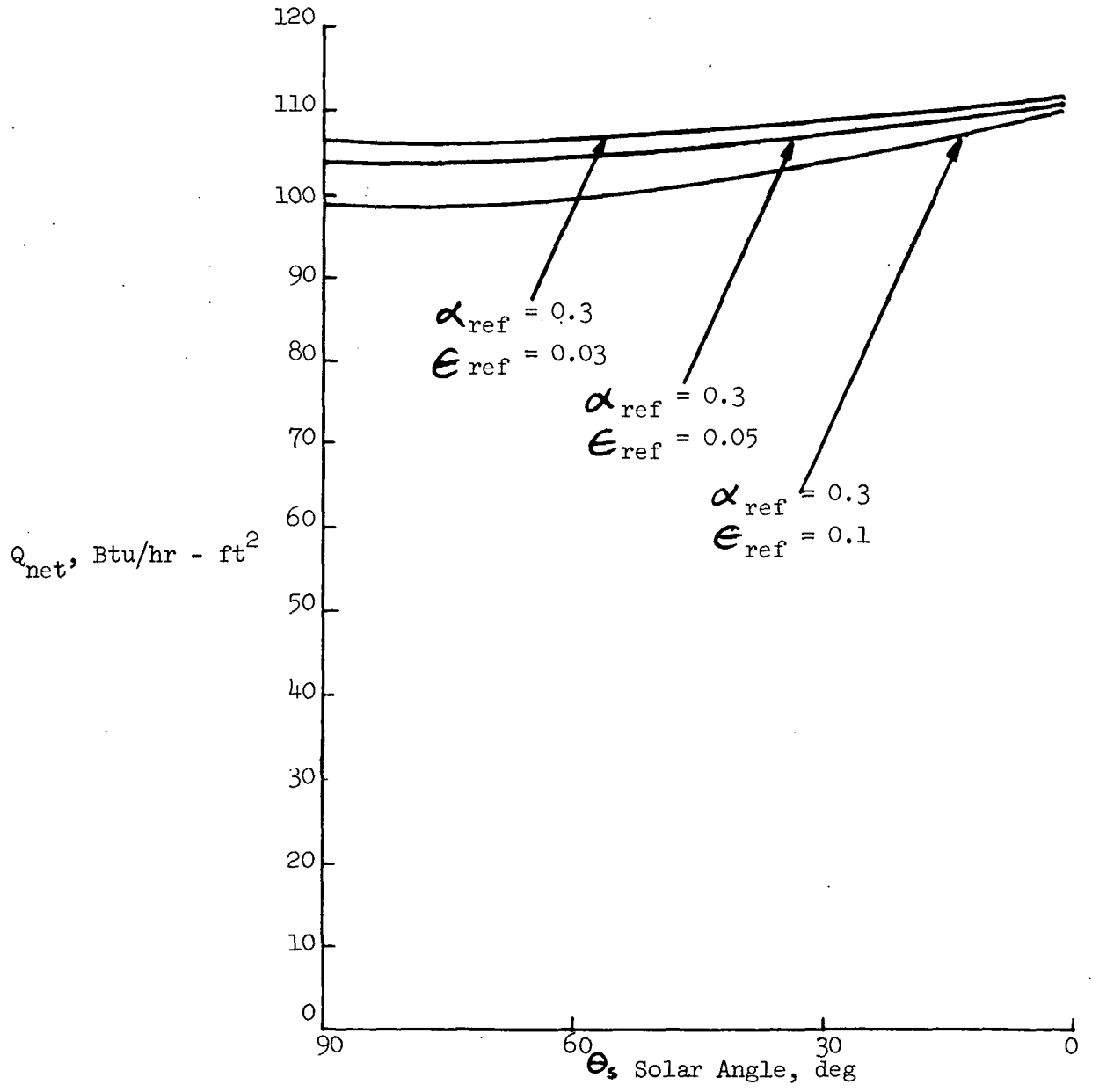

FIGURE 30

EFFECTS OF REFLECTOR NON-SPECULARITY ON GSR PERFORMANCE (WITHOUT VEHICLE INPUT)

$T = 65°F$ $\gamma = 90°$ (Sun on Edge)

$\epsilon^{rad} = 0.86$ $\epsilon^{ref} = 0.1$

$\alpha_{s\,rad} = 0.18$ $\alpha_{s\,ref} = 0.3$

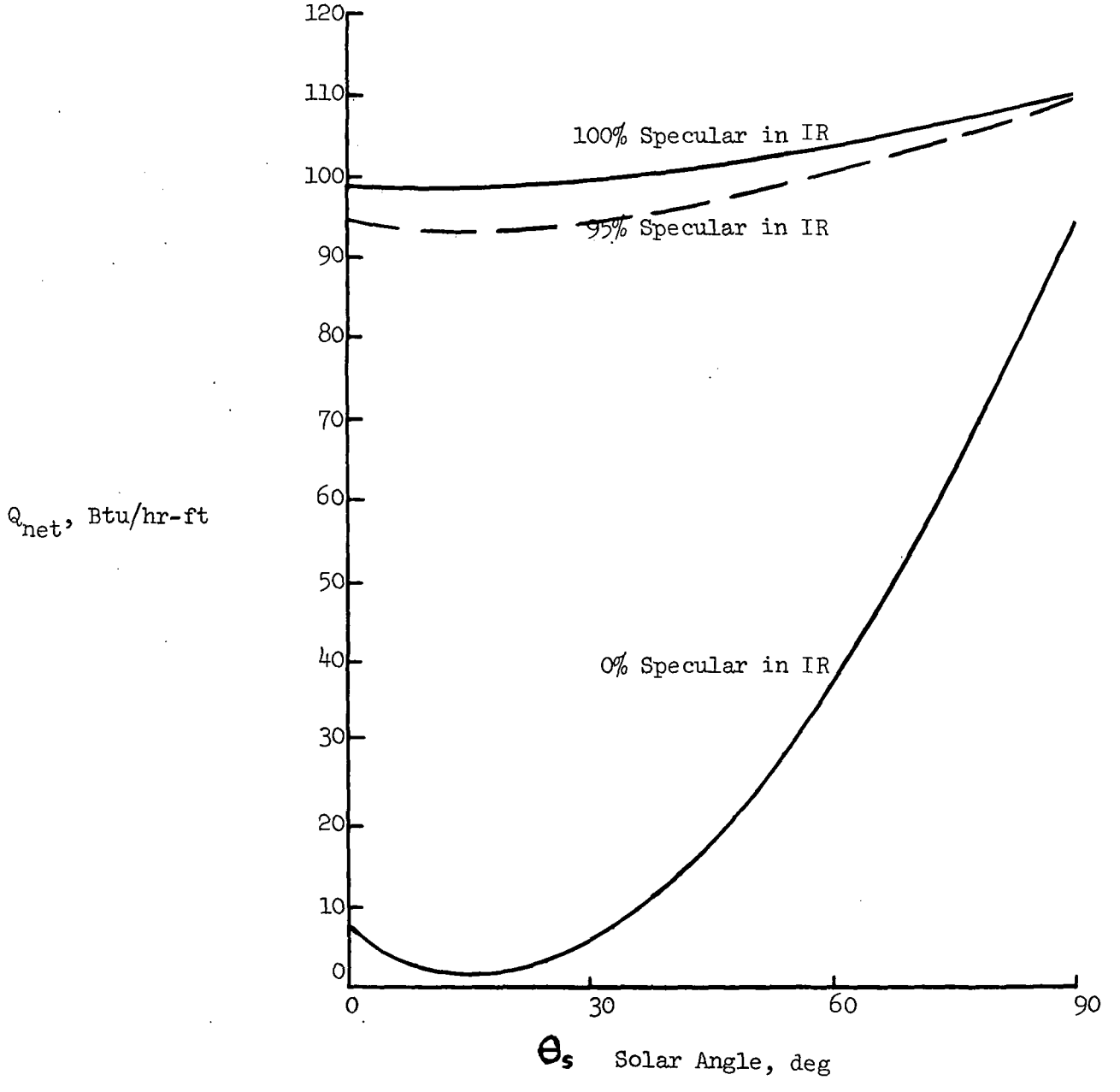

FIGURE 31

EFFECTS OF RADIATOR TEMPERATURE

ON GSR PERFORMANCE

(WITHOUT VEHICLE INPUT)

$\gamma = 90°$

ϵ Ref. = .1

α_s Ref. = .3

α_s Rad. = .17

ϵ Rad. = .92

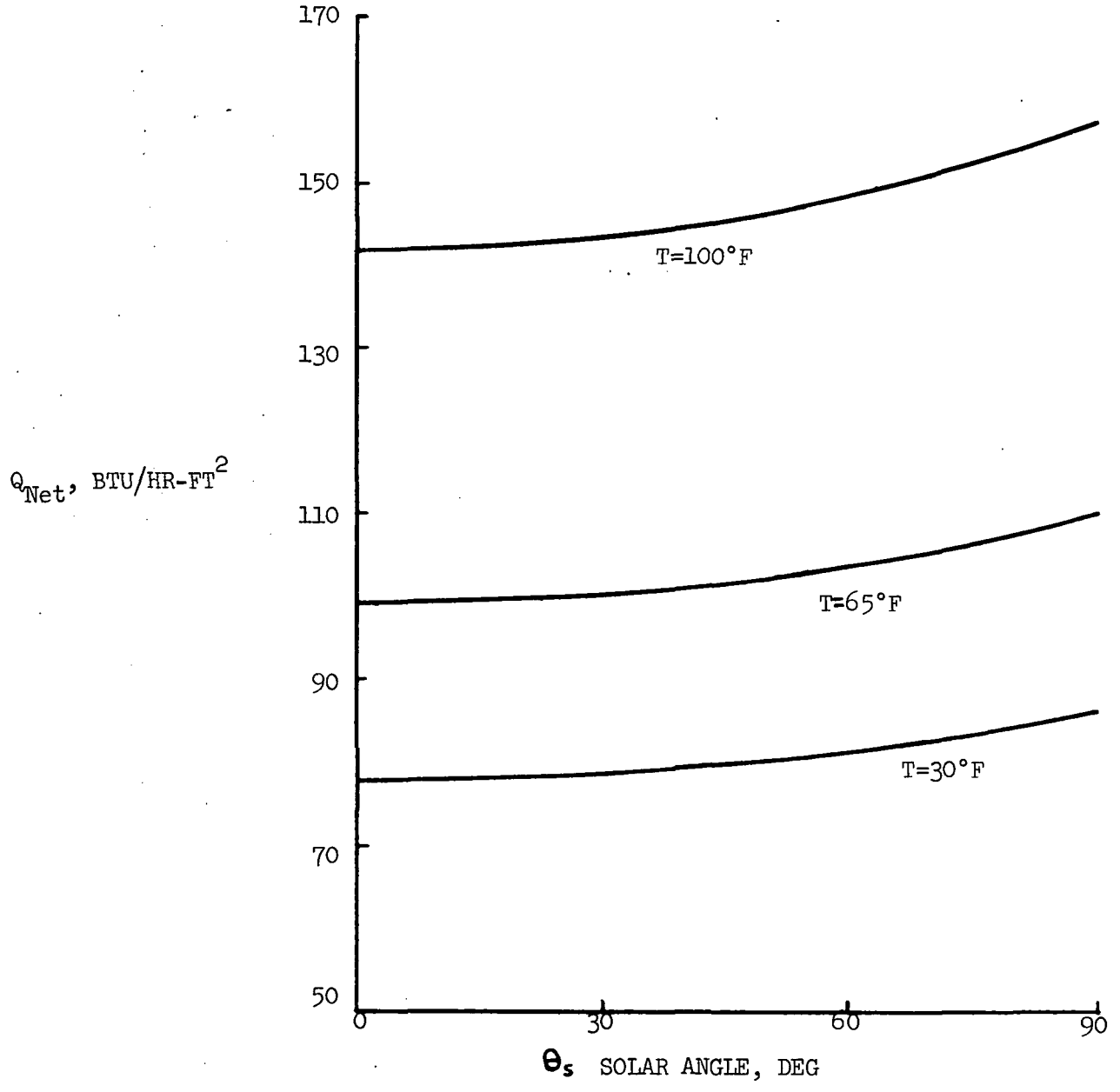

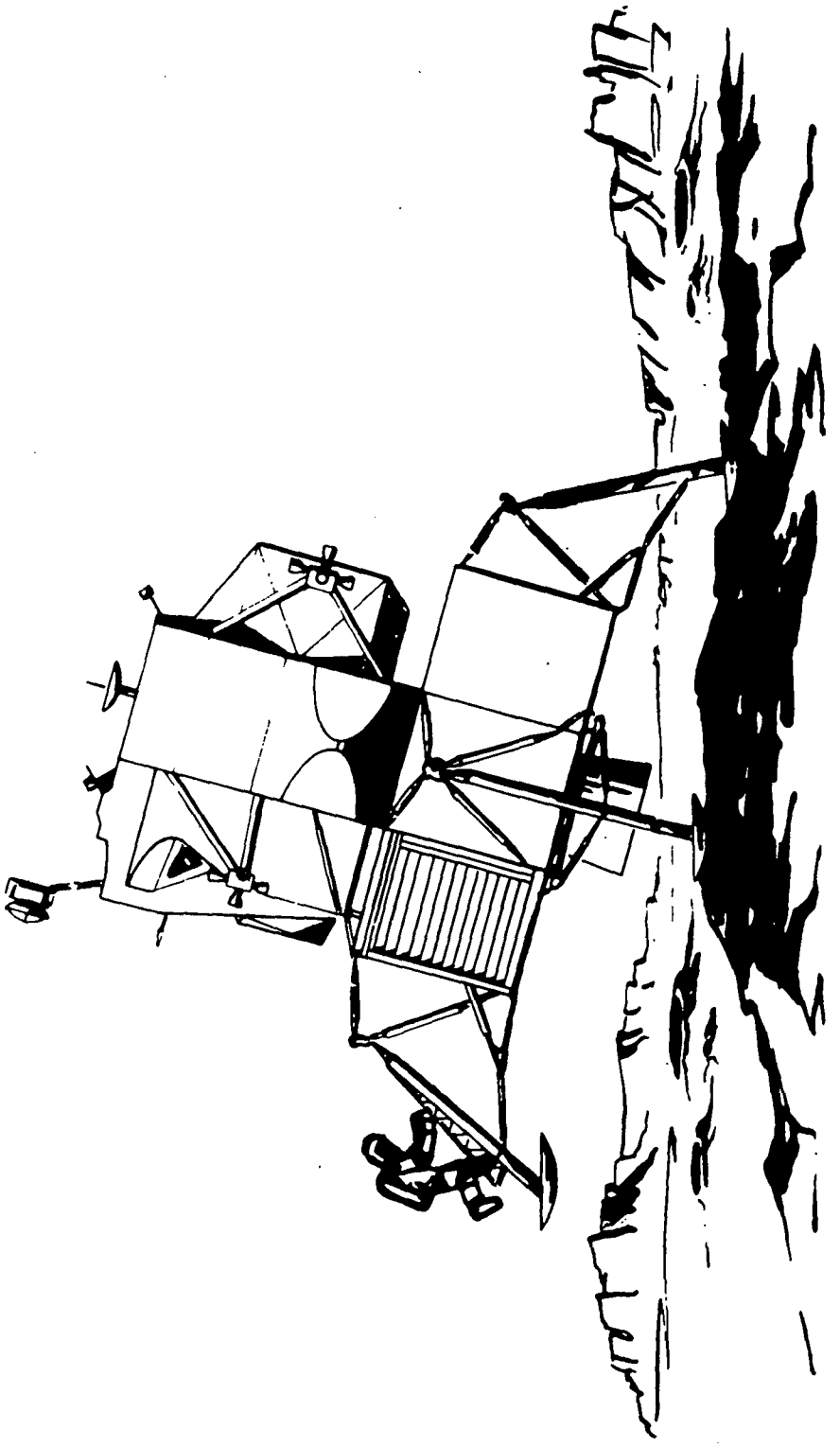

GSR DEPLOYMENT - STOWED RADIATOR

FIGURE 32

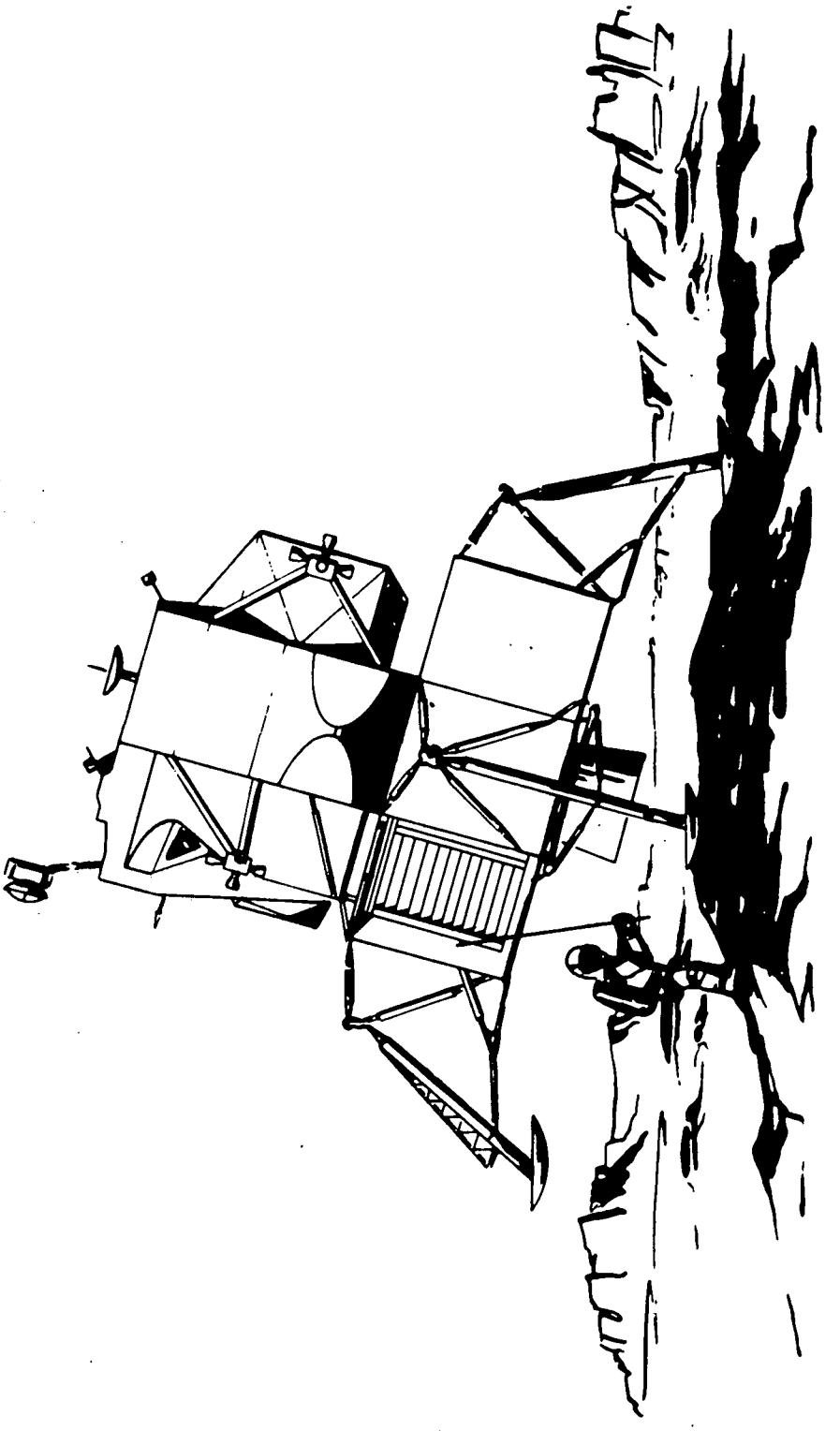

GSR DEPLOYMENT - SWINGING PANEL OUT

FIGURE 33

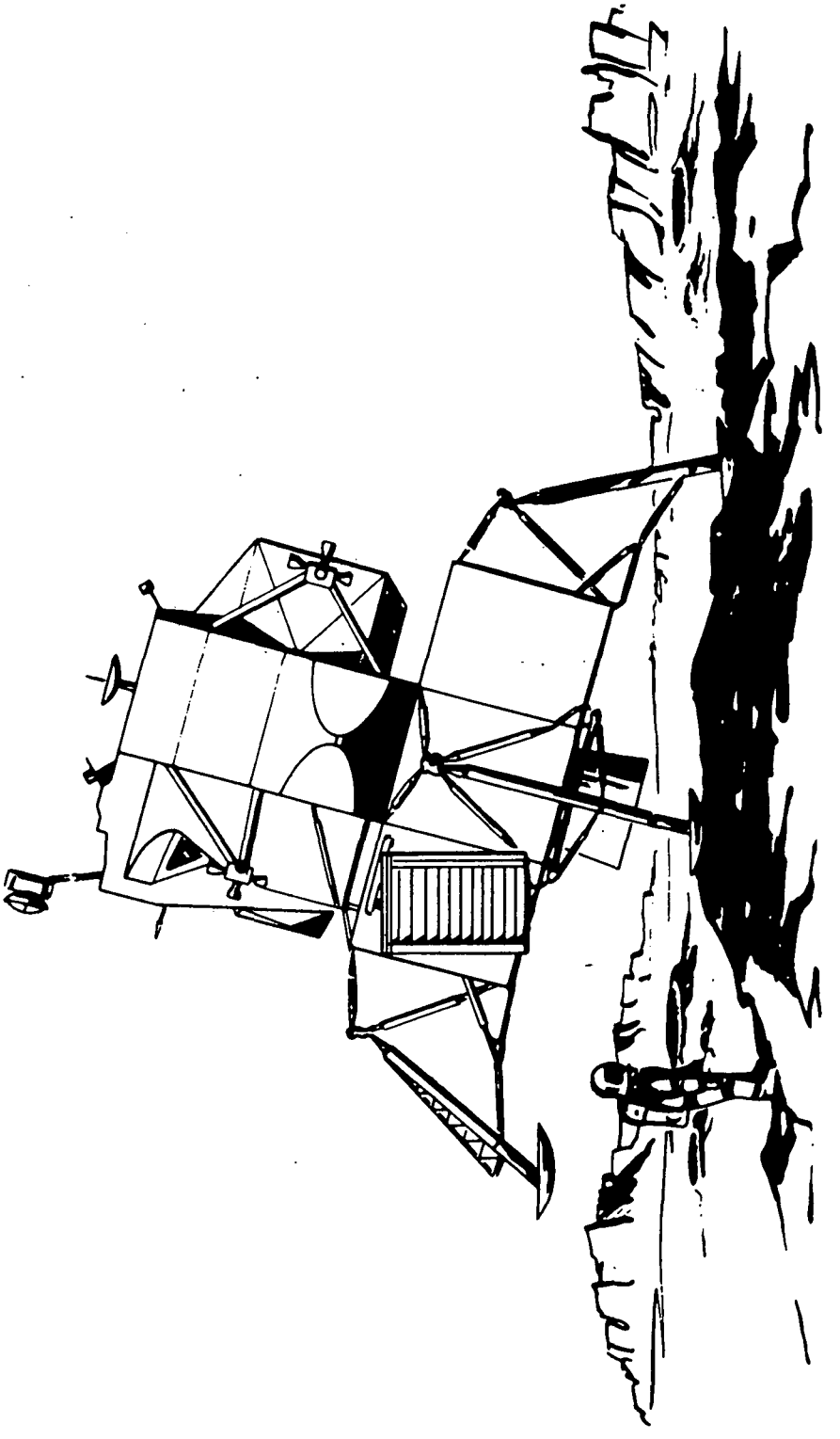

GSR DEPLOYMENT - FINAL VERTICAL POSITION

FIGURE 34

FIGURE 35

WATER BOILER

ESTIMATED PERFORMANCE

Ref. H.S. Memo LWH-1150-0312
Dated - 6/16/64
Extrapolated by Assuming
a Constant UA
of 280 BTU/HR°F

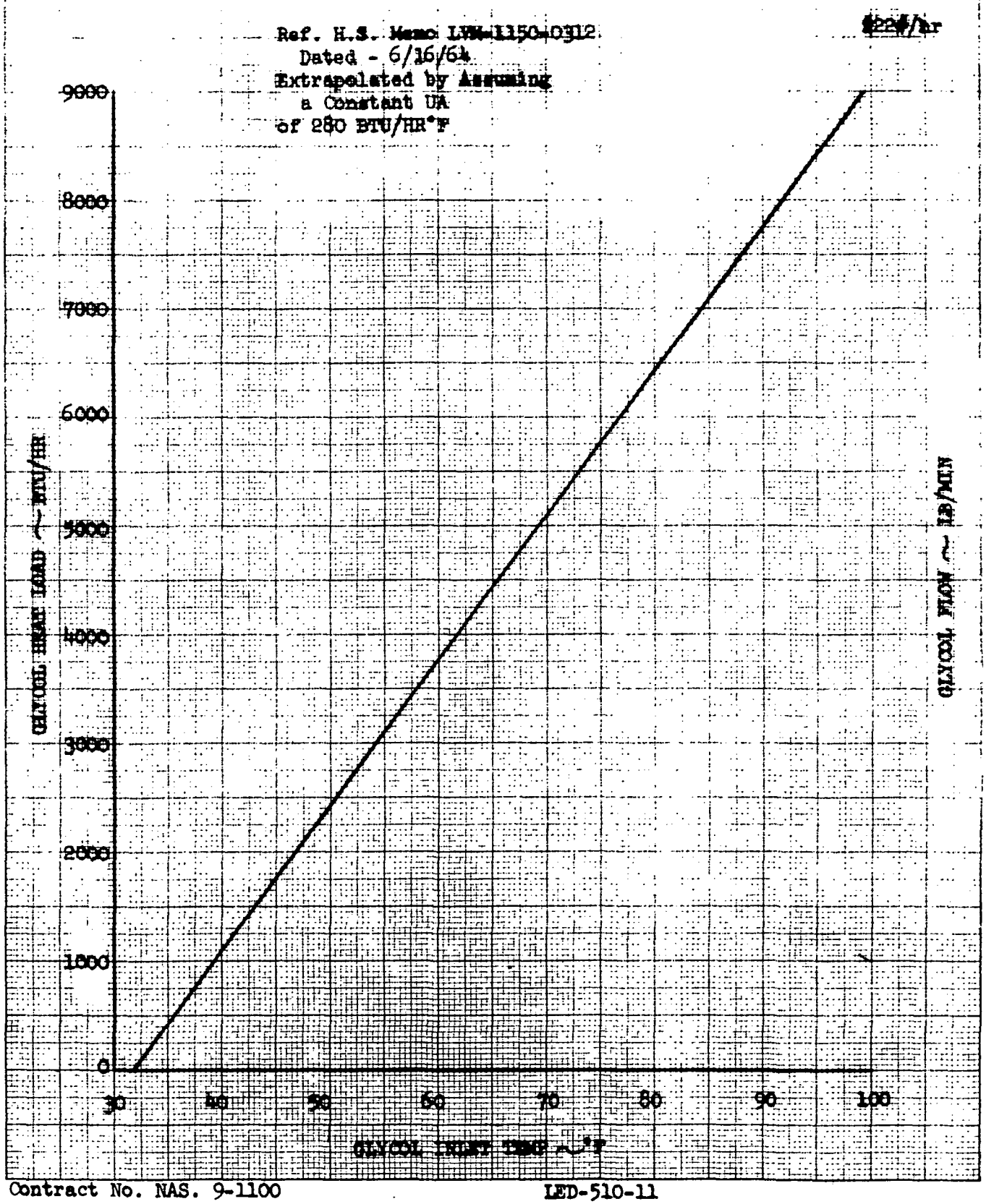

TABLE III

CYCLE CALCULATION RESULTS

RADIATION AREA = 52.25 FT^2

Q_{IN} VEHICLE $\neq 0$

AZIMUTH ANGLE = 0

SOLAR ANGLE, DEG	Q_{LOAD} BTU/HR	$Q_{IN\ VEH}$ BTU/HR/FT^2	$Q_{RAD\ NET}$ BTU/HR	H_2O RATE LBS/HR	FIN η	$T_{RAD\ IN}$ (FLUID)°F	$T_{RAD\ OUT}$ (FLUID)°F	$T_{BOIL\ OUT}$ (FLUID)°F
0	8759	35.60	3790	4.963	.8476	92.09	69.14	38.18
0	4549	35.60	2762	1.787	.8662	62.60	45.38	34.04
0	4573	35.60	2767	1.806	.8661	62.77	45.51	34.06
0	5184	35.60	2911	2.273	.8636	67.08	49.01	34.63
0	4645	35.60	2784	1.861	.8658	63.27	45.93	34.13
0	4657	35.60	2787	1.870	.8657	63.36	45.99	34.14
0	5264	35.60	2931	2.333	.8632	67.64	49.46	34.71
0	7968	35.60	3592	4.374	.8515	86.59	64.73	37.37
45	8593	30.60	4052	4.536	.8484	90.54	65.95	37.59
45	4383	30.60	3038	1.345	.8661	61.06	42.07	33.52
45	4407	30.60	3044	1.363	.8660	61.23	42.20	33.54
45	5018	30.60	3185	1.833	.8635	65.54	45.72	34.10
45	4479	30.60	3060	1.419	.8657	61.74	42.62	33.60
45	4491	30.60	3063	1.428	.8656	61.83	42.69	33.61
45	5098	30.60	3204	1.894	.8632	66.10	46.18	34.17
45	7802	30.60	3856	3.944	.8522	85.04	61.52	36.78
75	8482	20.20	4683	3.796	.8497	88.94	60.41	36.58
75	4272	20.20	3695	.5778	.8660	59.53	36.32	32.64
75	4296	20.20	3700	.5964	.8659	59.70	36.46	32.66
75	4907	20.20	3838	1.070	.8636	63.99	40.01	33.20
75	4368	20.20	3716	.6523	.8656	60.20	36.88	32.72
75	4380	20.20	3719	.6616	.8656	60.29	36.95	32.73
75	4987	20.20	3856	1.132	.8633	64.55	40.47	33.27
75	7691	20.20	4493	3.198	.8534	83.44	55.94	35.80

TABLE IV

CYCLE CALCULATION RESULTS

RADIATION AREA = 52.25 FT^2

Q_{IN} VEHICLE = 0

AZIMUTH ANGLE = 0

SOLAR ANGLE, DEG	Q_{LOAD} BTU/HR	Q_{IN} VEH BTU/HR/FT^2	Q_{RAD} NET BTU/HR	H_2O RATE LBS/HR	FIN η	$T_{RAD\ IN}$ (FLUID)°F	$T_{RAD\ OUT}$ (FLUID) °F	$T_{BOIL\ OUT}$ (FLUID) °F
0	8759	0	5126	3.630	.8489	90.38	59.16	36.36
0	4549	0	4146	.4034	.8651	61.05	35.02	32.44
0	4573	0	4151	.4221	.8650	61.22	35.16	32.46
0	5184	0	4287	.8966	.8627	65.50	38.71	33.00
0	4645	0	4167	.4782	.8647	61.73	35.58	32.53
0	4657	0	4170	.4875	.8647	61.81	35.65	32.54
0	5264	0	4305	.9585	.8624	66.06	39.17	33.07
0	7968	0	4937	3.031	.8526	84.91	54.68	35.58
45	8593	0	5205	3.386	.8499	89.09	57.34	36.04
45	4383	0	4232	.1509	.8657	59.76	33.13	32.16
45	4407	0	4237	.1696	.8656	59.92	33.27	32.18
45	5018	0	4373	.6453	.8634	64.21	32.83	32.71
45	4479	0	4253	.2258	.8654	60.43	33.69	32.25
45	4491	0	4256	.2352	.8653	60.51	33.76	32.26
45	5098	0	4391	.7075	.8631	64.77	37.29	32.78
45	7802	0	5017	2.785	.8533	83.61	52.84	35.27
75	8482	0	5448	3.034	.8506	88.00	54.70	35.59
75	4272	0	4272	0	.8697	51.65	24.50	24.50
75	4296	0	4296	0	.8693	52.45	25.17	25.17
75	4907	0	4625	.2827	.8637	63.14	34.12	32.31
75	4368	0	4368	0	.8681	54.84	27.18	27.18
75	4380	0	4380	0	.8679	55.23	27.51	27.51
75	4987	0	4642	.3451	.8634	63.70	34.58	32.38
75	7691	0	5260	2.431	.8536	82.52	50.20	34.83

TABLE V

CYCLE CALCULATION RESULTS

RADIATION AREA = 61.70 FT^2

Q_{IN} VEHICLE = 0

AZIMUTH ANGLE = 0

SOLAR ANGLE, DEG	Q_{LOAD} BTU/HR	$Q_{IN\ VEH}$ BTU/HR/FT^2	$Q_{RAD\ NET}$ BTU/HR	H2O RATE LBS/HR	FIN η	$T_{RAD\ IN}$ (FLUID)°F	$T_{RAD\ OUT}$ (FLUID)°F	$T_{BOIL\ OUT}$ (FLUID)°F
0	8759	0	5902	2.856	.8514	89.44	53.37	35.36
0	4549	0	4549	0	.8701	53.78	24.92	24.92
0	4573	0	4573	0	.8697	54.46	25.47	25.47
0	5184	0	4946	.2376	.8644	64.79	33.78	32.26
0	4645	0	4645	0	.8687	56.49	27.10	27.10
0	4657	0	4657	0	.8685	56.82	27.37	27.37
0	5264	0	4967	.2971	.8641	65.35	34.22	32.32
0	7968	0	5685	2.283	.8544	84.02	49.09	34.64
45	8593	0	5995	2.598	.8524	88.14	51.44	35.04
45	4383	0	4383	0	.8748	44.63	16.52	16.52
45	4407	0	4407	0	.8745	45.34	17.10	17.10
45	5018	0	5018	0	.8654	62.73	31.17	31.17
45	4479	0	4479	0	.8734	47.46	18.83	18.83
45	4491	0	4491	0	.8732	47.81	19.11	19.11
45	5098	0	5066	.0317	.8648	64.05	32.24	32.03
45	7802	0	5778	2.024	.8551	82.72	47.15	34.33
75	8482	0	6274	2.208	.8528	87.02	48.53	34.55
75	4272	0	4272	0	.8818	30.73	2.872	2.872
75	4296	0	4296	0	.8814	31.50	3.504	3.504
75	4907	0	4907	0	.8718	50.11	18.79	18.79
75	4368	0	4368	0	.8803	33.77	53.85	53.85
75	4380	0	4380	0	.8801	34.15	5.696	5.696
75	4987	0	4987	0	.8706	52.44	20.69	20.69
75	7691	0	6060	1.631	.8556	81.60	44.21	33.85

FIGURE 36

WATER CONSUMPTION, WITH AND WITHOUT
THE GSR SPACE RADIATOR
(WITH VEHICLE INPUT)

Sun Angle = 0° (Subsolar)
γ = 90° Sun On Edge
Q In Vehicle = 35.6
A = 52.25 ft^2

ΔH_2O = 92.628 lbs

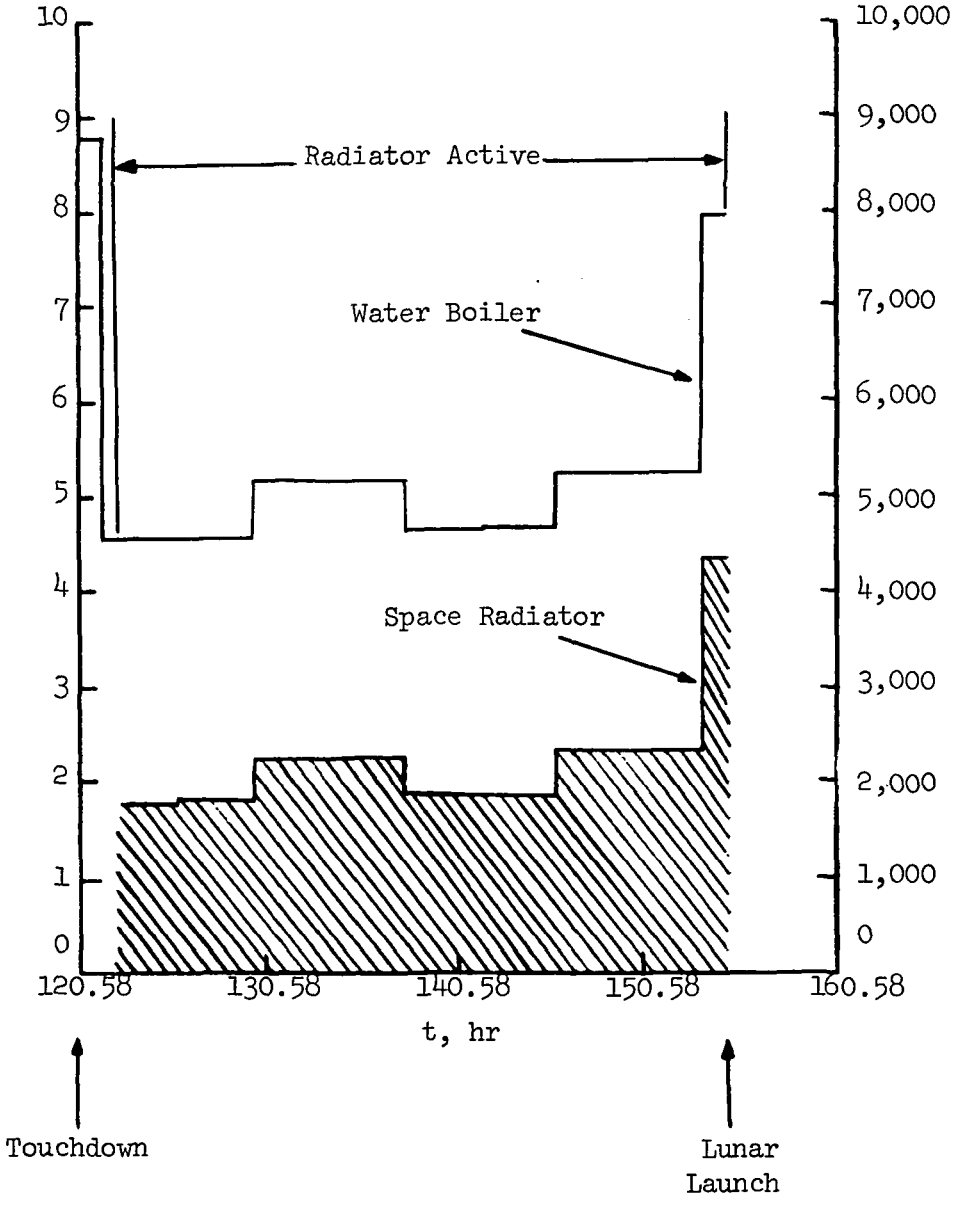

FIGURE 37

WATER CONSUMPTION, WITH AND WITHOUT
THE GSR SPACE RADIATOR
(WITHOUT VEHICLE INPUT)

Sun Angle = 0° (Subsolar)
γ = 90° Sun On Edge
Q In Vehicle = 0
Radiator Area = 52.25 ft^2

ΔH_2O = 136.995 lbs

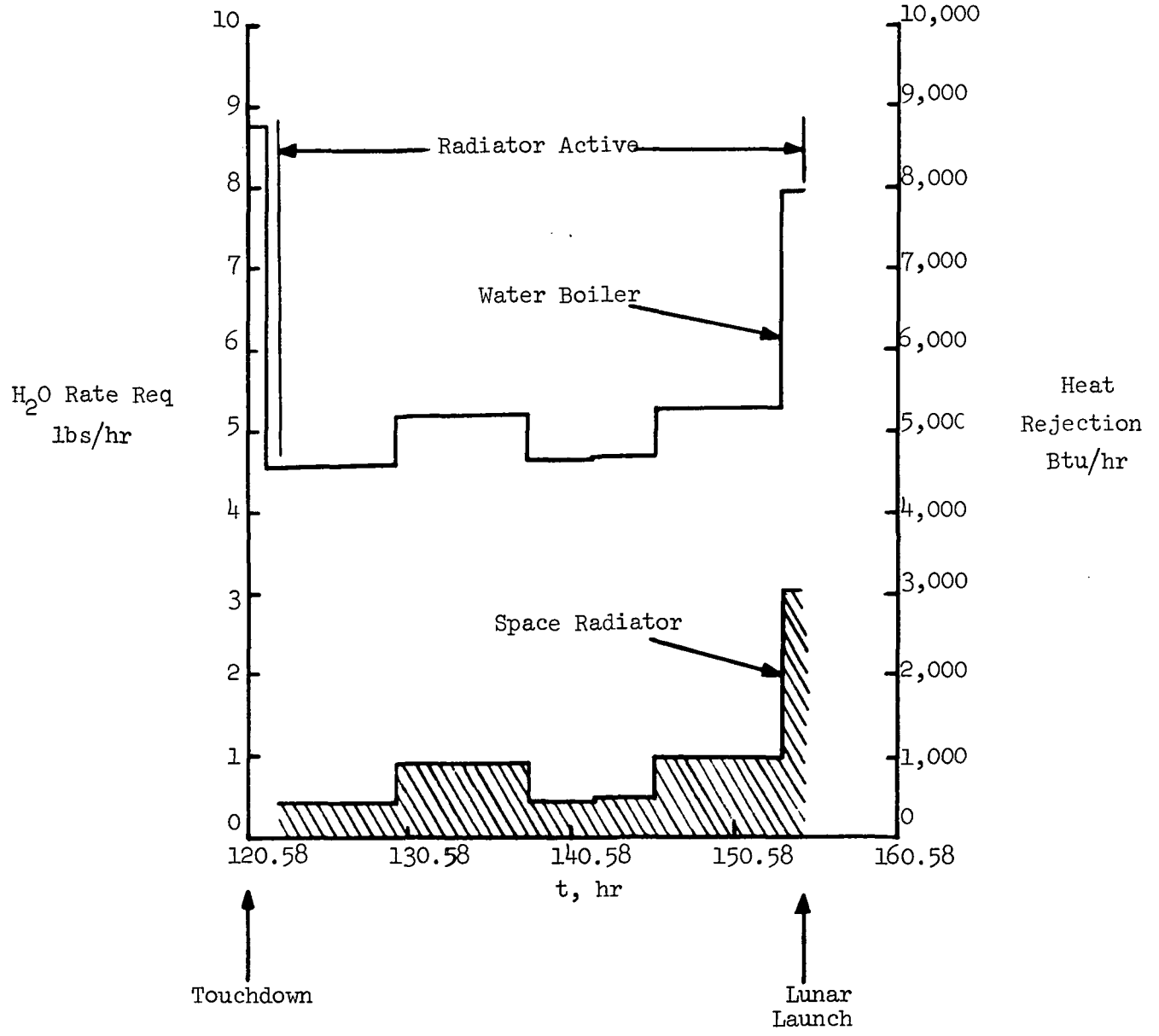

FIGURE 38

WATER CONSUMPTION, WITH AND WITHOUT TWR GBR SPACE RADIATOR

Sun Angle - 0° (Subsolar)

γ = 90°r Sun On Edge

Radiator Area = 61.7 ft^2

$Q_{in\ Veh} = 0$

ΔH_2O = 165.9

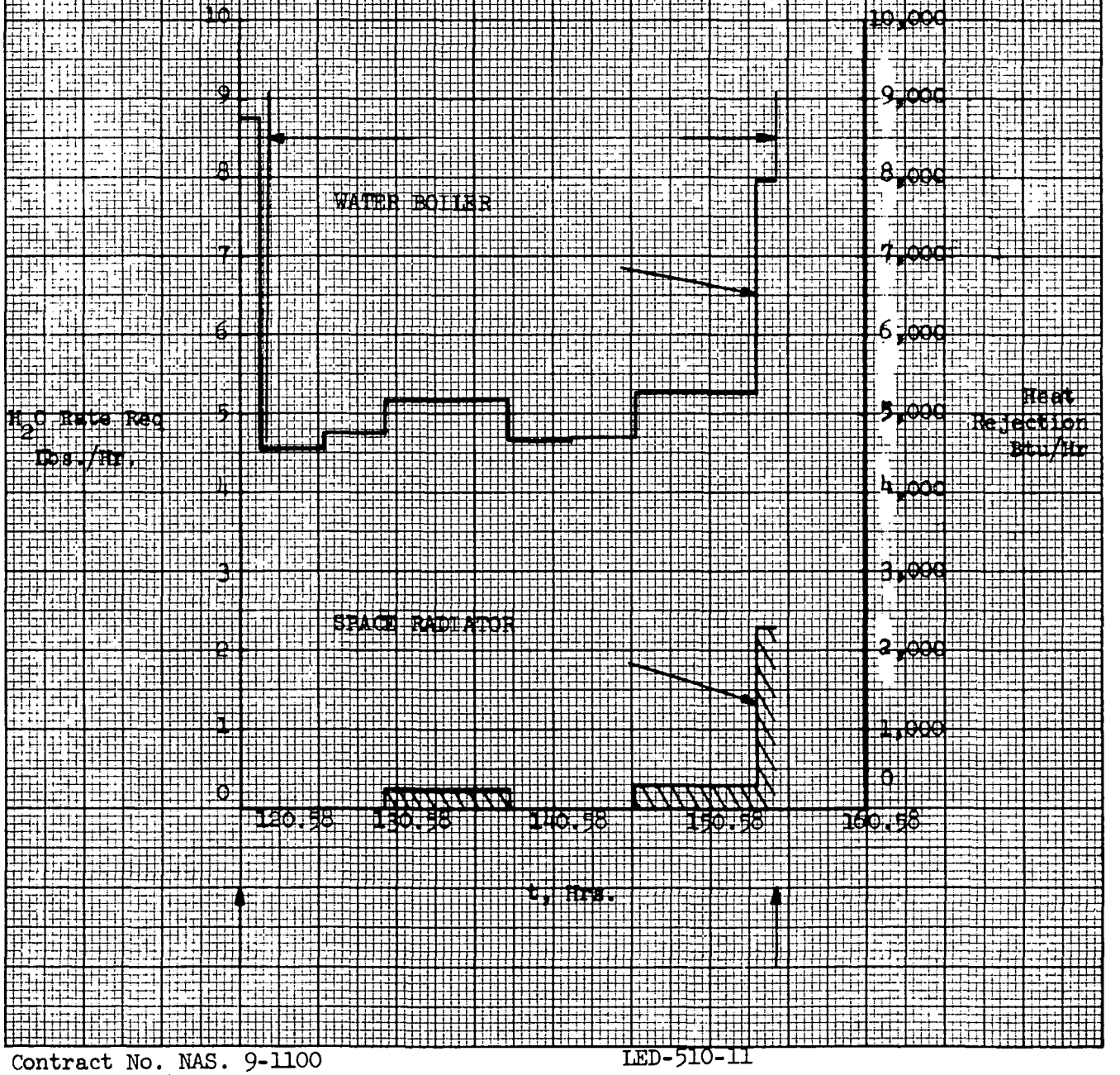

10 X 10 TO THE ½ INCH 359T-11
KEUFFEL & ESSER CO. MADE IN U.S.A.
ALBANENE ½

TABLE VI

GSR WATER SAVINGS, LB

Radiator Area - Ft^2	Solar Angle, deg	Without Vehicle Input	With Vehicle Input
52.25	0	137.0	92.6
52.25	45	139.7	101.5
52.25	75	145.3	122.5
61.7	0	165.9	-

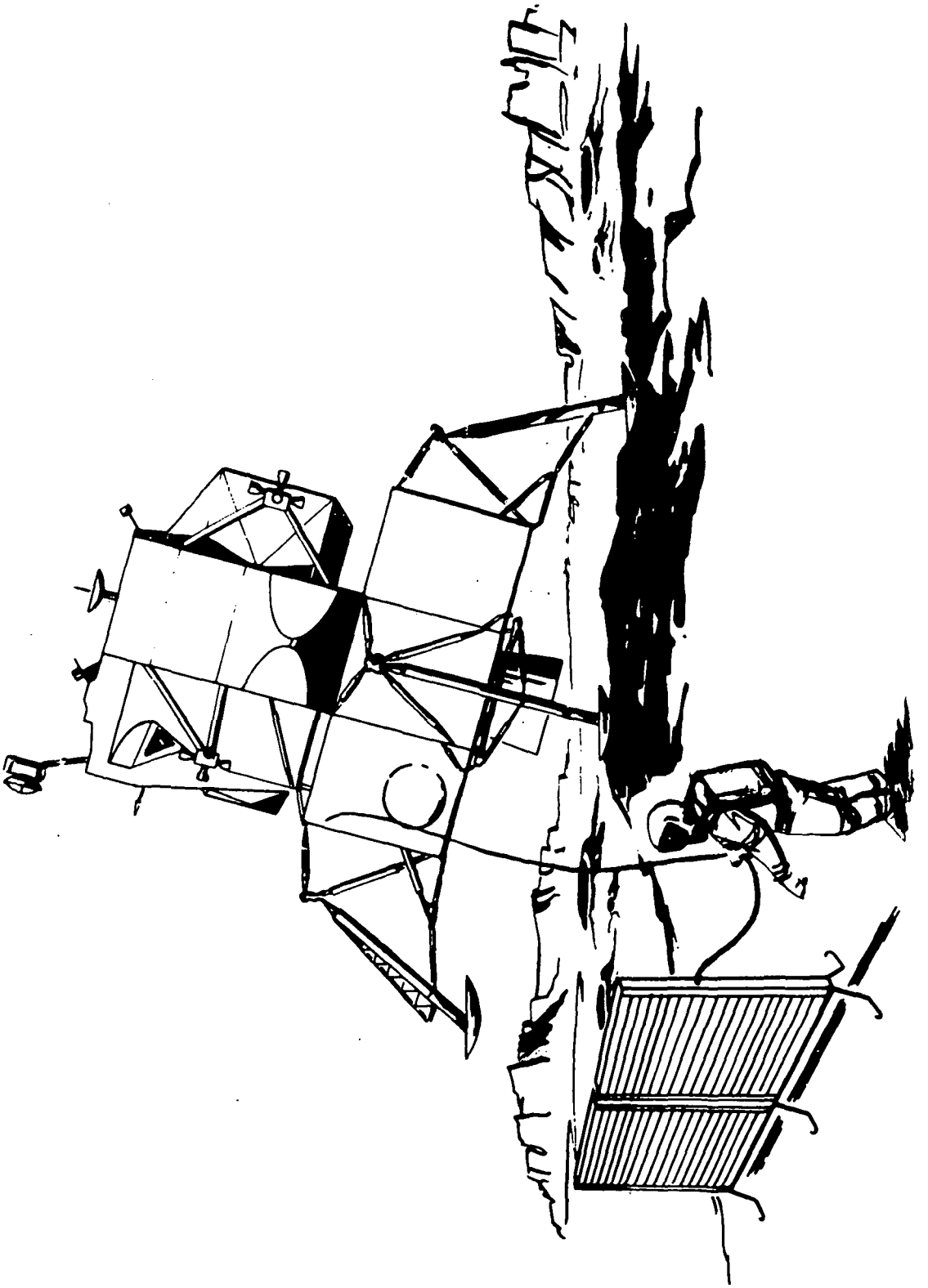

GSR CARRY OFF DESIGN

FIGURE 39

WEIGHT SAVINGS

In evaluating the potential worth of ECS radiators, the weight savings attained by modifying the present water boiler system must be considered. These modifications include:

1. The changes in ECS hardware located in both the ascent and descent stages. (The revised ECS loop will include provisions for attaching either or both radiators and this is accounted for in the weight calculation for both.)

2. The decreased amount of water which must be carried in the descent stage when a radiator system is utilized. (A single smaller water tank replaces the previous tank, i.e., the radiator tank is sized to carry the water required for a worst case landing.)

3. The radiator fluid pumping power weight penalty in the form of descent stage battery energy and a heavier glycol pump.

4. Changes to the basic LEM structure - mounts, fittings, etc.

5. The changes in propellant weight required for lunar descent and ascent.

The results are described as separation weight savings calculated as per Reference 3.

The separation weight savings for the flat radiators with vehicle interchange are shown as a function of the number of erected panels in Figure 40. Darkside savings were computed using only one center panel radiating from both sides. The performance of a set of three panels radiating from one side only is included for comparison. The night-time saving of almost 90 pounds is less than the peak day value because of the large drop in ECS load at the former landing location. For lunar stays at less than approximately 40° off subsolar, there is no advantage to using the deployable flat radiator. However, for θ greater than 40°, increasing gains are obtained and by varying the number of panels. A maximum separation weight saving of almost 150 pounds is evidenced with four panels at a near terminator stay.

The strong influence of radiator-vehicle radiant interchange and shadowing on radiator performance has been discussed. A comparison of weight savings with and without interchange for a six panel system is shown in Figure 41. A net weight saving could be realized at all possible landing sites if the radiators did not participate in radiant interchange with the vehicle. The effect of shadowing is quite pronounced. However, since there is no provision for controlling yaw on landing, weight benefits cannot be derived from shadowing.

A similar set of curves showing savings with and without vehicle interchange for the GSR appear in Figure 42. These are the results of combining the water weight savings (Table VI) with the GSR system weight as summarized in Table VII. Note that with vehicle/radiator interchange, the 52.25 ft^2 deployable GSR shows no saving for almost half of its possible operating range and at its best only saves 25 pounds. However, when vehicle interchange is eliminated, an almost constant 90 pound separation weight saving is obtained. This constant characteristic is of considerable value when lunar rotation is considered i.e., with the GSR, no significant drop in performance is expected during the lunation period.

In order to determine the optimum operating range for each radiator system, the results are replotted in Figure 43. Here the GSR and the flat radiators are compared both with and without interchange. Some specific conclusions are:

1. Considering only the systems which are fixed to the descent stage and deployed on landing, the GSR is valueless and the flat radiator has a performance range limited to landing sites more than 40° from the subsolar point.

2. The same panels in a "carry off" configuration, which would eliminate vehicle inputs, will always show a weight saving of not less than 75 pounds and as much as 150 pounds. The crossover from GSR to flat radiators occurs at about 30° off the subsolar point.

Projecting the results somewhat by eliminating a size limitation and using a 160 ft^2 maximum flat and 61.7 ft^2 GS radiator, savings shown in Figure 44 might be obtained. Almost the entire lunar stay ECS load could be handled by this system.

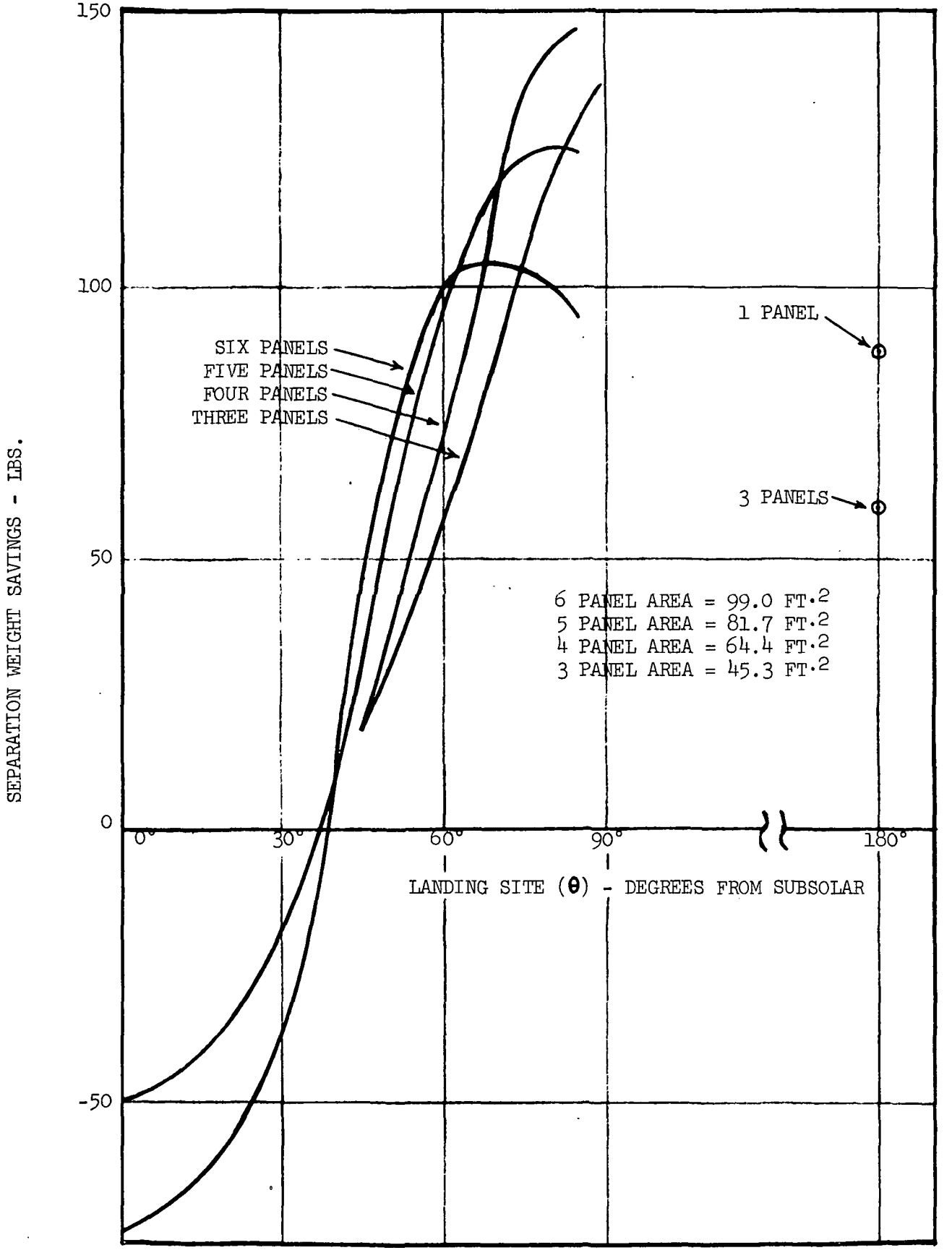

SEPARATION WEIGHT SAVINGS FOR RADIATORS WITH RADIANT INTERCHANGE

FIGURE 40

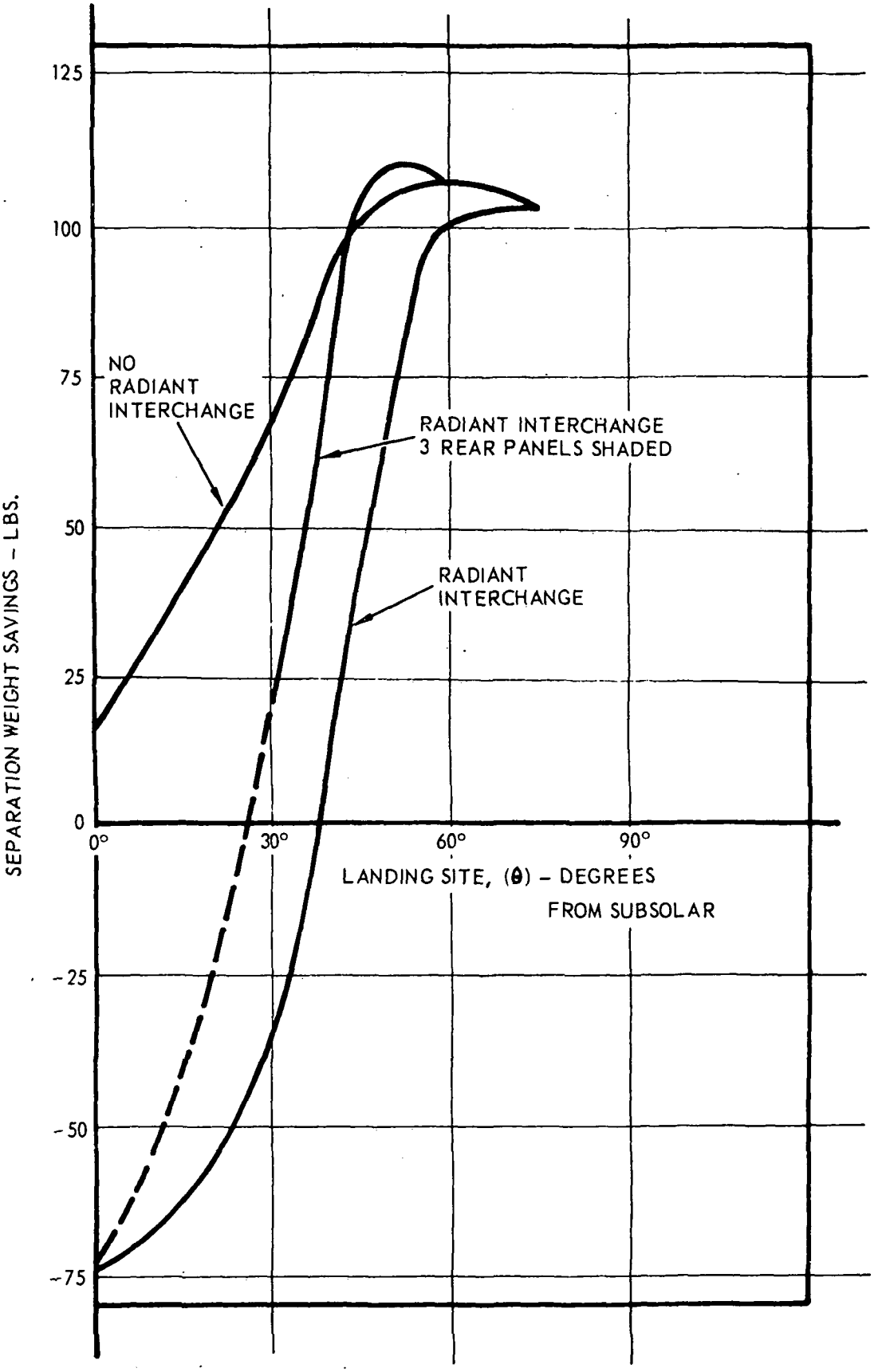

EFFECT OF RADIANT INTERCHANGE AND SHADOWING
ON WEIGHT SAVINGS FOR SIX PANEL, 99 FT.^{2} RADIATOR

FIGURE 41

FIGURE 42

WEIGHT SAVINGS AT SEPARATION

BOOM SUSPENDED GSR

Area = 52.25 Ft^2

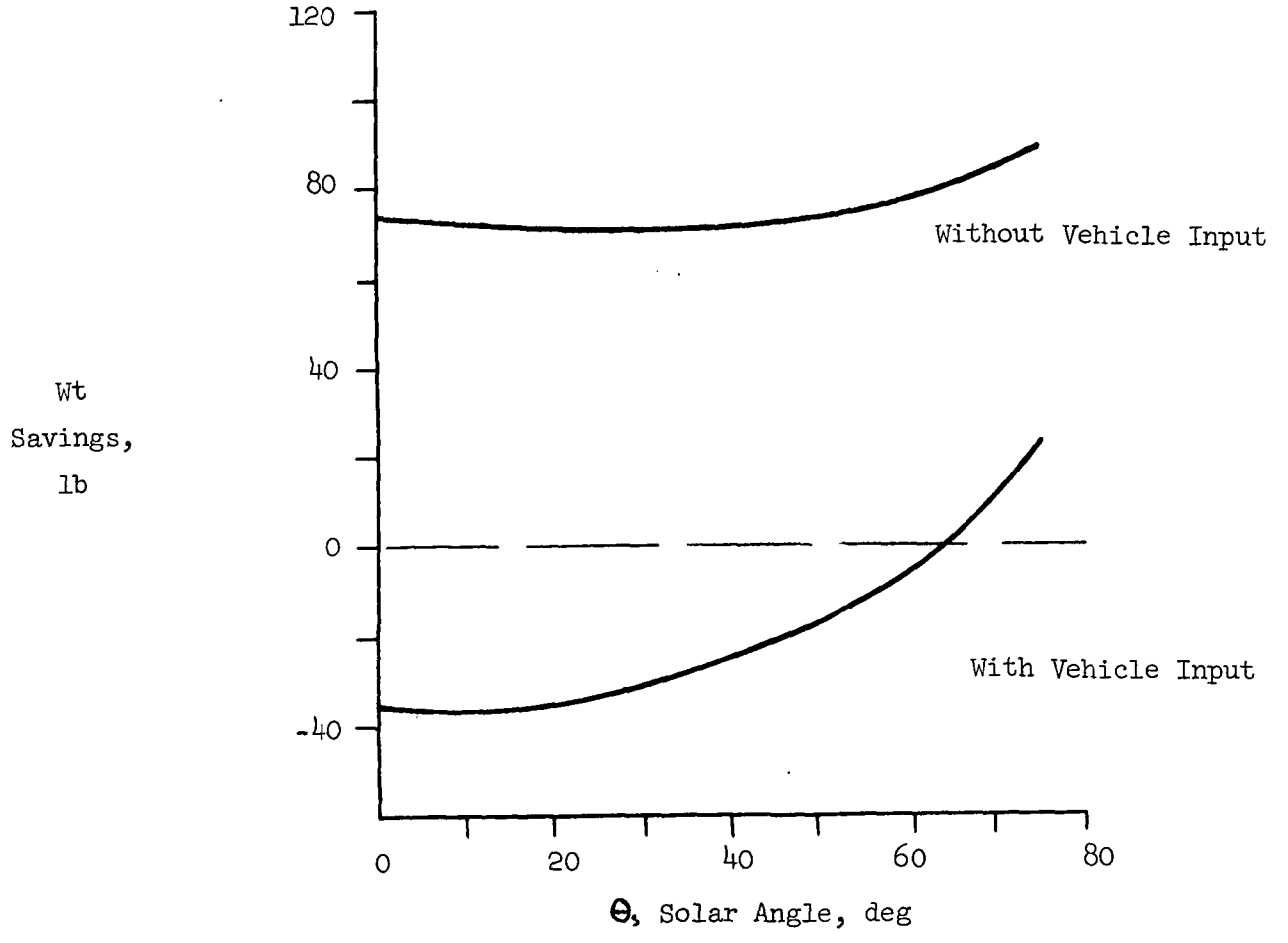

TABLE VII

GSR WEIGHT SUMMARY

- less water -

	Deployable		Carry Off	
DESCENT STAGE	52.25 ft^2		61.7 ft^2	
Wet Radiator Panel		63.0		71.0
Rad. Surface & Tubes, Thermal Paint, Flexlines	15.2		16.3	
Parabolic Reflectors	17.3		20.4	
Parabolic Reflectors Support Structure	2.41		2.9	
Longitudinal Reflector - Radiator Connectors	5.02		5.92	
Vertical End Panels	4.06		4.4	
Top Cover	.88		.96	
Bottom Cover	1.23		1.34	
Thermal Paint for Fiberglass Parts	1.38		1.56	
NRC-2 Superinsulation	3.46		4.06	
Insulation Support Rods	1.1		1.3	
Swivel Assembly	.56		-	
Hardware - Screws, Plate Nuts	2.4		2.86	
Fluid - Water Glycol	8.0		9.0	
RCS Thermal Shield Assembly		5.0		4.0
Glycol Reservoir - Dry		3.0		3.0
Booms & Supports		14.4		-
Flat Radiator Mount Brackets		3.0		3.0
GSR Mount Brackets		4.4		2.5
Panel Skids (Legs)		-		1.5
Valves & Lines		8.3		8.3
Water Tanks (Weight Reduction)		-5.0		-5.0
Battery Weight (Power Penalty)		2.0		2.0
ASCENT STAGE				
Disconnects & Manual Valves		1.8		1.8
Wet Plumbing		2.2		2.2
Hardware - Clamps, Screws		0.5		0.5
Accumulator		1.1		1.1
Pump		0.6		0.6

FIGURE 43

SEPARATION WEIGHT SAVINGS

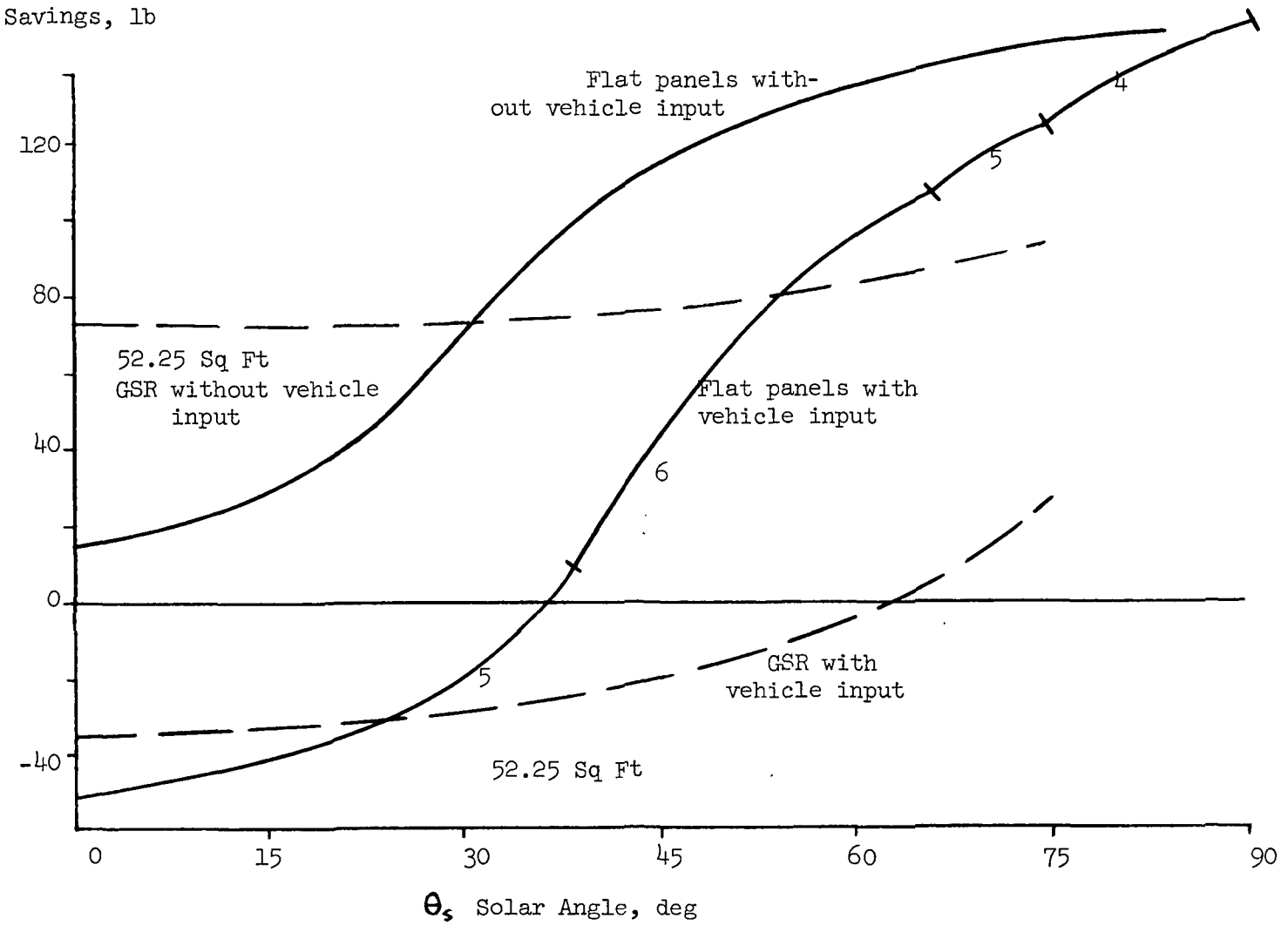

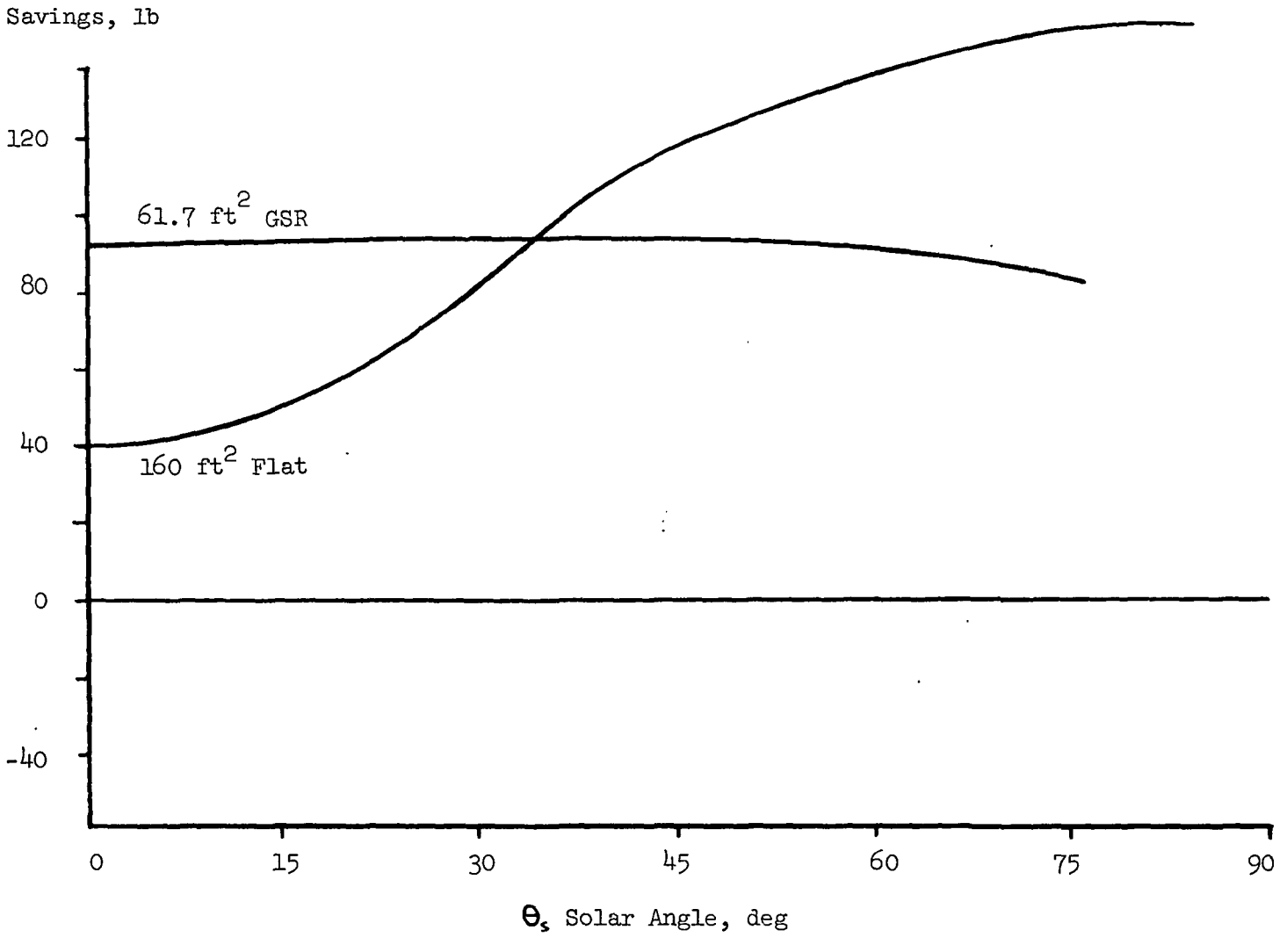

SEPARATION WEIGHT SAVINGS WITH OVERSIZED PANELS
WITHOUT VEHICLE INPUT

FIGURE 44

CONCLUSIONS

1. An ECS radiator subsystem can yield moderate weight saving when compared with the present LEM water boiler system for lunar landing sites beyond 45° from the subsolar point.

2. The radiator system could result in a weight saving for all possible landing sites if vehicle-radiator radiant interchange could be eliminated. This could involve either carrying them a sufficient distance from the vehicle or deploying them in a position where they cannot see the vehicle.

3. Weight savings will increase for lunar stay missions of longer (than 35-hour) duration.

RECOMMENDATIONS

Since the potential savings for an ECS radiator subsystem have been confirmed analytically, it is recommended that future efforts be concerned with developing and testing sample flight articles in order to experimentally verify weight and performance predictions. With such an effort successfully completed, future manned vehicles could consider the use of space radiators as practically "off the shelf" items.

It is, therefore, recommended that future efforts follow the outline below:

1. A limited investigation of new radiator concepts to implement the "carry-off" and/or remote deployment goal of eliminating significant vehicle radiation input.

2. Analyses to determine the operating characteristics of feasible designs from item 1. Included should be the effects of carry-off distance, lunarscape discontinuities and anomalies, RCS plume impingement, etc., in addition to the usual performance parameters.

3. Mechanical design, stress and vibration analyses of the most promising design(s).

4. Manufacture of working panels for testing.

5. Testing, to include: Vibration, thermal vacuum with solar simulation, EMC and deployment by suited astronaut in a Peter Pan type rig.

APPENDIX A

GSR Construction Details

The following discussion concerns the radiator depicted in figure 45. The radiating surfaces of this design are made up of aluminum alloy sheets 6061-T4 or similar weldable aluminum alloy. Each surface is 4.75 inches wide and has an aluminum alloy tube, seam welded to it along its center line. The gage of the sheets is kept at 0.020 for 0.20 down the center, 0.44 inches in from each edge and from each end for support attachments. The remainder is chem-milled to 0.008. The tube diameter is .375 inch OD with an .018 inch thick wall. The length of the radiator surface is 72.00 inches for the panel assembly mounted off of Quadrant I. It is 60.00 inches for the panel assembly mounted off of Quadrant III to allow clearance for access doors. Sufficient tube length is left over at each end of the radiator surface to allow welded connections to adjacent tubes. This puts the radiating surfaces in series. The tubes are bent up or down, as the case may be, and joined inside a short sleeve. There are 12 radiating surfaces to a panel giving an area of 28.50 square feet for the panel hung off of Quad I and 23.75 square feet for the other.

The main feature of this design is the parabolic reflector which permits reflection of radiator surface output to space and lunar input radiating below the horizontal (parallel to radiator surface) to reflect outside of the parabolic focus. Each parabolic surface is formed from aluminum alloy 2024-ST-6 in a back to back configuration. The parabolic curve, $Y^2 = 4fX$, (f=2.5) has the radiating surface on its principal axis with the vertex at the center of the surface. This places the focus off the edge of the surface by 0.125 inches $\left(2.50 - \frac{4.75}{2}\right)$.

The height of the reflector, at this point, (half of the latus rectum) is 5.00 inches. In order to form this back to back configuration from one sheet, the curve is bent on a suitable bend radius about 1.0 inch above the vertex. This separates the reflector from the radiating surface and permits some lunar radiation to pass by the reflector. The gage of the reflector is kept at 0.020 inches for 0.44 inches in from each edge, each end and for five cross strips equally spaced for support attachments. The remainder is chem-milled to 0.008 inches. In calculating weight of radiator surfaces and reflectors, 0.010 inch thick is used in place of .008 inch to allow for tolerances. The reflectors are the same length as the radiating surfaces.

The metal radiator surface is supported on its edges by longitudinal, angle shaped stiffeners formed of 0.020 inch thick fiberglass. This angle shape joins the surface edge with the reflector edge through a non-conductive path. The stiffener is bonded or riveted to the reflector edge and the surface is attached to it by means of #4-40 screws and plate nuts (approximately 4 inch spacing).

Fiberglass frames 0.020 inches thick serve to hold the parabolic shape of the reflector and also give intermediate support to the insulation blanket. There are five such open style frames to a surface - reflector module with a catenary shaped upper flange (0.44 inches wide). The 0.020 inch thick web material is allowed to protrude up at each end of the catenary to retain insulation blanket support rods. These frames are bonded to the reflector.

Fiberglass bulkheads 0.020 inches thick close off each end of the surface - reflector modules. They are bonded to the reflector and attached to the radiating surface and end covers with #4-40 screws and plate nuts. The upper flange is recessed for the 0.375 inch diameter tube and a catenary shaped support is bonded to the bulkhead to support the ends of the insulation blanket.

The insulation blanket is made up of 25 layers of NRC-2 (a mylar-aluminum sheet about .00025 inch thick). The blanket is hemmed on its longitudinal edges with small staples in such a manner as to retain nylon rods or tubes 0.093 inches in diameter, 72 inches long at a 0.375 inch distance from the blanket edge. The hem of this blanket is cut at each frame to permit the rod to be cradled in the frame support. The catenary shaped flanges give a natural support to this blanket at one foot spacings. The blanket reduces heat input from the reflectors to the under side of the radiator surface.

The twelve surface - reflector modules are held at a 5.12 inch stacked spacing by fiberglass end covers of .020 gage. These covers are 5.12 inches wide with 0.50 inch wide edge flanges for stiffness. A 1.00 inch wide, 1.75 inch deep longitudinal trough up the center provides protection for the tube connections.

Welding of the tube connections of the 12 unit assembly takes place in a fixture. The reflector assemblies and end covers are attached to this assembly, while in the fixture, with #4-40 screws to the plate nuts provided in the longitudinal stiffeners and end bulkheads. Cover patches are bonded to the end covers to cover portions of the trough not hidden by end bulkheads.

The bottom radiator surface is supported by a curved cover of 0.020 inch thick fiberglass. An insulation blanket lies on the inside of this cover to reduce lunar radiation input. The end covers conform to the bottom cover shape.

The top cover is an .020 inch thick flat sheet of fiberglass fastened to the two top longitudinal stiffeners, end bulkheads, and two swivel retainer supports. The two fiberglass supports straddle a fiberglass receptical and form a boxed in support for the swivel retainer. These supports are bonded and riveted to the top reflector. Insulation blankets are installed in the top reflector to reduce solar input from the top cover.

The swivel retainer is a spherical segment with a 1.31 inch inside radius and 0.050 gage fiberglass with a flange held to the two top longitudinal stiffeners and internal supports with four #8-32 screws and plate nuts.

The swivel fitting is hemispherically shaped with a 1.31 inch outside radius and .040 inch thick wall aluminum alloy 2024ST6 with top internally threaded stem. A 1/4 inch bolt attaches this fitting to the end of the boom. When the radiator is swung out from the LEM, it hangs from the swivel in a plane normal to the lunar surface regardless of the LEM attitude.

The boom is made in two sections, one 6 foot long supported from a titanium bracket off the corner post of the descent stage; the other, a 3 foot long section pivoted on the end of the 6 foot section. When unfolded, the total boom swing is 9 feet and provides for orientation of the panel assembly. The boom sections are constructed of 0.020 inch thick aluminum alloy 7075-ST6 in a hat shaped cross section with flat sheet closing the hat. The hat is 2.00 inches wide (3.00 inches across the flanges) and the 6 foot section tapers from 2.00 inches to 1.00 inch. The pivot pins at the main mounting bracket and at the sectional joing are tubular, about .50-.75 inches in diameter and held in split bearing sleeves with an adjustable clamp screw to regulate the friction at each pivot. This would enable the panel assembly to be moved out from the LEM and left at a position without additional restraints. The shorter boom nests back over the longer one in storage and the boom is intended to take 3 times the load of a panel assembly on earth.

Fluid is fed to the panel assembly from the descent stage through 0.375 inch rigid aluminum alloy lines with flex lines passing the two pivots and swivel joints. The flex lines tend to resist motion with their own torsional resistance. Sufficient length (about 2 feet) is allowed at each joint to minimize this. Standard aluminum alloy hydraulic swivel fittings serve to connect the rigid and

the flex lines. Some research will be necessary to check out flex lines in the proper environment to ascertain what handling difficulties might exist.

The panel assembly is mounted to the descent stage with four brackets made of .020 titanium sheet. Titanium is used because of its low conductivity. Fittings of titanium are attached in the bottom of each trough of the end covers. The two lower supports cradle the curved bottom cover at the troughs and "PIP" (Ball Detent) pins connect the fittings to the brackets. The two upper brackets support clevis type fittings which stradle the troughs below the top of the panel. "PIP" pins secure these fittings so that upward as well as downward motion is restrained. The four pins are connected with a lanyard so that a tug on each side releases them allowing the panel assembly to be deployed. The titanium brackets must support the panel assembly during launch and descent with a minimum deflection at the panel (about .003 inch). Attachment of these brackets and the boom support to the corner posts of the descent stage will necessitate some modification of the existing corner post design. Arrangements will also be made to change the thermal shield and insulation blanket of the descent stage where these brackets penetrate.

In order to protect the panel assembly from the Reaction Control exhausts, it is necessary to provide an overhanging canopy at the top of the descent stage. It will be a corrugated 0.010 inch thick titanium sheet, 14 inches wide by 77 inches long. Six channel shaped titanium brackets mounted from the top of the structural descent stage will cantilevered out to support the canopy. Here penetration of the thermal shield will have to be accounted for.

Carry-Off Design of GSR

In the carry-off radiator design, two panels can be hinged together with brackets supported from the longitudinal troughs on the end covers. During launch, these two panels are locked together with overlapping clevis joints on the unhinged ends and secured with "PIP" pins. The titanium canopy, in this instance, now becomes a structural support for a Block and Fall system which will lower the top panels to the lunar surface. At each end of each panel, there will be a pair of tubular "Legs" curved to allow a "castoring" alignment while the panels are dragged away from the LEM. Unfolded, end to end, the "Legs" can be adjusted to take care of irregularities on the lunar surface. The fluid will be fed through three sets of six foot long .375 inch diameter tubes connected up with flexible line joints. The pairs of lines will be surrounded with an insulated sleeve.

A ladder is provided here to facilitate access to the panel support mechanism. The weight of one structural support system and one canopy should come out a bit lighter than that of two booms and two canopys. The 18 foot fluid feed line might have more problems than envisioned at present.

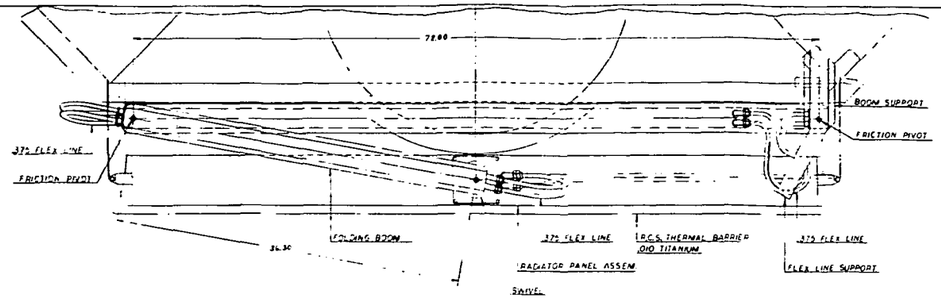

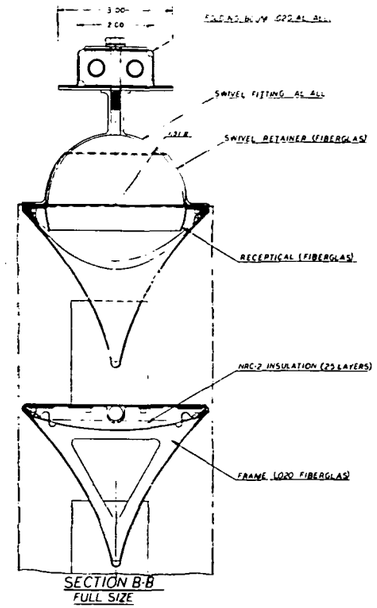

SECTION B-B
FULL SIZE

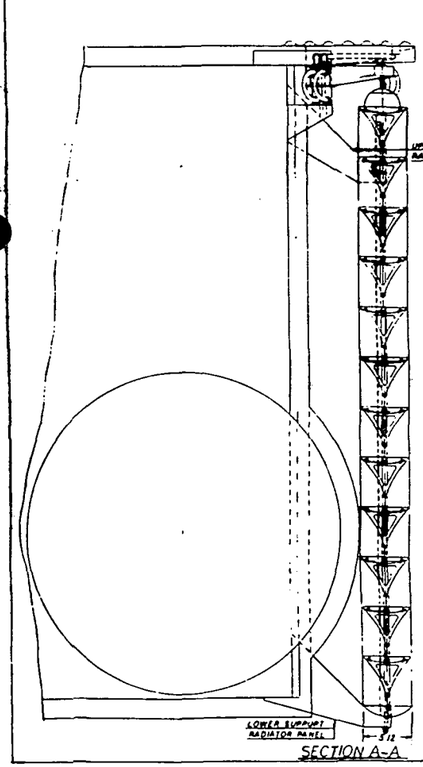

SECTION A-A

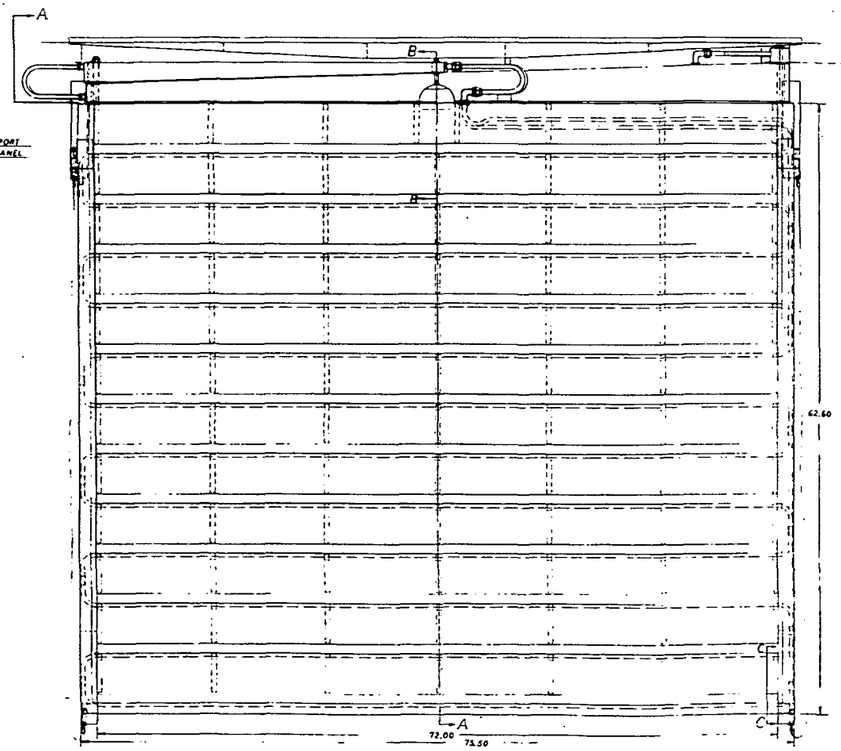

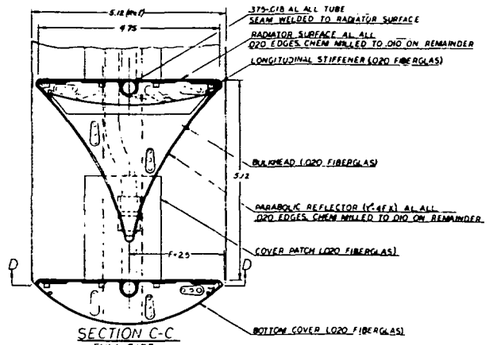

SECTION C-C
FULL SIZE

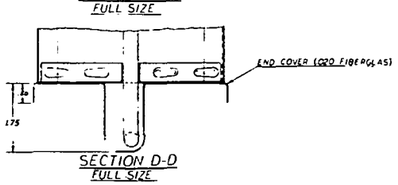

SECTION D-D
FULL SIZE

FIGURE 45

		GRUMMAN AIRCRAFT ENGRG CORP	
		RADIATOR, GSS TYPE BOOM SUPPORT	
		CONTRACT NO. 26512	LSK28C10738

APPENDIX B

GSR PERFORMANCE ANALYSIS

INTRODUCTION

For the purpose of predicting the performance of the Geometrically Selective Radiator (GSR), certain assumptions must be made regarding the surfaces themselves and the radiant interchange between them. The GSR, as analyzed, consists of a parabolic reflector segment (perfectly specular) and a flat radiator segment lying on the major axis of and touching at its vertex. For this development, the radiator is forced to various equilibrium temperature levels, and the reflector temperature and net heat rejection of the radiator is computed for various values of surface properties and solar and lunar inputs. The following algebraic relationships predict these effects and are based on the fact that radiation striking the reflector from below the horizon is always reflected to the moon and radiation striking the reflector from the horizon is always reflected into the radiators, providing the radiator is parallel to the lunar surface.

BASIC ASSUMPTIONS

1. Reflector and radiator are isothermal and there is no thermal conduction between them.

2. End effects are neglected.

3. Irradiation from all sources is uniform.

4. The reflector has a perfectly specular surface.

The analysis is based on the following graphic definition of areas:

① Reflector

② Radiator

③ Moon

④ Space

⑤ Exit plane

⑥ Reflector chord

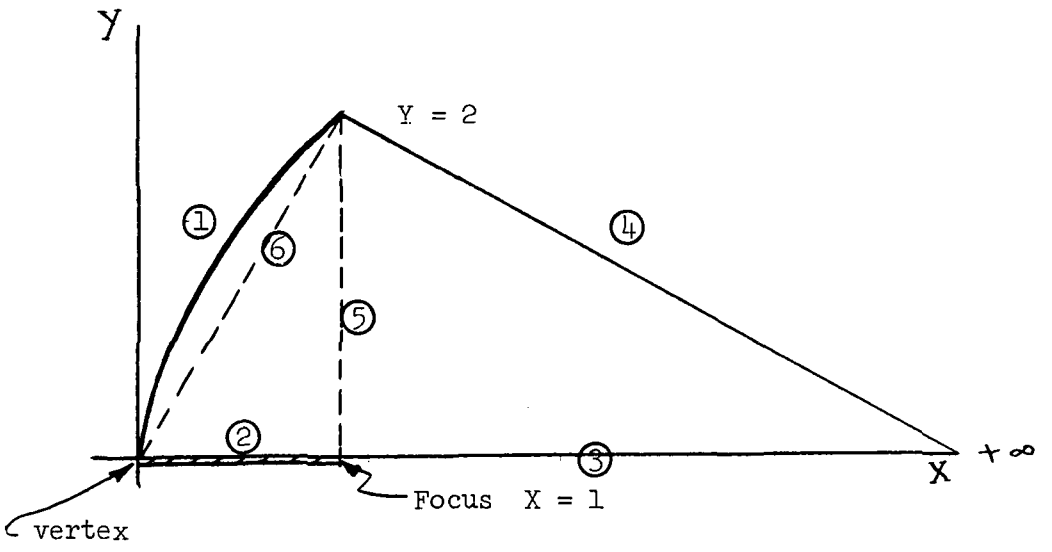

Equation of reflector:

$$Y^2 = 4X \quad \text{for} \quad 0 \leq Y \leq 2 \tag{1}$$

Equation of radiator:

$$Y = 0 \quad \text{for} \quad 0 \leq X \leq 1 \tag{2}$$

AREAS

For this development, since analysis is for a 1 unit (foot) longitudinal length.

Areas $\approx$ Lengths

and, by definition,

$$A_2 = 1 \tag{3}$$

From Analytic Geometry,

$$A_1 = \int_0^1 \sqrt{1 + \left(\frac{dy}{dx}\right)^2}\, dx \tag{4}$$

where $$\frac{dy}{dx} = \frac{2}{y} \tag{5}$$

Evaluating, by integrating between limits:

$$A_1 = 2.2955 \tag{6}$$

$$A_6 = \sqrt{5} = 2.2360 \tag{7}$$

$$A_5 = 2 \tag{8}$$

VIEW FACTORS

By inspection, the geometric view factor from surface 6 to surface 1 is:

$$F_{61} = 1 \tag{9}$$

By reciprocity

$$F_{16} = \frac{A_6}{A_1} F_{61} = 0.97407 \tag{10}$$

and

$$F_{11} = 1 - F_{16} = .0259 \tag{11}$$

For infinitely long right angle surfaces of finite width (Ref 4)

$$F_{25} = \tfrac{1}{2}(3 - \sqrt{5}) = 0.38196 \tag{12}$$

$$F_{21} = 1 - F_{25} = 0.61803 \tag{13}$$

Since all the radiator emitted by 2 which is directly incident on 5, is also absorbed by space,

$$F_{24} = F_{25} = 0.38196 \tag{14}$$

Now, by reciprocity

$$F_{12} = \frac{A_2 F_{21}}{A_1} = 0.26922 \tag{15}$$

By inspection

$$F_{53} = F_{54} = 0.5 \tag{16}$$

$$F_{32} = 0 \tag{17}$$

and

$$F_{34} + F_{31} + F_{32} = 1.0 \tag{18}$$

combining (17) and (18)

$$F_{34} + F_{31} = 1.0 \tag{19}$$

but

$$F_{35} + F_{34} = 1.0 \tag{20}$$

from (19) and (20), it is evident that

$$F_{35} = F_{31} \tag{21}$$

By reciprocity

$$F_{13} = \frac{A_3 \; F_{31}}{A1} \tag{22}$$

and

$$F_{35} = \frac{F_{53} \; A_5}{A_3} \tag{23}$$

combining (31), (33) & (23)

$$F_{13} = \frac{A_3 \; F_{53} \; A_5}{A_1 \; A_3} = \frac{F_{53} \; A_5}{A_1} \tag{24}$$

or,

$$F_{13} = 0.43561$$

$$F_{14} = 1 - F_{11} - F_{12} - F_{13} = 0.26922 \tag{25}$$

"SCRIPT F"

By assumption

$$\epsilon_3 = 1.0 \tag{26}$$

and since

$\overline{F}_{ij}$ = the fraction of energy emitted by surface i which is ultimately absorbed by surface j

by inspection,

$$\overline{F}_{24} = \epsilon_2 F_{24} + \epsilon_2 (1 - \epsilon_1) F_{21} \quad (27)$$

$$\overline{F}_{21} = \epsilon_2 F_{21} \epsilon_1 \quad (28)$$

$$\overline{F}_{13} = \epsilon_1 F_{13} \epsilon_3 = \epsilon_1 F_{13} \quad (29)$$

$$\overline{F}_{14} = \epsilon_1 F_{14} + \epsilon_1 F_{12} (1 - \epsilon_2) F_{24} \quad (30)$$

$$\overline{F}_{12} = \frac{A_2 \overline{F}_{21}}{A_1} \quad (31)$$

ALBEDO

Q_{alb} = solar energy diffusely reflected by the moon, 3, which is absorbed by surface 1

β_s = angle between the sun vector and moon's surface

By assumption,

$$\rho_3 = 0.07 \quad (32)$$

$$G_s = 443 \frac{Btu}{Hr\ Ft^2}, \text{ the solar intensity} \quad (33)$$

By inspection,

$$Q_{alb} = G_s \sin \beta_s \rho_3 F_{13} A_1 \alpha_1 \quad (34)$$

EFFECTS OF AZIMUTH ANGLE

Azimith angle is defined as the angle between the sun vector and the edge of the radiator (X = 1, Y = 0) when viewed from Y = $+\infty$. In this development, the effects of azimuth angle are accounted for by multiplying the solar constant by the cosine of the azimuth angle, or

$$G_{EQ} = G_S \cos \gamma \quad (35)$$

DIRECT SOLAR INPUT TO RADIATOR

In general, the sun will directly illuminate the radiator and energy will be absorbed along part of its area.

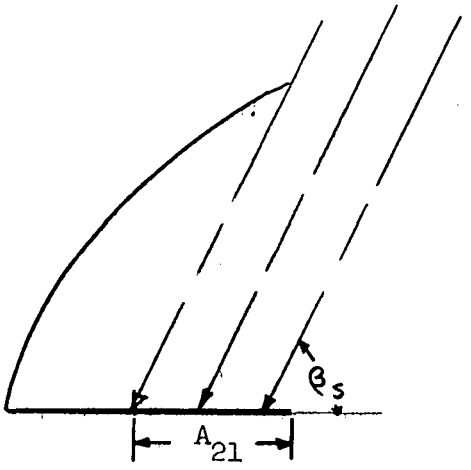

A_{21} = Directly illuminated area

$$\tan \beta_S = \frac{A_5}{A_{21}} \qquad (36)$$

and

$$A_{21} = A_5 \ \text{ctn} \beta_S = 2 \ \text{ctn} \beta_S \qquad (37)$$

modified to the limits,

$$0 \leq A_{21} \leq A_2$$

The projected area normal to the sun vector = $A_{21} \sin \beta_S$

and the total energy directly absorbed

$$Q_2 \text{ (sun direct)} = G_{EQ} \ A_{21} \ \sin \beta_S \alpha_2 \qquad (38)$$

$$= G_{EQ} \ 2 \ \text{ctn} \beta_S \ \sin \beta_S \alpha_2$$

SECONDARY RADIATION ABSORBED BY REFLECTOR

Some part of the radiation incident on the radiator will be diffusely reflected, some of this in turn will be absorbed by the reflector. For any calculations, the view factor from the directly illuminated portion of the radiator must be determined. From (reference 4).

$$F_{2\bar{I}-1} = 1 - \tfrac{1}{2}\left(1 + \frac{2}{A_{2I}} - \left(1 + \left(\frac{2}{A_{2I}}\right)^2\right)^{\frac{1}{2}}\right) \qquad (39)$$

heat reflected from $A_{2I} = G_{EQ}\ 2\ \mathrm{ctn}\,\beta_S\ \sin\beta_S \alpha_2$

heat reflected from $A_{2\bar{I}}$ which is absorbed by (1)

$$Q_1 \text{ (sun indirect)} = G_{EQ}\ 2\ \mathrm{ctn}\,\beta_S\ \sin\beta_S \rho_2\ F_{21-1} \alpha_1 \qquad (40)$$

RADIATION DIRECTLY ABSORBED BY REFLECTOR

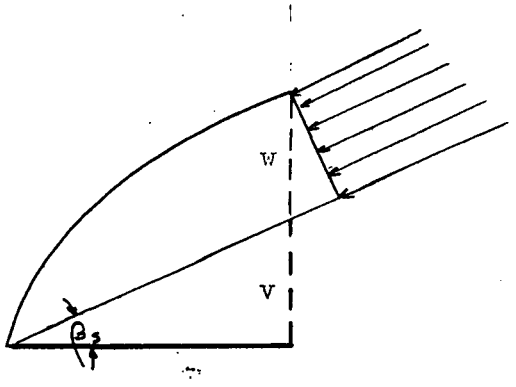

Projected area of reflector = $w \cos\beta_S$ (41)

but

$$w = 2 - v \qquad (42)$$

and

$$v = \tan\beta_S \qquad (43)$$

combining (41) (42) and (43)

$$\text{Projected area} = (2 - \tan\beta_S) \quad \cos\beta_S \tag{44}$$

valid for

$$0 \leq \text{projected area} \leq 2$$

the corresponding energy absorbed is

$$Q_1 \text{ (sun direct)} = G_{EQ} \ (2-\tan\beta_S) \cos\beta_S \alpha_1 \tag{45}$$

SOLAR RADIATION INDIRECTLY ABSORBED BY THE RADIATOR

All of the solar radiation directly incident on the reflector is specularly reflected to the radiator, i.e. with a view factor of unity.

$$\text{heat reflected from reflector} = G_{EQ} \ (2-\tan\beta_S) \cos\beta_S \rho_1 \tag{46}$$

and the corresponding amount absorbed by the radiator is:

$$Q_2 \text{ (sun indirect)} = G_{EQ} \ (2-\tan\beta_S) \cos\beta_S \rho_1 \alpha_2 \tag{47}$$

VEHICLE INPUT

The thermal heat input from the vehicle is assumed uniform and its numerical value is computed based on orientation of the GSR panel and solar angles. Here it is used as a constant Q_{veh}.

OVERALL HEAT BALANCE

Since the temperature of the radiator is fixed and isothermal, a heat balance is taken around the reflector.

$$(\text{heat in})_{\text{reflector}} = (\text{heat out})_{\text{reflector}} \tag{48}$$

$$\text{heat in} = Q_{alb} + Q_2 \text{ (sun direct)}$$

$$+Q_1 \text{ (sun indirect)} \quad + \quad Q_1 \text{ (sun direct)}$$

$$+Q_2 \text{ (sun indirect)} + \sigma \bar{F}_{13} A_3 (T_3^4 - T_1^4) + Q_{veh} \quad (49)$$

$$\text{heat out} = \sigma A_1 \bar{F}_{12} (T_1^4 - T_2^4) + \sigma A_1 \bar{F}_{14} T_1^4 \quad (50)$$

Combining eqs (48), (49), (50), and solving for T_1, the reflector temperature yields:

$$T_1 = \sqrt[4]{\frac{\sigma A_1 \bar{F}_{13} T_3^4 + \sigma A_1 \bar{F}_{12} T_2^4 + Q_{alb} + Q_2 \text{ (sun direct)} + Q_1 \text{ (sun indirect)} + Q_1 \text{ (sun direct)} + Q_2 \text{ (sun indirect)} + Q_{veh}}{\sigma A_1 \bar{F}_{13} + \sigma A_1 \bar{F}_{12} + \sigma \bar{F}_{14} A_1}} \quad (51)$$

and the corresponding net heat loss from the radiator is

$$Q_{2net} = \sigma A_2 \bar{F}_{24} T_2^4 + \sigma A_2 \bar{F}_{21} (T_2^4 - T_1^4)$$
$$-Q_2 \text{ (sun direct)} - Q_2 \text{ (sun indirect)} - Qveh \quad (52)$$

APPENDIX C

GSR - ECS SYSTEM ANALYSIS PROGRAM

A digital program was developed to examine the GSR in the LEM system environment for a full mission profile. The program was designed to account for the following physical phenomena and components.

Thermal Inertia

The ECS system was broken up into major groups of heat dissipating equipment. These were chosen as (1) the aft bay electronic equipment, (2) the cabin electronic equipment. These two groups of components have significant thermal inertia and the digital program was designed to account for it using the conventional lumped-parameter technique.

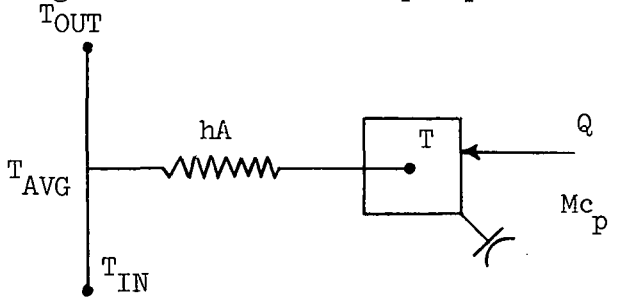

Shown in the above sketch are the average temperatures of the lumped mass, T, the total heat dissipated in the component, Q, the average overall coefficient of heat transfer between the mass and the average fluid temperatures, h, and the inlet, average and outlet fluid temperatures as T_{IN}, T_{AVG} and T_{OUT}. This model is reduced to the following system of equations.

$$Q = hA(T-T_{AVG}) + (Mc_p)\ \frac{dT}{d\theta} \qquad (1)$$

$$T_{AVG} = \frac{T_{IN} + T_{OUT}}{2} \qquad (2)$$

and

$$(W_{cp})\ (T_{OUT} - T_{IN}) = hA\ (T - T_{AVG}) \qquad (3)$$

Where (Mc_p) is the thermal mass of the dissipating component and (W_{cp}) is the product of mass flow rate and specific heat capacity of the fluid. In this discussion, the specific heat capacity is always evaluated at the average fluid temperature.

APPENDIX C - Continued

Since the program can utilize only algebraic equations, the first equation is converted, using the backward finite difference definition, to:

$$\Delta\Theta \cdot Q = h \cdot T \cdot \Delta\Theta - h \cdot T_{AVG} \cdot \Delta\Theta + (Mc_p)(T - T_o) \qquad (4)$$

where,

$\Delta\Theta$ = finite time increment used by the program for indexing

T_o = initial temperature at beginning of a time increment

T = final temperature at the end of a time increment

Equations (2), (3) and (4) are subsequently set up in determinant form in the program and solved simultaneously using the XSIMEQ routine, available from SHARE.

Transport Delay

Since the total time for a fluid particle to traverse the complete ECS is about 10 minutes, a technique was devised to move, or more correctly index, the fluid around the circuit. The ECS circuit was conveniently divided into 11 length which represent adiabatic lines between components. Each length has its own average inside diameter and mass flow rate. Based on this data, the time it takes for the fluid in each line to travel its length was computed as follows, where ρ is the fluid density:

$$\Delta\tau_i = \rho \frac{D^2 \pi L}{4 W}$$

The smallest of these 11 time values, $\Delta\tau_{MIN}$, was then selected and this value assigned for the transient computer interval. The balance of the remaining 10 line lengths are then divided into a number of smaller line segments each of which exhibits a transport time equal to $\Delta\tau_{MIN}$. Thus, by indexing the fluid temperature from line node to line node for each value of real time, the program keeps track of the fluid temperatures in the lines.

Water Boiler Equations

The ECS water boiler component is positioned between the radiator and the regenerator (which was not used) in the glycol circuit. Its performance is represented by the following equations:

APPENDIX C - Continued

$$QWB = 133.62\ (T_{IN} - 32) \tag{5}$$

$$T_{OUT} = T_{IN} - \frac{QWB}{(W_{cp})g} \tag{6}$$

$$W_{H_2O} = QWB/1000.0 \tag{7}$$

$$W_{lb} = W_{lbo} + W_{H_2O} \cdot \Delta\Theta \tag{8}$$

where:

QWB = Net heat rejected by water boiler

T_{IN} = Glycol inlet temperature to water boiler

T_{OUT} = Glycol outlet temperature from water boiler

$(W_{cp})g$ = Specific heat capacity times mass flow rate of glycol

W_{H_2O} = Water consumption rate

W_{lb} = Integrated water lost by boiler summed to the end of a time increment

W_{lbo} = Initial integrated water at the beginning of a time increment

$\Delta\Theta$ = Finite time increment used by program for indexing

When the inlet temperature to the water boiler is less than $32^{\circ}F$, the net heat rejection is set to zero since the water boiler would then freeze up.

GSR Equations

Since three dimensional GSR performance was not established, the radiator equations incorporated in the system analysis assume that the radiator performs as if the root of the fin were fixed at a temperature value equal to the average temperature of the glycol in the radiator.

APPENDIX C - Continued

With this approximation, a fin effectiveness is used (as defined in the GSR performance section) and the following set of equations represent the GSR performance in the ECS system:

$$(W_{cp})g\left(T_{IN} - T_{OUT}\right) = \eta_f \; A\, T_{AVG}^{4} + (Mc_p)_R \, d\, \frac{T_{AVG}}{d\theta} \qquad (9)$$

$$T_{AVG} = \frac{T_{IN} + T_{OUT}}{2} \qquad (10)$$

where the variables are consistantly defined, and,

η_f = fin effectiveness

A = total surface area

$(Mc_p)_R$ = mass times specific heat capacity of radiator

Equation (9) is converted to finite difference form before use in the program.

Regenerator Heat Exchanger Equations

The regeneration heat exchanger is considered as a constant "UA" device and the following equations were used to predict its performance.

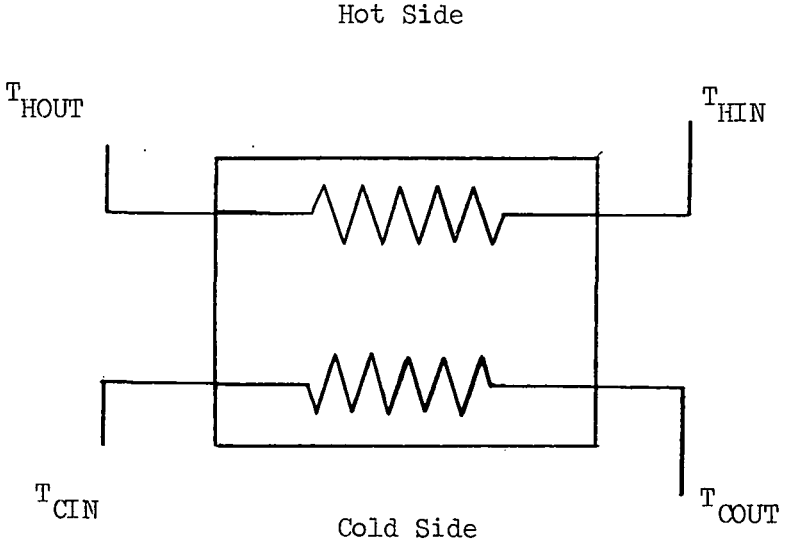

APPENDIX C - Continued

$$Q_{reg} = (UA) \frac{(T_{HIN} - T_{COUT}) + (T_{HOUT} - T_{CIN})}{2} \quad (11)$$

$$Q_{reg} = (W_{cp})g \ (T_{HIN} - T_{HOUT}) \quad (12)$$

$$Q_{reg} = (W_{cp})gc \ (T_{COUT} - T_{CIN}) \quad (13)$$

$(W_{cp})gs$ = a function of the temperature compensated bypass control valve setting (14)

where:

Q_{reg} = Net heat rejected from hot side to cold side of the regenerator

$(W_{cp})gc$ = Cold side mass flow times specific heat capacity.

Cabin Heat Exchanger Equations

The cabin heat exchanger and its related environment is represented by the following equations:

$$Q_{CHX} = (W_{cpe})_o \ (T_{HIN} - T_{GIN}) \quad (15)$$

$$T_{HIN} = T_{AIR} + \frac{Q_{FAN}}{(W_{cp})_o} \quad (16)$$

$$Q_{CHX} = (W_{cp})g \ (T_{GOUT} - T_{GIN}) \quad (17)$$

$$T_{HOUT} = T_{HIN} - \frac{Q_{CHX}}{(W_{cp})_o} \quad (18)$$

$$C_{WA} \ (T_W - T_{AIR}) + Q_{FAN} = Q_{CHX} \quad (19)$$

where:

Q_{CHX} = Net heat rejected from cabin heat exchanger to the glycol

T_{HIN} = Upstream cabin heat exchanger air

APPENDIX C - Continued

T_{GIN} = Upstream glycol temperature

$(W_{cpe})_o$ = Mass flow times specific heat capacity times heat exchanger effectiveness of cabin oxygen

T_{AIR} = Cabin air temperature

T_{GOUT} = Outlet glycol temperature

Q_{FAN} = Power of heat exchanger fan

T_W = Characteristic cabin wall temperature

C_{WA} = Thermal conductance between cabin air and walls

$(W_{cp})_o$ = Mass flow times specific heat capacity of cabin oxygen

Program Logic

Since it takes an integral number of finite time increments for the fluid "lumps" to move from one component to the next downstream component, it is immaterial in what order the calculations for each component occur. It is important only to "index" the fluid around the circuit after all new temperatures and other variables have been computed. In schematic form:

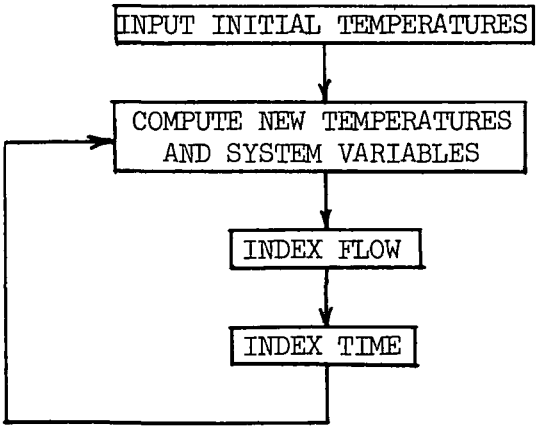

APPENDIX C - Continued

Program Results

The most significant variable in the ECS system analysis is the total cumulative water expended by the water boiler.

For a typical mission profile and a 52.25 ft^2 GSR with no vehicle heat input, 126 pounds of water are used with a radiator in the loop, versus 268 pounds without a radiator.

These values agree well with those obtained from the more simplified steady state "cycle" calculations.

APPENDIX D

GSR FIN EFFECTIVENESS PROGRAM

The GSR analysis as previously developed assumes that the radiator fin is at a constant temperature. This assumption was subsequently removed and an additional routine was added to account for the effects of a temperature gradient in the fin. Only gradients normal to the fluid flow are considered and the problem retains its two dimensional aspects.

This routine is designed to compute the temperature distribution across the fin and the corresponding distribution of net heat rejection. The total heat rejection is then obtained by summation. Defining a new parameter called fin effectiveness, a table of numbers is generated which is useful for obtaining GSR performance in particular systems in or out-of-program computations.

Fifty nodes were used to break the fin into strips parallel to the tube.

No direct solar illumination of the radiator or reflector was considered in the heat balance involving fin nodes.

A thermal balance on an arbitrary node includes conduction to and from adjacent nodes, radiation to space and radiation coupling to the reflector.

Based on this heat balance, the temperature of each node and the reflector are determined for a particular "forced" value of root temperature. The net heat rejected from each node, q_i, is then determined.

$$q_i = \sigma A_i \bar{F}_{i-s} T_i^4 - \sigma A_i \bar{F}_{i-r} \left(T_r^4 - T_i^4 \right)$$

where:

A_i = surface area of each radiator node

$\bar{F}_{i-s}$ = "script F" value from radiator node to space

$\bar{F}_{i-r}$ = "script F" value from radiator node to reflector

T_i = node temperature, absolute

T_r = reflector temperature, absolute

APPENDIX D - Continued

The net heat rejected, under these conditions, by the radiator is merely the sum of the q_is

$$q_{NET} = \sum_{i=1}^{50} qi$$

Since an overall performance parameter is needed to describe these results, namely the effects of temperature gradients of the radiator fin on net heat rejection, we define a "fin effectiveness", η_f

$$\eta_f = \frac{\text{Net Heat Rejected by Radiator}}{\text{Heat rejected to a non-reflecting environment by a black body radiator at a uniform temperature equal to the root temperature}}$$

or,

$$\eta_f = \frac{q_{net}}{\sigma A T_{Root}^4}$$

The table below lists calculated values of fin effectiveness for the 52.25 ft^2 design GSR as a function of root temperature.

η_f	Root Temperature ^oF
.683	0.0
.707	20.0
.713	40.0
.721	60.0
.725	80.0
.728	100.0

The equation defining fin effectiveness is rewritten:

$$q_{net} = \eta_f \sigma A \ T_{Root}^4$$

and is used with the table of fin effectiveness values to predict the performance of the GSR in the ECS system analysis.

The results of this analysis substantiate the simplified cycle calculation results.

REFERENCES

1. Phase I Report, LEM Space Radiator Study. LTV Report No. 00.655 submitted on 11 June 1965.

2. LEM Systems Specification LSP-470-1.

3. Application of Mass Ratios for Weight Optimizing System Staging Arrangements LMO-490-152, Revision A.

4. Radiation Heat Transfer, F. Kreith, Internation Textbook Company, 1962.

GRUMMAN AIRCRAFT ENGINEERING CORPORATION

BETHPAGE · LONG ISLAND · NEW YORK